DETERMINATION OF THE ACCURACY OF NON-DESTRUCTIVE RESIDUAL STRESS MEASUREMENT METHODS

by

TENDAI CHIPANGA

Thesis submitted in partial fulfilment of the requirements for the

Master of Technology Degree in Mechanical Engineering

in the Faculty of Engineering
at the

CAPE PENINSULA UNIVERSITY OF TECHNOLOGY

Internal Supervisor: Prof. G.J. Oliver

External Supervisor: Prof. J. Gryzagoridis

Bellville, Cape Town
AUGUST 2009

DECLARATION

I, Tendai Chipanga, declare that the contents of this thesis represent my own unaided work, and that the thesis has not previously been submitted for academic examination towards any qualification. Furthermore, it represents my own opinions and not necessarily those of the Cape Peninsula University of Technology.

30/09/2009

Signed **Date**

ABSTRACT

Sophisticated measurement methods are currently used extensively to determine the residual stresses in materials. The capabilities of the Hole-Drilling Method, Debro-30 Ultrasonic System and Digital Shearography to determine residual stresses have been explored. The accuracy of these techniques in measuring residual stresses in mild steel specimens is thoroughly examined and discussed. The results obtained from the experiments are consistent with the expected outcomes. Related literature review, experimental procedures, results and their discussion have been outlined. It is hoped that the information provided in this thesis will be of importance to end users, especially engineers and technologists who use these non-destructive methods to evaluate residual stresses in components and materials.

ACKNOWLEDGEMENTS

I would like to extend my profound gratitude and appreciation to God for His guidance, protection, provision, unconditional love and courage without which successful completion of this work was not going to be possible.

I am indebted to my Professors, Jasson Gryzagoridis and Graeme Oliver for their constructive criticism, guidance and encouragement.

Many thanks to Mr Walter Kolhoffer for assisting me in servicing some of the equipment and machines that were used to conduct this research. Prof. Dr. Szelazek, head of Ultrasonic Testing of Materials Laboratory in Poland, your willingness to send a manual for the Debro-30 Ultrasonic System through Prof. J. Gryzagoridis is acknowledged with thanks. Thanks also to Associate Professor Philander in the department of Mechanical Engineering for unselfishly making available the shearography measuring equipment.

Mr Francois Hoffman, co-ordinator of Mechatronics programme in the department of Mechanical Engineering allowed me to lecture whilst undertaking my research, your confidence and trust in me is greatly appreciated. Mr Waleed Kahn, my student, thank you for your assistance in procuring materials.

A special word of thanks to my wife, Unity, whose unwavering support kept me going miles away from home in Zimbabwe. I also acknowledge the moral support and encouragement provided by my parents and family members.

The financial assistance offered by the department of Mechanical Engineering (Cape Peninsula University of Technology) through the acting head of department, Mr Zwelethu is gratefully acknowledged.

DEDICATION

To the darling of my heart Unity and our future children.

TABLE OF CONTENTS

DECLARATION ii
ABSTRACT iii
ACKNOWLEDGEMENTS iv
DEDICATION v
TABLE OF CONTENTS vi
LIST OF FIGURES viii
LIST OF TABLES x
GLOSSARY xi
CHAPTER ONE 1
INTRODUCTION 1
1.1 STATEMENT OF THE PROBLEM 1
1.2 INTRODUCTION AND BACKGROUND OF THE PROBLEM 1
1.2.1 DEFINITION OF RESIDUAL STRESSES 1
1.2.2 CLASSIFICATION OF RESIDUAL STRESSES 2
1.2.3 FORMATION OF RESIDUAL STRESSES 2
1.2.3.1. Thermal deformation 3
1.2.3.2. Mechanical deformation 4
1.2.4.3. Combined thermal and plastic deformation 5
1.3 HYPOTHESES OR RESEARCH QUESTIONS 5
1.4 AIMS AND OBJECTIVES OF THE RESEARCH 6
1.5 RESEARCH DESIGN AND METHODOLOGY 6
1.6 DELIMITATION OF THE RESEARCH 6
1.7 SIGNIFICANCE OF THE RESEARCH 6
1.8 EXPECTED OUTCOMES, RESULTS AND CONTRIBUTIONS OF THE RESEARCH 7
1.9 CONCLUSION 7
CHAPTER TWO 8
LITERATURE REVIEW ON THE CHARACTERISATION 8
OF RESIDUAL STRESSES 8
2.1 HOLE-DRILLING TECHNIQUE 8
2.1.1 THE PRINCIPLE AND THEORY OF THE HOLE-DRILLING STRAIN GAUGE METHOD 9
2.1.1.2 STRESS EVALUATION METHODS 11
2.1.1.3 Blind Hole Analysis 12
2.1.1.4 Surface Preparation for Strain Gage Bonding 13
2.2 ULTRASONIC METHODS 15
2.2.1 THE ACOUSTOELASTIC THEORY 15
2.2.2 ULTRASONIC WAVES 15
2.2.2.1 Fundamental properties of waves: 16
2.2.2.2 Characteristic Properties of Ultrasonic Waves 16
2.2.3 EFFECTS OF STRESSES ON THE PROPAGATION OF ULTRASONIC WAVES 18
2.2.4 ULTRASONIC STRESS MEASUREMENT TECHNIQUES 19
2.2.5 Preparatory work 21
2.3 DIGITAL SHEAROGRAPHY 22
2.3.1 DESCRIPTION OF DIGITAL SHEAROGRAPHY TECHNIQUE 22
2.3.2 PHASE STEPPING 26
2.3.3 CONCLUSION 27
CHAPTER THREE 28
USING THE HOLE DRILLING METHOD ON A SPECIMEN SUBJECTED TO FOUR POINT BENDING 28
3.1 INTRODUCTION 28
3.2 MANUFACTURE OF SPECIMEN 28
3.3 ANNEALING PROCEDURE 28
3.3.1 Precautions during Annealing 28
3.4 MATERIAL AND EQUIPMENT 29
3.4.1 Specimen Surface Preparation for Strain Gage Bonding 30
3.4.2 Strain Gage Rosettes 31
3.4.3 Conventional Strain Gages 32
3.4.4 Instrumentation 33
3.5 FOUR POINT BENDING TEST 33
3.6 DERIVATION OF THE APPLIED FORCE USING MACAULAY'S METHOD 35

3.6.1 Procedure for conducting a Four Point Bending Test 37
3.7 DESCRIPTION OF THE RS-200 MILLING GUIDE 37
3.7.1 Procedure for the Measurement of Residual Stress Using the RS-200 Milling Guide 38
3.7.2 Procedure for Using the Milling Rod Assembly 39
3.8 PRESENTATION AND DISCUSSION OF RESULTS 40
3.9 VALIDATION OF RESULTS USING ANSYS 42
3.10. CONCLUSION 42
CHAPTER FOUR 43
EXPERIMENTAL WORK 43
4.1 INTRODUCTION 43
4.2 MANUFACTURE OF THE SPECIMENS 43
4.3 ANNEALING PROCEDURE 44
4.4 INDUCING STRESSES ON THE SPECIMEN SURFACE BY SHOT PEENING 45
4.4.1 Classification of Almen strips 47
4.5 MATERIAL AND EQUIPMENT 49
4.5.1 Debro-30 Ultrasonic stress meter 49
4.5.2 Calibration Procedure 50
4.5.3 Measuring Procedure 52
4.5.4 Compression Test 54
4.6 DISCUSSION OF CALIBRATION RESULTS 56
4.7 STRESS MEASUREMENTS ON SPECIMENS 56
4.7.1 Discussion of Ultrasonic Stress Measurement Results 58
4.8 THE HOLE DRILLING METHOD 59
4.8.1 Discussion of the Hole Drilling Method Stress Measurement Results 62
4.9 DIGITAL SHEAROGRAPHY 63
4.9.1 Introduction 63
4.10 Surface Preparation of Specimens 63
4.11 Material and Equipment 64
4.12 Experimental Procedure 64
4.13 Shearography Measurement Procedures 66
4.14 Discussion of Shearography Results 68
4.15 Conclusion 69
CHAPTER FIVE 70
ANALYTICAL RESULTS 70
5.1 INTRODUCTION 70
5.2 ANALYTICAL RESULTS 70
5.3 Shearography Measurements 77
5.4 Strain Gauge Measurements 80
5.5 Comparison of Strain Gauge and Shearography Results 82
5.6 Finite Element Analysis on “Stress Free” Specimen 82
CHAPTER SIX 85
CONCLUSIONS AND RECOMMENDATIONS 85
6.1 CONCLUSIONS 85
6.2 RECOMMENDATIONS 87
REFERENCES 88
APPENDICES 90
APPENDIX A: STRAIN RESULTS AND COMPUTATION OF STRESSES 90
APPENDIX B: Fundamental Properties of Ultrasonic Waves in some solid media 96
APPENDIX C: Debro-30 Measurement Results 97
APPENDIX D: Shearography Results for all the Four Specimens 99

LIST OF FIGURES

Figure 1.1:	An illustration of the effect of thermal phase transformations upon the residual stresses induced in the surface of a component	4
Figure 1.2:	An illustration of the effect of mechanical deformation upon the residual stresses induced in the surface of a component	4
Figure 1.3:	An illustration of the effect of a combination of thermal and plastic deformations upon the residual stresses induced in the surface of a component	5
Figure 2.1:	Stress states at a point before the introduction of a hole	10
Figure 2.2:	Stress states at a point after the introduction of a hole	10
Figure 2.3:	Sketch of the propagation of the wave from the emitter to the receivers	19
Figure 2.4:	Velocity of plane waves and stress field in orthogonal directions	21
Figure 2.5:	Typical Shearography set up	24
Figure 3.1:	Thickness versus hole diameter over gauge circle diameter ratio	30
Figure 3.2:	Specimen with bonded strain gauges and soldered electrical wires	31
Figure 3.3:	Strain Gauge Rosette Grid Orientation	32
Figure 3.4:	Bonded Strain Gauges for measuring tensile strains due to bending	32
Figure 3.5:	Four Point Bending Beam loading set-up	33
Figure 3.6:	Specimen subjected to load during the four point bending test	34
Figure 3.7:	Beam sectioned in the middle with uniformly distributed load consideration	35
Figure 3.8:	Free body diagram of beam	35
Figure 3.9:	Hole-drilling equipment set-up using compressed air	38
Figure 3.10:	Hole-drilling equipment set-up using milling rod assembly and electric drill	39
Figure 3.11:	Graphical projection of surface stress by Uniform Stress Method	41
Figure 3.12:	FEA - Stress distribution in the specimen	42
Figure 4.1:	Combined Heating and Cooling Cycle Graphs at intervals of 100 °C	45
Figure 4.2:	An illustration of the Shot Peening Process Phenomenon on a given metal surface	46
Figure 4.3:	Shot Peening Intensity Curve	48
Figure 4.4:	Ultrasonic Stress Meter – Debro-30 and Accessories	50
Figure 4.5:	Schematic of the Specimen used for the calibration in uniaxial loading	52
Figure 4.6:	Tensile Test set-up for calibrating the Debro-30 Ultrasonic system	53
Figure 4.7:	Determination of Acoustoelastic constant of specimen using the Debro-30 6L Probehead	54
Figure 4.8:	Compression Test set-up for calibrating the Debro-30 system	55
Figure 4.9:	Determination of Acoustoelastic constant of specimen using the 6L Probehead in a compressive test	55
Figure 4.10:	Specimen surface impacted with the tips of bristles of a wire brush	57
Figure 4.11:	Specimen surface subjected to hammering the 1.5 mm steel bearing balls that covered the surface	57
Figure 4.12:	Specimen surface heated to dull orange colour with oxy-acetylene flame and quenched in water	58
Figure 4.13:	CEA-06-062UM-120 rosette	59
Figure 4.14:	Soldering of electrical wires on the tabs of the CEA-06-062UM-120 rosette	60
Figure 4.15:	Milling Guide Base Assembly with a microscope assembly	61
Figure 4.16:	Strain Gauge cemented on specimens	63
Figure 4.17:	Digital Shearographic Unit System	64

Figure 4.18:	Shearography Experimental set-up	65
Figure 4.19:	Schematic of the Mechanical Loading of the Cantilever	66
Figure 4.20:	Captured filtered phase image during measurement	68
Figure 4.21:	Phase Images for stress free and wire-brush impacted specimens	69
Figure 5.1:	Cantilever Beam loading set-up	70
Figure 5.2:	Variation of bending stress with distance from the built-in support	73
Figure 5.3:	Variation of deflection with distance from the built-in support to the free end	73
Figure 5.4:	Variation of slope with distance from the built-in support to the free end	74
Figure 5.5:	Variation of strain with distance from the built-in support to the free end	77
Figure 5.6:	Variation of slope with distance from the built-in support to the free end for all specimens (analytical and experimental)	78
Figure 5.7:	Variation of bending stress with distance from the built-in support to the free end	80
Figure 5.8:	Variation of measured surface strain with mass for all specimens	81
Figure 5.9:	Variation of measured surface strain with distance for all specimens	81
Figure 5.10:	Effect of elastic constants on displacement	83
Figure 5.11:	Variation of displacement from the built-in support to the free end	83
Figure 5:12	Variation of stress from the built-in support to the free end	84
Figure A1:	Data reduction coefficients graphs	91
Figure A2:	Stress versus depth for a heated and quenched specimen	94
Figure A3:	Stress versus depth for a dimpled specimen	94
Figure A4:	Stress versus depth for a specimen impacted with tips of bristles of a wire brush	95
Figure D1:	Phase Image for stress free specimen	99
Figure D2:	Gradient Image for stress free specimen	99
Figure D3:	Displacement Image for stress free specimen	99
Figure D4:	Phase Image for surface impacted with the tips of bristles of a wire brush	100
Figure D5:	Gradient Image for surface impacted with the tips of bristles of a wire brush	100
Figure D6:	Displacement Image for surface impacted with the tips of bristles of a wire brush	100
Figure D7:	Phase Image for surface produced by hammering 1.5 mm steel bearing balls in contact with the surface	101
Figure D8:	Gradient Image for surface produced by hammering 1.5 mm steel bearing balls in contact with the surface	101
Figure D9:	Displacement Image for surface produced by hammering 1.5 mm steel bearing balls in contact with the surface	101
Figure D10:	Phase Image for surface heated with oxy-acetylene flame and quenched in water	102
Figure D11:	Gradient Image for surface heated with oxy-acetylene flame and quenched in water	102
Figure D12:	Displacement Image for surface heated with oxy-acetylene flame and quenched in water	102

LIST OF TABLES

Table 4.1:	**Chemical composition of mild steel alloy**	**43**
Table 4.2:	**Annealing heating and cooling cycles**	**44**
Table 4.3:	**Ultrasonic stress measurement results for the three mild steel specimens**	**58**
Table 4.4:	**Hole Drilling stress measurement results**	**61**
Table 5.1:	**Computed stress values for all the specimens**	**82**
Table A1:	**Computed stresses for specimens**	**92**
Table B1:	**Fundamental Properties of Ultrasonic Waves in some solid media**	**96**
Table C1:	**Calibration Results for Acoustoelastic Constant Determination by Compression Test**	**98**

GLOSSARY

Symbols/Acronyms	Meaning
A, a	Cross sectional area (m^2), Amplitude (m)
b	Section Breadth/Width (m)
D, d	Gauge Circle Diameter (m), Section Depth (m)
G	Modulus of rigidity (N/m^2)
P	Applied load (N), Acoustic pressure (Pa)
N	Number of Fringes (dimensionless)
E	Young's Modulus of Elasticity (N/m^2)
I	Intensity distribution, Acoustic intensity (W/m^2)
K	Sensitivity coefficient (dimensionless)
S	Magnitude of shear (m)
T, t	Period (s), Time (s), Temperature (ºC), Thickness (mm)
f	Frequency (Hz or s^{-1})
I	Second moment of area (m^4)
M	Moment (Nm)
EI	Bending stiffness or Flexural rigidity ($MN\ m^2$)
V	Velocity (m/s)
V_L	Longitudinal wave velocity (m/s)
V_T	Transverse wave velocity (m/s)
y	Deflection (mm) or distance from the neutral axis to the uttermost fibres (mm)
L	Length of a beam
R, r	Radius
Z	Acoustic impedance (Pa s/m), Depth (m)
α	Phrase difference/Direction of principal stresses/Coefficient of Linear Expansion
β	Acoustic-elastic constant
δ	Deformation
σ_x	Stress in x direction (MPa)
σ_y	Stress in y direction (MPa)
σ_z	Stress in z direction (MPa)
ε_x	Strain in x direction
ε_y	Strain in y direction
ε_z	Strain in z direction
ν	Poisson's ratio
π	Pi
ρ	Density (kg/m^3)
τ	Shear stress (MPa)
ϕ	Phase
λ	Wave Length (m)
Ω	Resistance (ohms)
Ø	Diameter (m)
Δ	Change in a variable

ASTM	**American Society for Testing Materials**
CCD	**Charge Coupled Device**
FEA	**Finite Element Analysis**
PC	**Personal Computer**
UTM	**Universal Testing Machine**

CHAPTER ONE

INTRODUCTION

1.1 STATEMENT OF THE PROBLEM

Residual stress characterisation poses a great challenge in both the mechanical formulation of the problem and modelling prediction. Experimental techniques have been developed over the past years to determine the existence and measurement of residual stresses. Factors such as design optimisation and manufacturing cost reduction are further creating a need to experimentally obtain information with a higher degree of reliability; hence direct comparison of the existing techniques regarding residual stress characterisation becomes important.

1.2 INTRODUCTION AND BACKGROUND OF THE PROBLEM

Residual stresses occur as a result of the imbalance of outer and inner conditions of a material. Typically plastic deformation or microstructural changes in the material prevent the unloading of previously applied external loads. This usually occurs as a result of three principal mechanisms namely; mechanical processes, chemical treatment and heat treatment (Hearn, 1985). According to Wyatt & Berry (2006), residual stresses are formed basically in one of the three ways; thermal deformation, mechanical deformation and combined thermal and plastic deformation. There is consensus amongst researchers that residual stresses do exist in engineering components due to the above-mentioned processes and others, but their characterisation is complex. For example, in the past, engineers have been conservative in their designs by using large factors of safety to account for the existence of residual stresses (Smith et al, 2001 & James et al, 2007). The need to optimise components' designs and reduce their related manufacturing costs has attracted an increasing interest among researchers. Residual stresses are more difficult to predict and measure reliably than in-service stresses and can have either a beneficial or detrimental effect on the fatigue life of components and therefore cannot be ignored (Withers & Bhadeshia, 2001). A better understanding of residual stresses will alleviate component failure problems and maximise its benefits. Thus, the magnitudes and distribution of these stresses need to be measured or predicted. The techniques that are now available to measure residual stresses, that this study presents are; Hole Drilling, Debro-30 Ultrasonic System and Digital Shearography.

1.2.1 DEFINITION OF RESIDUAL STRESSES

These are stresses that are inside or locked into a component or stresses that remain after the original cause of the stresses such as those resulting from external loading, have been

removed. According to Duggan & Byrne (1979), the importance of residual stress depends upon:

(1) its magnitude, sense and direction relative to the applied stress;
(2) the material properties; and
(3) its stability with respect to time-temperature recovery processes occurring during cyclic stressing.

It is very important to know the magnitude and distribution of residual stresses since the mechanical behaviour of the material will be affected when they are present. Residual stress may be regarded as a superimposed mean stress that locally modifies the overall loading. Additionally, its introduction can modify the material's response to loading. Irrespective of their nature, large residual stresses can cause dimensional instability through phenomena such as creep, fatigue and stress corrosion cracking (Mordfin, 1988). Residual stresses cause warping during machining. As soon as a stressed region is removed, the part will deform in such a way as to maintain internal force and moment balances (Hosford, 2005).

1.2.2 CLASSIFICATION OF RESIDUAL STRESSES

Residual stresses may be classified by the scale over which they are significant, and hence the type of measurement technique used to study them.

- Macro-level stresses – those stresses that traverse distances that are larger than the material grains size (Wyatt & Berry, 2006). They can also be referred to as macroscopic residual stresses. These stresses are the ones of main interest in design and failure analysis.
- Micro-level stresses – those stresses that are within the crystal lattice that cover distances less than the size of the grain (Wyatt & Berry, 2006). They are also known as microscopic residual stresses.

Both types may be present at any one time in a material or component. Accordingly, in order to assess the likely performance of a component, knowledge of the residual stresses levels within that component is of fundamental importance.

1.2.3 FORMATION OF RESIDUAL STRESSES

The formation of residual stresses is influenced by the interactions of time, temperature, deformation and microstructure. Characteristics of material that influence the development of residual stresses include thermal conductivity, heat capacity, thermal expansion , elastic modulus and Poisson's ratio, plasticity, thermodynamics and kinematics of transformations,

mechanisms of transformations, and transformation plasticity. Totten et al (2005) reported that macroscopic residual stresses can be induced due to:

- Non-homogeneous plastic flow under the action of external treatment (shot peening, autofretting, roller burnishing, hammer peening, shock laser treatment).
- Non-homogeneous plastic deformation during non-uniform heating and cooling (ordinary quenching, moulding of plastics)
- Structural deformation from metalworking (heat treatment).
- Heterogeneity of a chemical or crystallographic order (nitriding or case hardening).
- Various surface treatments (enamelling, nickel plating, chrome plating, PVD and CVD coating).
- Differences in expansion coefficients and mechanical incompability of different components of composites.

Thus residual stresses are produced by heterogeneous plastic deformations, thermal contractions and phase transformations induced by manufacturing and fabricating processes. According to Wyatt & Berry (2006), residual stresses can be formed in one of the three ways;

- Thermal deformation
- Mechanical deformation
- Combined thermal and plastic deformation as discussed in the following section.

1.2.3.1. Thermal deformation

When heat is added to most materials, the average amplitude of the atoms vibrating within the material increases. This, in turn, increases the separation between the atoms by stretching the molecular bonds causing the material to expand. If the material does not go through a phase change, the expansion can be easily related to the temperature change. If the thermal energy of a material decreases, the material will shrink or contract. For example thermal deformation of a length of bar is given by:

$$\delta_{th} = \alpha(\Delta T)L \qquad (1.1)$$

Where α is linear coefficient of expansion for the material, and is the fractional change in length per degree change in temperature, ΔT is the temperature change (°C), δ_{th} is the thermal deformation, and L is the length of the bar (m).

The **thermal stress** which develops if a structure or member is completely constrained (not allowed to move at all) is the product of the coefficient of linear expansion and the temperature change and Young's modulus, mathematically given by:

$$\sigma = \alpha(\Delta T)E \qquad (1.2)$$

In Figure 1.1 the application of heat causes a change in volume in the surface layers of the component. If there is a phase change that causes the volume of the surface layers to decrease, the surface layers will tend to contract. However, the bulk of the component material will try to resist this contraction which will cause the surface layer to go into tension.

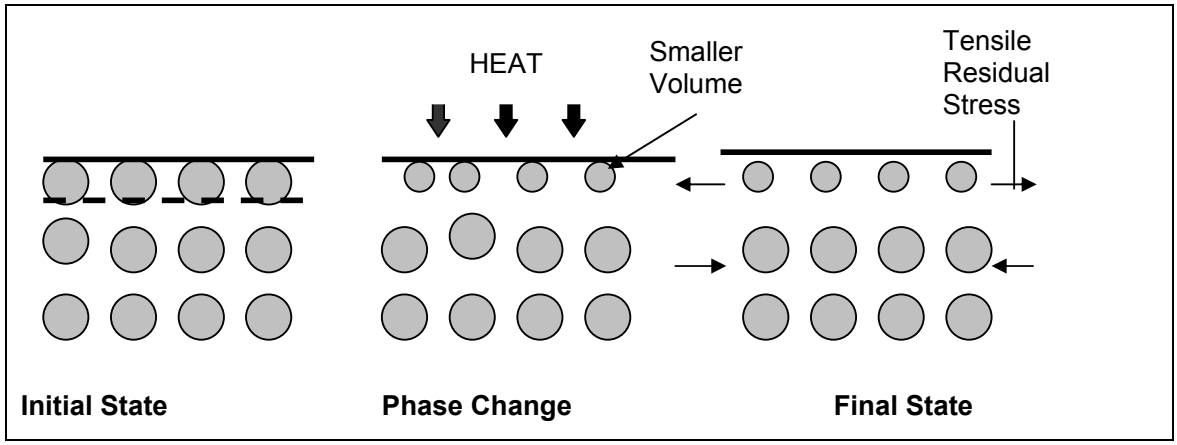

Figure 1.1. An illustration of the effect of thermal phase transformations as residual stresses are induced in the surface of a component, according to Griffiths (Wyatt & Berry, 2006).

1.2.3.2. Mechanical deformation

It occurs when the surface layers of the material undergo compaction. There is no significant heating of component surface and residual stresses are compressive in nature. Shot peening is an example of such phenomenon, see Figure 1.2 below.

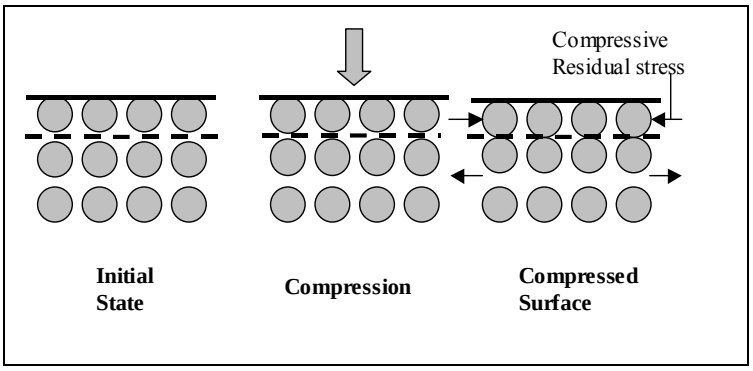

Figure 1.2. An illustration of the effect of mechanical deformation as residual stresses are induced in the surface of a component according, to Griffiths (Wyatt & Berry, 2006).

1.2.4.3. Combined thermal and plastic deformation

Deformations of this nature are induced during machining operations. The machining operation heats the component surface which expands. This expansion is then relieved by plastic flow, which is restricted to the surface layer. When the heat is removed the surface layer contracts which results in a tensile stress at the surface of the work piece, as can be seen in Figure 1.3 below.

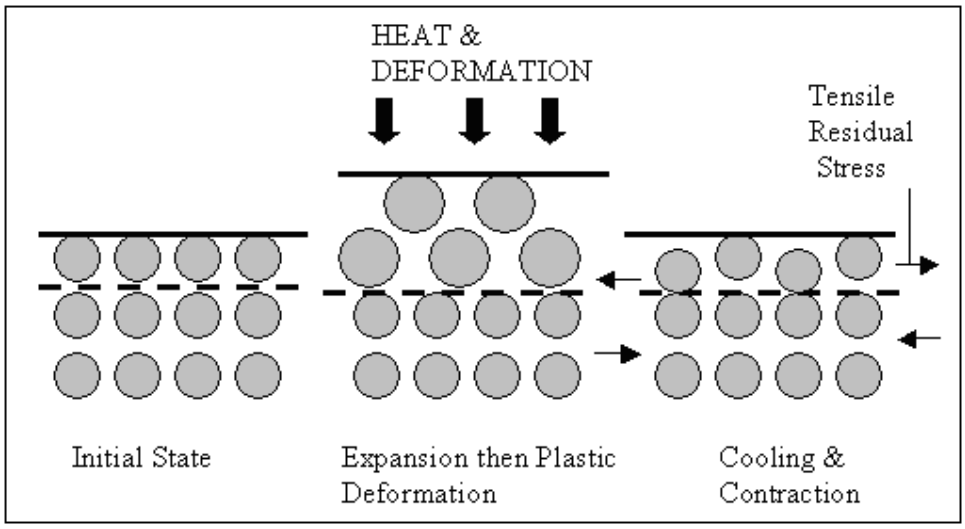

Figure 1.3. An illustration of the effect of a combination of thermal and plastic deformations as residual stresses are induced in the surface of a component, according to Griffiths (Wyatt & Berry, 2006).

The discussion above has shown that different processes produce residual stresses differently. For example, a study on castings done by Seetharamu et al quoted in Totten et al (2005) came up with following findings which they documented. In a solidifying material there will be various deformation regimes:

1) A plastic zone in tension at the solidification front, since the strength of the solid is low;
2) A central region where the stresses are in the elastic range;
3) A zone at the surface of the casting where there is plastic flow in compression.

1.3 HYPOTHESES OR RESEARCH QUESTIONS

- When are residual stresses beneficial or detrimental?
- What contribution do residual stresses have on the components and designs during failure?

1.4 AIMS AND OBJECTIVES OF THE RESEARCH

The aim of this research is to investigate and possibly quantify residual stresses identified by the three different techniques mentioned earlier and the results are critically compared. The objective is as follows:

- Investigate the magnitudes and possibly the distribution of residual stresses using the previously identified techniques in components where the presence and magnitude of residual stress is already known by other means or can be predicted.

1.5 RESEARCH DESIGN AND METHODOLOGY

The following are methods of investigation that were employed in undertaking this research:

- ❖ Laboratory experiments – A number of experiments for each technique were conducted. The data collected were carefully analysed and discussed. The following techniques were used in this work; Hole drilling, Debro-30 Ultrasonic system, and Digital Shearography. For each experiment all factors inter-alia, the accuracy and reliability of measuring instruments, experimental set up and quality of specimens were observed to ensure that reasonable and accurate results were obtained.
- ❖ Finite Element Analysis – static structural analysis was performed on specimen models to predict the stress distribution and the effect of residual stresses on the actual specimens.

1.6 DELIMITATION OF THE RESEARCH

- Limited only to selected techniques of measuring residual stresses.
- Effects of residual stresses on fatigue lifetimes are not covered.

1.7 SIGNIFICANCE OF THE RESEARCH

The ever-increasing need to optimise designs and reduce manufacturing costs has led to investigations of residual stresses and their effects on service life of components. Some designs and components have failed in service and no concrete scientific evidence has been found as to what contributions residual stresses may have had in those instances. Many industries such as the aerospace, nuclear, automotive and others will benefit as a result of reliable techniques of measuring residual stresses.

1.8 EXPECTED OUTCOMES, RESULTS AND CONTRIBUTIONS OF THE RESEARCH

- Identify perhaps the simple, cheaper and reliable way of determining residual stresses.
- To provide relevant and pertinent information to engineers to reliably measure residual stresses.
- To use knowledge of some principles of the techniques such as Digital Shearography in predicting the behaviour of engineering components and designs.

1.9 CONCLUSION

This chapter has outlined the background and motivation of the research. The Chapters that follow present an in-depth review of literature on the three methods used in this work for determining residual stresses, the experiments performed and the presentation of the experimental and FEA results, discussion and recommendations.

CHAPTER TWO

LITERATURE REVIEW ON THE CHARACTERISATION OF RESIDUAL STRESSES

2.1 HOLE-DRILLING TECHNIQUE

Mathar (Hearn, 1985) initially proposed the hole-drilling technique for measuring residual stress in 1933. In 1985 the technique was regulated by ASTM E837 (Totten et al, 2002). The hole-drilling technique is one of the most commonly used semi-destructive mechanical methods for experimental residual stress analysis. It is regarded as semi-destructive because of the small amount of damage that is produced in the specimen. It involves the drilling of a small hole normal to the surface at the point of interest and measurement of the resulting local surface deformations or strains. The creation of the hole redistributes the stresses in the material surrounding the hole. Thus the hole-drilling technique consists of applying a special strain gage rosette, drilling a hole at the rosette centre, measuring the relaxed strains and computing the residual stress field by means of appropriate stress-strain relationships.

The hole drilling method offers the following advantages:

- Any qualified stress analysis technician can apply it, since no special expertise is required for making the measurements.
- The method is versatile in that it can be performed either in the laboratory or field, on test objects ranging widely in size and shape.
- It is considered a “semi-destructive” technique, since the small hole will not in many cases significantly impair the structural integrity of the part being tested.

The measurement of strains is effected by the use of electrical resistance strain gauges. However at the time of discovery of this technique, measurement of relaxations was done using mechanical extensometers that offered limited accuracy (Hearn, 1985). Although recent workers are using the electrical resistance strain gauges, accuracy is still a major problem. The use of these traditional strain gauge rosettes presents some practical disadvantages. The following are some of the disadvantages of the hole-drilling technique:

- The long gauge length of a resistance strain gauge results in difficulties in measuring steep stress gradients.

- The technique cannot be used in notched regions or small parts where high concentrations of residual stresses are common because of limited space.
- The accurate drilling of the hole at the centre of the rosette is not always easy.
- It is time consuming to mount a rosette and installing a milling guide, hence its limited use in industry.
- It can be destructive especially on small components where after test; the component may be rendered useless.

One of the challenges experienced during the use of the hole drilling method is the inevitable generation of heat during the drilling operation. According to Honner et al (2004), the drilling process is usually accompanied with some amount of heat manifesting itself by a temperature rise. The strain measured by a strain gauge rosette in the vicinity of the hole is sensitive to errors caused by increasing temperature. Strain gauge thermal output (apparent strain) is one of the largest sources of error associated with the measurement of strain when temperature rises. Apparent strain comprises of two components namely, the change of electrical resistivity of the gauge material due to the temperature change, and the electrical resistivity change produced by thermal expansion of the material to which the gauge is bonded. The strain induced by the residual stress relief during the drilling process is thus combined with this apparent strain.

Furthermore, the possible source of error caused by the temperature rise can also be due to thermal stress induced by non-homogenous temperature field. Temperature rise induced by drilling also lowers the material yield strength. It can result in a plastic deformation and changes of the residual stress in the sample near the hole, where the residual stress is measured.

Currently, researchers are focusing on overcoming some of these difficulties in order to obtain more reliable results.

2.1.1 THE PRINCIPLE AND THEORY OF THE HOLE-DRILLING STRAIN GAUGE METHOD

The introduction of a hole into a residually stressed body relaxes the stresses at that location. The removal of stresses on the hole surface changes the stress in the immediately surrounding region, causing the local strains on the surface of the test object to change correspondingly.

In most practical applications of the method, the drilled hole is blind, with a depth which is: (a) about equal to its diameter, and (b) small compared to the thickness of the test object. According to Vishay Micro-Measurements(Tech Note 503-6), the blind hole geometry is so

complex that no closed-form solution is available from the theory of elasticity for direct calculation of the residual stresses from the measured strains except by the introduction of empirical coefficients. It is however simpler to carry out such an analysis of a through hole on a thin plate in which residual stress is uniformly distributed through the plate thickness. Therefore the theoretical basis for the hole drilling method will first be developed for a through hole geometry.

Through Hole Analysis

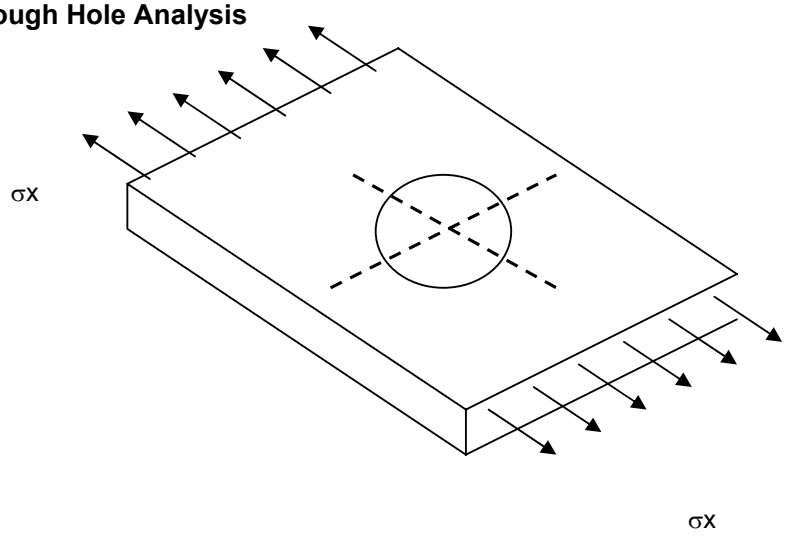

Figure 2.1. Stress states at P(R,α) before the introduction of a hole (Vishay Micro-Measurement – Tech Note 503-6).

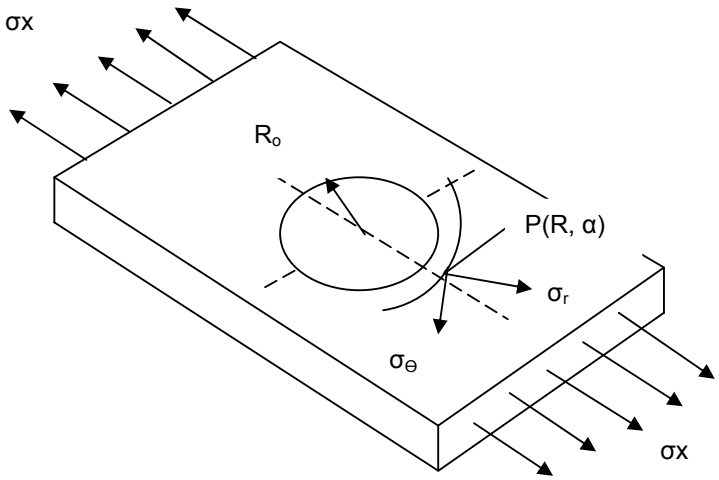

Figure 2.2. Stress states at P(R,α) after the introduction of a hole (Vishay Micro-Measurement – Tech Note 503-6).

Subtraction of initial stresses from the final stresses after drilling gives the change in stress, or relaxation at point P(R, α). The mechanics of stress relief is complex. Thus the relieved strains vary in a complex way with distance from the hole surface. The relieved strains generally decrease as distance from the hole increases. For this reason it is desirable to measure the strains close to the edge of the hole in order to maximise the strain gauge output signal.

2.1.1.2 STRESS EVALUATION METHODS

The evaluation procedures of the hole-drilling method are based on linear-elastic equations. When variable through-thickness residual stresses are expected, the hole is executed in many steps and the relaxed strain is recorded at each step. Residual stress through-thickness distribution can be deduced by a proper elaboration of the relaxed strain profiles versus the hole depth.

The incremental hole drilling method is based on the following assumptions (Totten et al, 2002):

1) The directions of principal stresses are generally unknown;
2) The dimensions of the hole are small compared with the rest of the part;
3) The residual stress distribution is such that the stresses are uniform in each layer removed;
4) The material is homogenous, isotropic, elastic and linear;
5) The small strain hypothesis is used for the numerical computation;
6) The normal stress is negligible;
7) The shearing is nil between the successive layers removed;
8) The rosette geometry is perfect in comparison with the other dimensions.

2.1.1.2.1 Incremental strain method

It involves the measurement of the strain relaxation after successive increments of the drilled hole depth. The stresses existing within each depth increment are calculated by assuming that the strain relaxation is wholly due to stresses that existed within the depth increment. Thus values of the calibration constants need to be used. However, this is not the case because after the first increment is drilled, subsequent strain relation combine the effect of the stresses within the new increment and effect change in the hole geometry.

2.1.1.2.2 Average stress method

This method was introduced to overcome the shortcomings of the incremental strain method using the equivalent uniform stress. It assumes that the equivalent uniform stress equals the

average stress over the whole depth, whereas stress closer to the surface contributes more to the surface strain relations.

Schaej (Totten et al, 2002) concluded that the incremental strain and average stress methods give unsatisfactory results with regard to non-uniform stresses due to calibrations using uniform stress. However, for smoothly varying stress fields, with many depth increments the power series method gives the best results while the integral method is best suited in cases where the residual stresses vary abruptly. These two methods (the integral method and power series method) are based on the numerical simulation of a unit residual stress relaxation (computed for three typical hole radii **r**, and several partial hole depths) thus obtaining influence coefficients relating relaxed strain and residual stress.

2.1.1.2.3 Power Series Method

This is an approximate method, but theoretically acceptable method of calculating non-uniform stress fields from incremental data. It is only suitable for smoothly varying stress fields.

2.1.1.2.4 Integral Method

The integral method is the most viable and practical for computing non-uniform residual stresses from strain relaxation data measured using the incremental hole drilling method.

2.1.1.2.5 Schwartz-Kockelmann Method

Due to the residual stresses in the vicinity of the hole not being completely released when using the hole drilling method, the determination of the residual stresses cannot be calculated from measured relaxed strains using the Hooke's law formula as in the case with general stress analysis. For this reason a calibration constant, using experimental and computational methods needs to be added to take into account the partially relieved strains. With experimental calibration, the residual stresses are simulated by the external loading stresses normally in a uniaxial tensile or bending test.

2.1.1.3 Blind Hole Analysis

The through hole analysis is based on a small hole being drilled completely through a thin, wide, flat plate subjected to uniform plane stress. However, the reality is that most ordinary machine parts and structural members requiring residual stress analysis may be of any size, shape, and rarely thin or flat. The introduction of a blind hole into a field of plane stress produces a complex local stress state. The findings of Rendler and Vigness (Weng & Lo, 1992) though reveal that the relieved strains due to drilling the blind hole still vary sinusoidally along a circle concentric with the hole making the equations for relieved strains

for thin sections still valid if appropriate blind hole drilling coefficients are used. The coefficients can only be obtained by experimental calibration or numerical procedures such as finite element analysis as opposed to calculations for the through-hole drilling case.

Beaney (Hearn, 1985) gives a formula that may be used to evaluate the principal residual stresses σ_1 and σ_2 :

$$\left.\begin{matrix}\sigma_1 \\ \sigma_2\end{matrix}\right\} = -\frac{1}{K_1}\cdot\frac{E}{2}\left\{\frac{(\varepsilon_1+\varepsilon_3)}{1-\nu\left(K_2/K_1\right)} \pm \frac{1}{1+\nu\left(\frac{K_2}{K_1}\right)}\sqrt{(\varepsilon_3-\varepsilon_1)^2+\left[(\varepsilon_1+\varepsilon_3)^2-2\varepsilon_2\right]^2}\right\} \qquad (2.1)$$

Where K_1 and K_2 are sensitivity coefficients obtained by calibration. It should be noted that correction factors may be introduced to account for the variation of stress with depth, effects of surface preparation when mounting gauges and for plastic yielding at the hole edge.

According to Withers & Bhadeshia (2001), the general formula applicable to a rosette of strain gauges in determining residual stress is given below.

$$\sigma = (\sigma_{\max}+\sigma_{\min})A + (\sigma_{\max}-\sigma_{\min})B\cos\alpha \qquad (2.2)$$

Where A and B are hole drilling constants; α is the angle from the x-axis to the direction of maximum principal stress, σ_{max}. The values of σ_{max} and σ_{min} are calculated from strains recorded by the gauges.

2.1.1.4 Surface Preparation for Strain Gage Bonding

All open surfaces not thoroughly and freshly cleaned must be considered contaminated and therefore must be cleaned immediately prior to gauge bonding. Furthermore, it is imperative that all materials used in the surface preparation be fresh, clean and uncontaminated. The purpose of surface preparation is to develop a chemically clean surface compatible with the gauge installation requirements, resulting in strong stable bonds. Such surface preparation includes five basic operations discussed below, in the usual order of execution (Vishay Micro-Measurement – Tech Note 515).

1. *Solvent Degreasing*

Degreasing is done to remove oils, greases, organic contaminants, and soluble chemical residues. It can be accomplished using a hot vapour degreaser, aerosol type spray cans of CSM-2 Degreaser or wiping with GC-6 Isopropyl Alcohol. In cases of dissolved contaminants

on small test pieces, the entire test piece should be degreased. In the case of bulky objects which cannot be completely degreased, an area covering 100 to 150 mm on all sides of the gauge should be cleaned.

2. *Surface Abrading*

This is done to remove any loosely bonded adherents such as scale, rust, paint, galvanised coatings and oxides, and to develop a surface texture suitable for bonding. The abrading operation can be performed in a variety of ways, depending on the initial condition of the surface and the desired finish for gauge installation. The optimum surface finish acceptable for general stress analysis applications is a roughness of the order of 2.5 μm which is a relatively smooth surface.

3. *Gauge-Location Layout Lines*

Reference lines for accurately locating and orienting the gauges are marked on the test surface where strain measurement is to take place. The lines should be made with a tool that burnishes, rather than scores or scribes, the surface to avoid stress concentration risers. The gauge is then installed so that the marks defining the longitudinal and traverse axes of the grid are aligned with the reference lines on the test piece surface. All residues from the burnishing operation should be removed by scrubbing using Conditioner A (a mild acid).

4. *Surface Conditioning*

After the layout lines are marked, Conditioner A should be applied repeatedly, and the surface scrubbed with cotton-tipped applicators until a clean tip is no longer discoloured by scrubbing. Drying of the cleaned surface is accomplished by wiping using a sponge with a single slow stroke. The sponge should never be wiped back and forth, since this may redeposit the contaminants on the cleaned surface.

5. Neutralising

This final step is done to bring the surface back to normal conditions by applying a neutraliser (a base chemical). The cleaned surface should be kept completely wet with a neutraliser throughout this operation. Drying is done in the same way as described under surface conditioning. The gauges should be installed immediately after the neutralisation process.

More on surface preparation for strain gage bonding is covered under the section for the measurement of strains using the Hole Drilling Technique.

2.2 ULTRASONIC METHODS

Ultrasonic testing methods are powerful tools used in the fields of Science and Technology. Application of these methods is found in areas such as medicine and engineering. In the context of this work, ultrasonic testing methods are used to examine and study the stresses locked inside materials as a result of manufacturing and forming processes. Ultrasonic techniques are regularly used for flaw detection in mechanical components and systems, and more recently for stress evaluation. The determination of both surface residual stresses and bulk stresses in all three principal stress directions is very complex. These two types of stresses are interrelated in such a way that a slight change in one type affects the other. The knowledge of all these stresses is essential to avoid premature failure of components.

Ultrasonic methods provide a measure of the macro residual stresses over a large volume of material. The stress measurement utilises the change in velocity of ultrasonic sound waves as they pass through a solid material. The speed of ultrasonic waves in a material is directly affected by the magnitude and direction of stresses present.

Ultrasonic stress measurement techniques are based on the acousto-elasticity effect, to which the velocity of elastic wave propagation in solids is dependent on the mechanical stress (Kudryavtsev et al, undated). Put differently, ultrasonic techniques rely on the variations in the time of flight difference of ultrasonic waves which can be related to the residual stress state through third order elastic constants of the material. The ultrasonic velocity in stressed materials can be determined by estimating the phase change of the propagating wave.

2.2.1 THE ACOUSTOELASTIC THEORY

The study of the acoustoelastic effect in materials requires a derivation of stress and strain relationships of the initial state and final state of a body through the use of material and spatial coordinates respectively. The formulation of mathematical expressions for wave velocity dependence on static deformation and after dynamic disturbances (acoustic waves) is quite tedious. For purposes of this study, the complete tensorial description of the acoustoelastic effect in isotropic materials is not covered.

2.2.2 ULTRASONIC WAVES

Ultrasonic waves are mechanical vibrations with different wavelengths propagated through a medium. Ultrasonic waves can exist in all known media including gases, liquids, and solids. According to Baldev Raj et al (2004), ultrasonic waves are classified in four different categories based on the mode of vibration of the particle in the medium with respect to the direction of the propagation of the initial waves.

- Longitudinal or compressional waves – each particle of the medium vibrates about its mean position in a direction parallel to the direction of wave propagation.
- Transverse or shear waves – vibration of particles are perpendicular to the direction of propagation of wave motion.
- Surface or Rayleigh waves – the motion of particles is elliptical and contains both transverse and longitudinal. These waves can only travel on the surface layer of solids.
- Plate or Lamb waves – material vibrates as a plate since the wave encompasses the entire thickness of the material.

2.2.2.1 Fundamental properties of waves:

- Wave speed
- Reflection
- Attenuation
- Refraction

All these properties depend on the medium properties and conditions through which they pass.

2.2.2.2 Characteristic Properties of Ultrasonic Waves

Velocity

The velocity of propagation of ultrasonic waves depends on the nature of the materials. However, in a given material, it is independent of frequency of the wave and the dimension of the material. The following are the equations for calculating the velocities of the longitudinal, shear and surface waves (Baldev Raj et al (2004).

$$V_L = \left[\frac{E(1-\nu)}{\rho(1+\nu)(1-2\nu)} \right]^{\frac{1}{2}} \qquad (2.3)$$

Where V_L = longitudinal wave velocity (m/s)

E = Young's Modulus of Elasticity (N/m^2)

v = Poisson's ratio of the material

ρ = density of the material (kg/m^3)

$$V_T = \left[\frac{E}{2\rho(1+\nu)}\right]^{\frac{1}{2}} \quad \text{or} \quad V_T = \left[\frac{G}{\rho}\right]^{\frac{1}{2}} \tag{2.4}$$

Where V_T = transverse wave velocity (m/s)

G = Modulus of rigidity (N/m^2)

$$V_S = 0.9V_T \tag{2.5}$$

Where V_S = surface wave velocity (m/s)

Appendix B gives the longitudinal and shear wave velocity of some of the selected materials.

Specific acoustic impedance

It is the resistance offered by a material to the propagation of ultrasonic waves. It depends only on the physical properties of the material and is independent of wave characteristics and frequency. The acoustic impedance in a material is given by the following equation (Baldev Raj et al, 2004):

$$Z = \rho V \tag{2.6}$$

Where V = ultrasonic velocity (m/s)

Z = acoustic impedance (Pa s/m)

Acoustic intensity and pressure

Acoustic intensity is the energy flowing per second per unit area normal to the direction of the propagation of the ultrasonic waves. The intensity of the ultrasonic waves in a material depends on the acoustic pressure and impedance. Acoustic pressure, P is the amplitude of alternating stresses on the material through which ultrasound propagates. It is given by:

$$P = Za \tag{2.7}$$

Where **a** is the amplitude of particle vibrations.

$$I = \frac{P^2}{2Z} \tag{2.8}$$

Where I = acoustic intensity (W/m^2)

P = acoustic pressure (Pa)

2.2.3 EFFECTS OF STRESSES ON THE PROPAGATION OF ULTRASONIC WAVES

- Variation of wave velocity propagation, i.e. the velocity is dependent on the density of the medium (waveguide). Wave velocity is the speed at which energy moves in a medium. The denser the medium is, the faster the waves will travel as particles are closer to each other, thus energy can be transferred among them at a greater rate. The universal wave equation:

$$v = \lambda f = \frac{\lambda}{T} \qquad (2.9)$$

  Where v = wave velocity (m/s), λ = wave length (m), f = frequency (Hz or s^{-1}), T = period (s).

- Variation of the amplitude of ultrasonic waves

In general, the change in the ultrasonic wave velocity in structural materials under mechanical stress amounts to tenths of a percentage point, hence the equipment for practical application of ultrasonic technique for residual stress measurement should be of high resolution, reliable and fully computerised (Kudryavtsev et al, undated). Baldev Raj et al (2004) mention that the change in ultrasonic velocity due to stress is usually less than 1%.

The main effect of stresses on the propagation of ultrasonic waves in a material is the variation of wave velocity of propagation. Another effect, to a lesser extent, is the variation of the ultrasonic waves.

When waves oscillate along the axis of wave propagation, they are called longitudinal waves and when oscillation occurs perpendicularly to the direction of wave propagation they are called traverse waves e.g. electro-magnetic waves.

Factors that may have an effect on the results obtained from measurement are material texture and thickness, and temperature.

Advantages of ultrasonic techniques

- They are by nature non-destructive.
- It enables the measurement of residual stresses at the same location repeatedly, studying, for instance, the changes of residual stresses under the action of service loading or effectives of stress-relieving techniques (Kudryavtsev et al, undated).

- Measurements of residual stresses are obtained either in surface layers or averaged through the thickness.

Disadvantages of ultrasonic techniques

- Ultrasonic instrumentation is usually very costly
- Some ultrasonic instruments are not portable.
- Higher-order elastic constants which must be experimentally determined to relate the ultrasonic velocity measurements to stresses require careful interpretation of micro-structural texture of a particular material under test.

2.2.4 ULTRASONIC STRESS MEASUREMENT TECHNIQUES

Different techniques of measuring residual stresses have now been developed. The choice of a particular technique over the other depends on a number of factors inter-alia, the position and type of specimen under review, reliability of results expected and availability of measuring instrumentation.

In their study of subsurface stress evaluation in steel plates and bars, Bray and Tang (Bray, 2001), employed the critically refracted longitudinal wave technique. The waves are emitted from a piezoelectric transducer into a sample. They propagate in a specific area of the sample and are detected by one or two receivers. The mean stress is measured in the area where the waves propagate. Figure 2.3 below shows the description of this measuring technique.

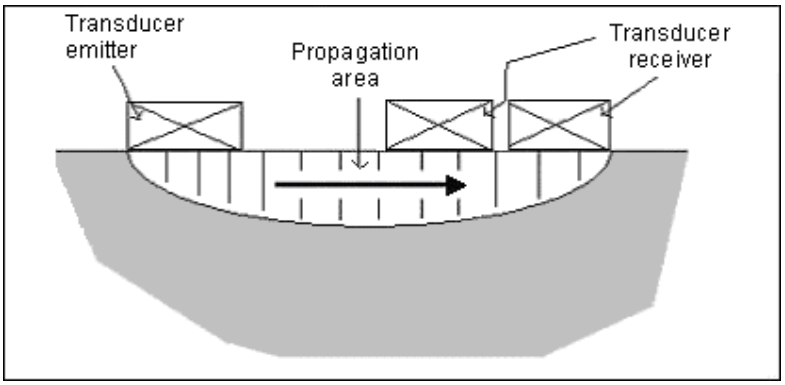

Figure 2.3. Sketch of the propagation of the wave from the emitter to the receivers (Ya et al, 2004).

Bray (2000, 2001) found out that the most significant variation in travel time with the strain was for longitudinal waves, followed by the shear waves when the particles vibrate in the

direction of the load. The greatest sensitivity is obtained when the wave propagates in the same direction as the stress. The stress can be calculated according to:

$$\frac{V_{11} - V_L^0}{V_L^0} = \beta_1 \sigma_p + \beta_2 (\sigma_{22} + \sigma_{33}) \qquad (2.10)$$

$$\frac{V_{12} - V_T^0}{V_T^0} = \beta_3 \sigma_{11} + \beta_4 \sigma_{22} + \beta_5 \sigma_{33} \qquad (2.11)$$

Where V_T^0 and V_L^0 are the isotropic longitudinal and transverse velocities in an unstressed medium, V_{ij} is the velocity of a wave travelling in the direction *i* polarized in direction *j,* in the presence of stresses σ_{11}, σ_{22} and σ_{33} , and $\beta_{1,\ldots}$ β_5 are acousto-elastic constants (Ya et al, 2004).

The diagrams below show a bar in tension with wave propagation in three perpendicular directions. The first index in the velocities represents the propagation direction whilst the second one represents the movement of the particles.

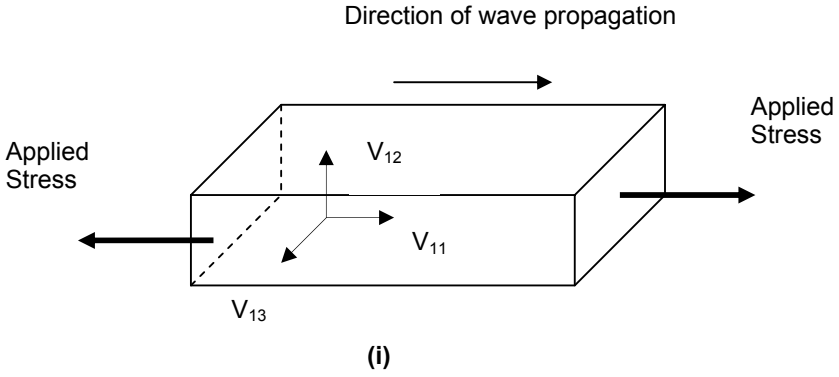

(i)

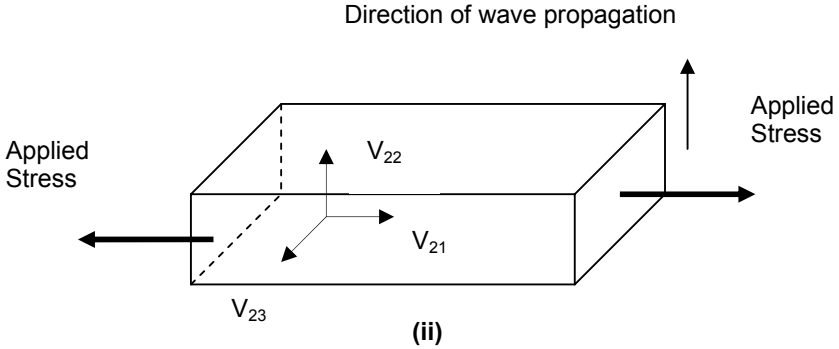

(ii)

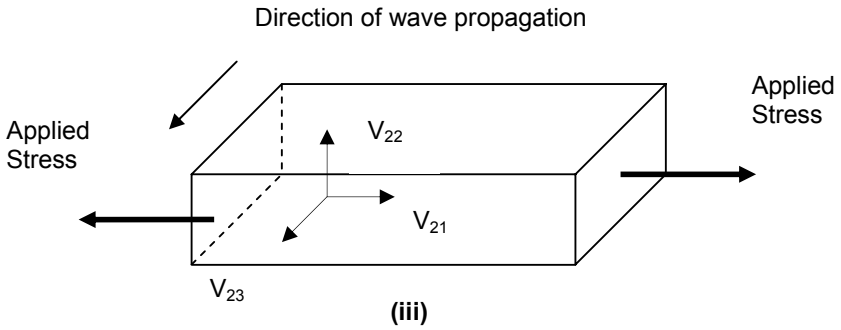

Figure 2.4. Velocity of plane waves and stress field in orthogonal directions.

Generally, the relative change of wave velocity is proportional to stress (Duquennoy et al, 2001). The stress induced velocity change is described by the equation (Baldev Raj et al (2004) :

$$V_{str} = V_o + \beta\sigma; \qquad (2.12)$$

Where V_{str} is the ultrasonic velocity in the presence of stress, V_o is the stress free velocity, σ is the stress and β is acousto-elastic constant. The acousto-elastic constant is material dependent. Dobmann et al (1997) mention that knowledge of these constants is prerequisite for quantitative stress analysis using the ultrasonic techniques.

2.2.5 Preparatory work

The use of the stress induced velocity change equation requires that a prior determination of the acousto-elastic constant be done by testing a standard specimen having the same composition as that of the component for which residual stress have to be determined. The tests are usually done in a Universal Testing Machine (UTM) and specimens are fabricated as per ASTM standards.

Procedure for determining residual stresses using the ultrasonic methods is as follows (Baldev Raj et al, 2004):

(a) Determination of acousto-elastic constant of the material or component using standard tensile specimen with applied loads.
(b) Ultrasonic velocity measurements in the material or component of interest.
(c) Determination of residual stresses using the acousto-elastic constant.

2.3 DIGITAL SHEAROGRAPHY

Shearography is an optical method that measures the rate at which an object deforms under applied stress and it produces fast, high resolution, full-field and reliable measurement of gradients of surface displacements. It allows the measurement of in-plane and out-of plane displacement derivatives of object surfaces (Hathway et al, 1997, Groves et al, 2004). Hung, (1999) mentions that shearography overshadowed holography because the later is limited by vibrations and environmental disturbances.

Advantages of Shearography

- Surface preparation is likely not required.
- Full-field measurement, and defect identification.
- Low sensitivity to vibrations.
- Simple optical set-up

Disadvantages of Shearography

Although it indicates the presence of a flaw and the appropriate size, it does not indicate the position of the defect depth wise, relative to the surface under inspection.

Three versions of shearography employing different recording media exist, namely; photographic emulsion, thermoplastic and video (Hung, 1999). For purposes of this study, the video version known as digital shearography will be used.

According to Hung (2000:355), digital shearography extracts deformation-related phases, Δ, directly from measured intensities using computer programs as opposed to film-based shearography which relies on visible fringes for quantitative interpretation of test data.

Shearography although invented as a strain measuring technique is vastly gaining recognition as a technique used to undertake full field examination and quick qualitative analysis of defects in components. Findeis & Gryzagoridis (2004) used this technique to identify delaminations in composite structures.

2.3.1 DESCRIPTION OF DIGITAL SHEAROGRAPHY TECHNIQUE

Digital shearography employs a computerised process using a digital camera to acquire images which are recorded on an image digitiser. Appropriate software is used to process the images. The essence of this technique is to examine the image of two states; before and after deformation. (Hung, 1999) mentions some of the stressing techniques that can be

employed to cause deformation, such as temperature change, pressure change and vibrations (acoustic or ultrasonic). Figure 2.5 shows a typical digital shearography set-up.

The part being tested is illuminated by an expanding beam from a monochromatic light source i.e. a laser. A video camera is used to view the object through a shearing device, for example, a modified Michelson interferometer. One of the mirrors of the modified Michelson is tilted to obtain the out-of-plane surface gradients along the shear direction while the other one which is fixed reflects light back into the beam-splitter. The light waves, the normal one and the other one coming from the titled mirror are focussed on the camera image plane through the camera lens. The recombined light waves interfere with each other producing a speckle pattern. The intensity of the interferogram registered by the CCD camera is saved in the computer through an image digitiser (frame grabber board).

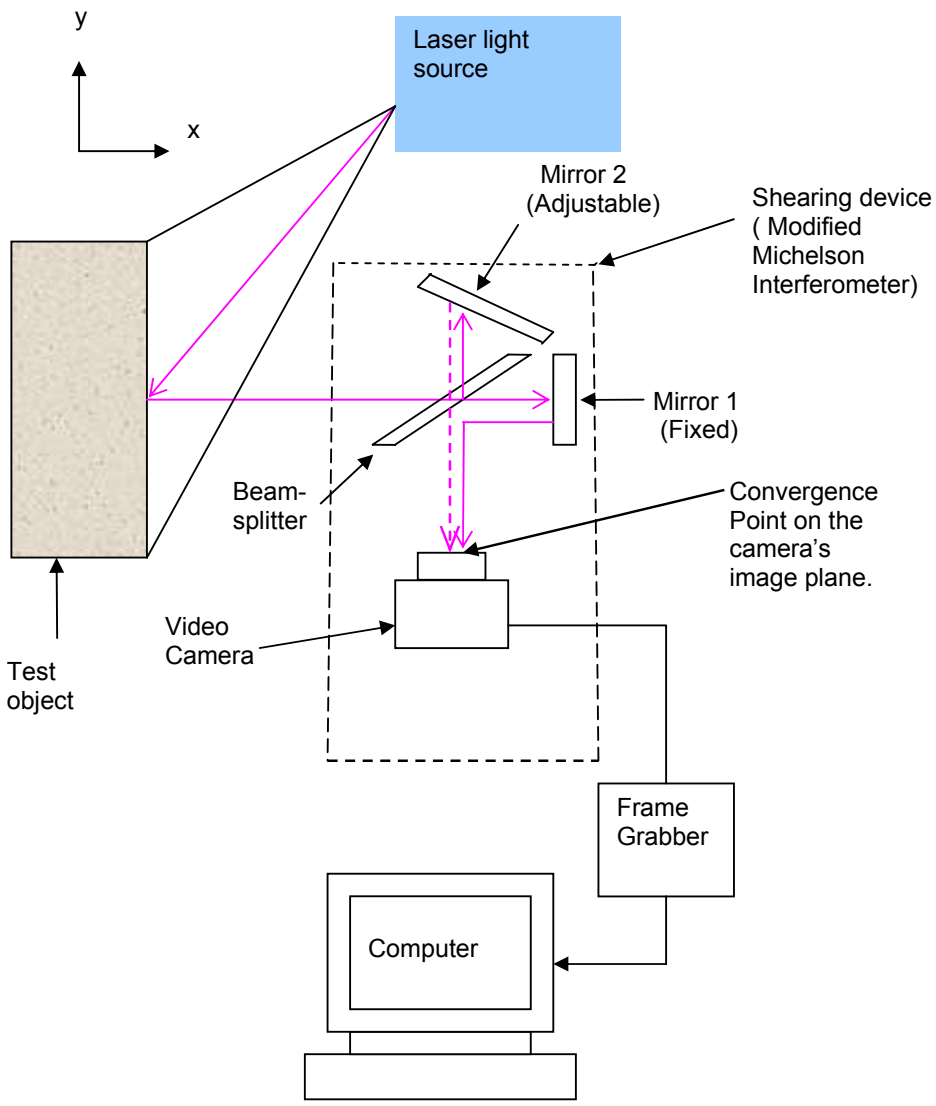

Figure 2.5. Typical Shearography set up

Hung, (2000) expresses the intensity of distribution before deformation as:

$$I_p = 2A^2\left[1 + \cos(\phi_1 - \phi_2)\right] \qquad (2.13)$$

Where A is the real amplitude of light wavefront; ϕ, is the phase related to the optical path length measured from the laser to the camera, hence, $\phi_1 - \phi_2$ is the phase difference of two neighbouring points, 1 and 2 and can be represented by an angle α. Equation 2.13 can be rewritten as:

$$I_p = 2A^2\left[1 + \cos\alpha\right] \qquad (2.14)$$

If the object is stressed, the deformation on the surface changes the original positions of points 1 and 2 to 1′ and 2′ respectively. This causes a change in the respective optical path lengths with a corresponding phase-change, Δ of the light arriving at the common point **p.**

Assuming that the amplitude, A of the light wavefront remains the same, then;

$$I_{p'} = 2A^2\left[1 + \cos(\alpha + \Delta)\right] \tag{2.15}$$

The resulting intensity distribution, I_r is obtained from the difference between $I_{p'}$ and I_p given by the following expression;

$$I_r = \left|-4A^2\left[\sin\left(\alpha + \frac{\Delta}{2}\right)\right]\sin\frac{\Delta}{2}\right| \tag{2.16}$$

Gryzagoridis & Findeis (2005:3) give a different form of the equation for this resulting intensity distribution as follows:

$$I_r = I_i - I_f = 4\sqrt{I_1 I_2}\,\sin\left[\left(\theta_1 - \theta_2\right) + 0.5\Delta\varphi\right]\sin 0.5\Delta\varphi \tag{2.17}$$

Where I_i and I_f are intensities of the object's image before and after stressing, and Δφ is the phase change that occurs due to the speckle pattern being changed.

According to Gryzagoridis & Findeis (2005:3), the gradient of out-of-plane surface displacement is approximated by the following expressions:

$$\Delta\delta p = \frac{\partial\delta p}{\partial x} S \tag{2.18}$$

Where $\Delta\partial p$ is the out-of-plane surface displacement; S is the distance between the two points on the object and can also be regarded as magnitude of shear since shearing takes place in the direction in which the two points on the surface of the object are oriented.

The phase change for arriving at this common point, **p** is also given by;

$$\Delta\varphi = \frac{4\pi\Delta\delta p}{\lambda} \tag{2.19}$$

Where $\Delta\varphi$ is the phase change, λ is the wave-length of the laser light. The phase change can also be written in terms of number of fringe patterns, N, i.e.

$$\Delta\varphi = 2N\pi \qquad \text{N = 0,1,2,3} \tag{2.20}$$

Equations 2.18, 2.19 and 2.20 can be combined to get:

$$\frac{\partial \delta p}{\partial x} = \frac{N\lambda}{2S} \tag{2.21}$$

Equation 2.21 shows that the spacing between adjacent fringes is a function of the displacement gradient. The final image produced has black and white zebra-like fringes superimposed on the object's image. Findeis et al (2005) mention that, the black and white fringes do not provide information pertaining to the direction of surface displacement and quantity of the rate of displacement unless a technique known as phase stepping is done during image capturing. The following section discusses the phase stepping technique.

2.3.2 PHASE STEPPING

The evolution of phase stepping technique is as a result of on going research to increase the sensitivity of shearographic unit and obtain quantitative information regarding the formation of the interference fringes. It is different from conventional shearography in that a calibrated piezo-electrically driven mirror moves in predetermined phase-steps enabling the CCD camera to register intensities of micro-displacements. According to Andhee et al, (2005), phase-stepping allows three, four or more interferograms to be calibrated at phase shifts and compared to the reference image whilst conventional shearography captures only one interferogram. The phase-steps are in increments of π/2 for four measurements or interferograms. This changes the wavelengths between images for both stressed and unstressed states. Findeis et al (2005) present the equations for the intensities of any stepped image as:

$$I_i(x,y) = I_B(x,y) + I_{MP}(x,y)\cos(\phi(x,y) + i.\alpha) \quad \text{i = 1,2,3,..N} \tag{2.22}$$

Where:

I_i (x , y) measured intensity of the interferogram at any given co-ordinate;

I_B (x , y) is the intensity of the background noise during image capturing;

I_{MP} (x , y) is the modulation intensity;

ϕ (x , y) is the phrase difference between the object and the reference beam.

α the relative phase step i.e. π/2 for four stepped images.

Hence the phase difference, ϕ(x , y) is described as a function of the four intensities by the following the following equation:

$$\phi(x,y) = \arctan\left(\frac{I_3(x,y) - I_1(x,y)}{I_4(x,y) - I_2(x,y)}\right) \quad (2.23)$$

Equation 2.23 enables the phase distribution of the speckle interference pattern to be determined as:

$$\beta(x,y) = \phi_a(x,y) - \phi_b(x,y) \quad (2.24)$$

$\phi_a(x,y)$ = phase distribution after stressing

$\phi_b(x,y)$ = phase distribution before stressing

Equation 2.24 can be used to calculate the phase change of the laser light due to surface displacement. Since β repeats itself at 2π intervals, the final profile of the fringes of the image is of a saw tooth profile; hence the slope of the profile determines the direction of object displacement (Findeis et al (2005). The calculation of the phase difference is facilitated by image processing software. Filtering the original phase fringe patterns reduces the noise intensity and improves the quality of the fringes. On the final image, black represents the smallest phase difference and white the largest (Andhee et al, (2005).

Phase stepping shearography thus produces intensity fringe patterns that provide quantitative information about the direction of surface displacement gradients relative to the observer.

2.3.3 CONCLUSION

This chapter has presented background information regarding residual stress characterisation by the three non-destructive testing techniques chosen for the purpose. The next Chapter deals with the experimental set-up and procedures of the Hole Drilling Technique using the Four Point Bending Fixture and RS-200 Milling Guide.

CHAPTER THREE

USING THE HOLE DRILLING METHOD ON A SPECIMEN SUBJECTED TO FOUR POINT BENDING

3.1 INTRODUCTION

This section deals with the experimental details of the Hole-Drilling Method where the four point bending test was used to induce “residual” stresses in the specimen. The preparation or manufacturing and heat treatment of specimens, experimental procedures and methodology, and description of all the apparatus used is covered. The results are also presented.

Briefly the specimen was subjected to a four point loading hence one of the surfaces would be in compression while the opposite surface would be in tension. Thus the hole drilling could be validated against a known stress.

3.2 MANUFACTURE OF SPECIMEN

The specimen was machined on a milling machine. To ensure flatness and also to provide a clean surface for strain gage bonding, the specimen was ground on the surface grinder. The final dimensions of the specimen were 221 mm long, 60 mm wide and 4.5 mm thick

Since it is well known that machining processes induce residual stresses on any work piece, in order to relieve these stresses, the specimens must be annealed.

3.3 ANNEALING PROCEDURE

The specimen was placed in an oven for two hours with the temperature set at 650°C. The temperature was then lowered to 250°C at intervals of 100°C, each hour. The high temperatures involved are meant to accelerate the unloading of stresses. The specimen was left in the furnace to cool. Slow cooling allows the material’s microstructure to attain equilibrium state. The final state of the specimen was a more ductile, and possibly had a lower yield and tensile strength; however this was not a factor affecting the experiment.

3.3.1 Precautions during Annealing

To avoid or minimise warpage of the specimen during the heat treatment process, the specimen was suspended in the middle of the oven. Suspension of the specimen discourages direct contact with the refractory bricks and promotes uniform heat distribution over the specimen. Usually if the specimen is not suspended, bending is caused by

differences in the cooling rate of the bottom part in contact with the refractory bricks and the top part of the specimen.

3.4 MATERIAL AND EQUIPMENT

The test for determining “residual” or the stresses induced by the four point loading was done by the hole drilling strain gauge method that complies with the American Standards Test Methods (ASTM). According to these standards (ASTM – E 837 01), the specifications for the specimen are as follows:

1. A specimen whose thickness is at least 1.2D is considered to be ‘thick’ and therefore eight sets of strain readings should be obtained as the hole depth is increased in increments of 0.05D. D represents the diameter of the gauge circle i.e. the pitch circle of all the gauges.
2. A specimen whose thickness is less than 0.4D is considered to be ‘thin’ and only one set of strain readings is required for a through hole. The intermediate case when the specimen thickness is between 0.4D and 1.2D is not within the scope of the Standard Test Method.

The gage diameter for the strain gages is 10.26 mm, and multiplying this gage diameter by 0.4 constant will give a thickness of 4.1 mm. The specimen must therefore be less than 4.1 mm to be considered thin. Since the thickness of the plate is 4.5 mm, the analysis will be treated as an intermediate case that requires interpolation of calibration constants.

In order to facilitate easy interpolation of constants and thicknesses, a graph in figure 3.1 overleaf was drawn from the standard constants data to project the outside limits for a gauge circle diameter of 10.26 mm.

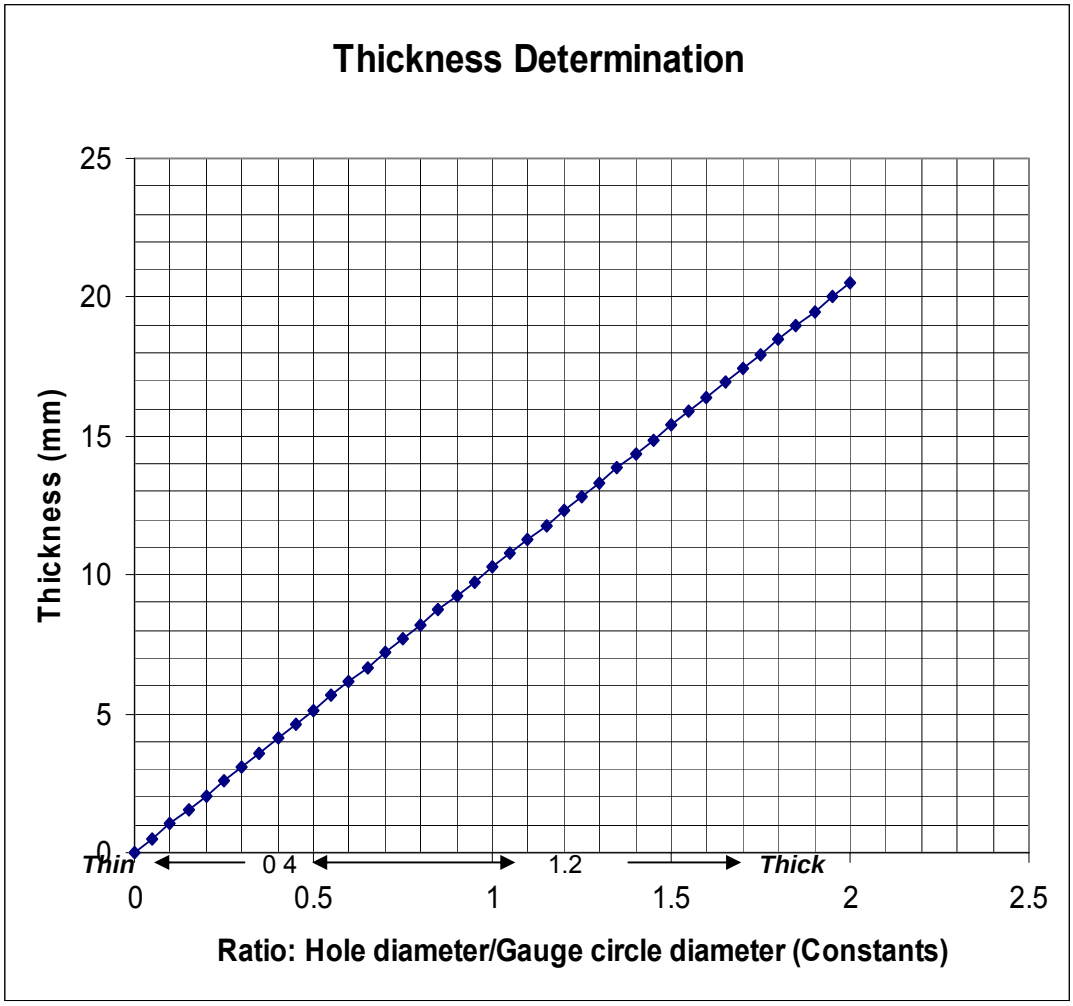

Figure 3.1. Thickness versus hole diameter/gauge circle diameter ratio

3.4.1 Specimen Surface Preparation for Strain Gage Bonding

Before the gauges were bonded to the surface of the test specimen, the surface was cleaned of oxide or scaling. The surface was cleaned with M5 solvent to remove grease and other related lubricants. The next step was to clean the surface with a mild acid (metal conditioner) followed by wiping clean with a clean tissue. The final step was to wash the surface with a mild base neutralising agent and wiping clean the surface with a single stroke of clean tissue.

The strain gages were bonded using epoxy adhesive with the correct orientation of the gages. After curing, the lead wires were carefully soldered on the gage grids. The lead wires were then connected to the Strain Indicators.

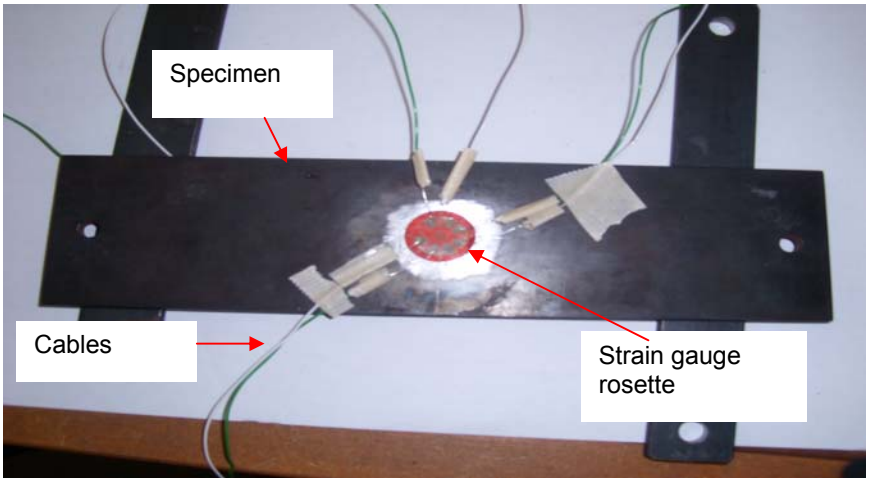

Figure 3.2. Specimen with bonded strain gauges and soldered electrical wires

3.4.2 Strain Gage Rosettes

Different types of rosettes are available for various requirements for measuring residual stresses. Rosette type A strain gages were used in this work. This type is used for general purpose and is available in several different sizes. The orientation of the strain gage grids is 45° - rectangular i.e. three grids, with the second and third grids angularly displaced from the first grid by 45° and 90°, respectively (see figure 3.3). They are applicable where the directions of the principal strains are unknown and are most popular because of data-reduction relationships which are simpler. The grid numbers 1 and 3 are assigned to two mutually perpendicular grids and the axis of grid 2 must be 45° away in the same rotational, typical arrangement of the gage grids. Although grid 2's actual position is 2a, its effect is felt at position 2b. The gages were bonded on the top surface of the specimen. The strains relieved when the hole was drilled were converted to stresses using the equation below ("Strain Gages and Instruments", Tech Note TN – 515, Vishay Micro-Measurements).

$$\sigma_{P,Q} = \frac{E}{2}\left[\frac{\varepsilon_1 + \varepsilon_2}{1-\nu} \pm \frac{\sqrt{2}}{1+\nu}\sqrt{(\varepsilon_1 - \varepsilon_2)^2 + (\varepsilon_2 - \varepsilon_3)^2}\right] \qquad (3.1)$$

The subscripts P and Q denote the maximum and minimum stress values respectively while E and ν represent Young's Modulus and Poisson's ratio respectively.

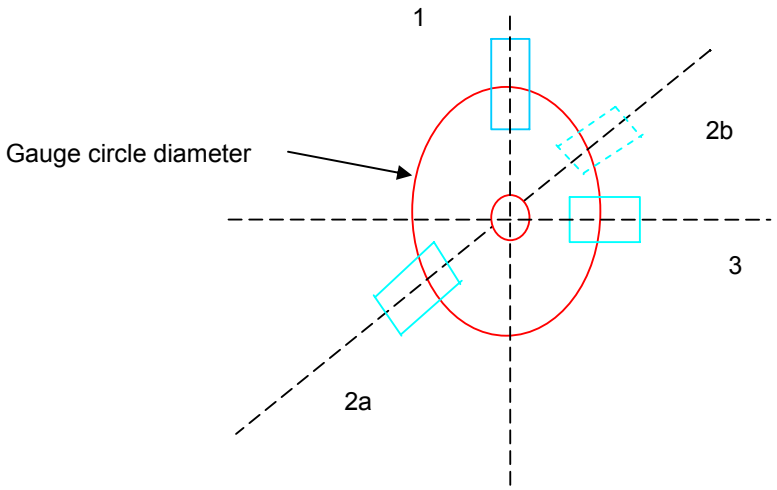

Figure 3.3. Strain Gauge Rosette Grid Orientation

3.4.3 Conventional Strain Gages

Strain gages work on the principle that when they are bonded to an elastic material which is loaded and stretched, the strain due to the load is determined by measuring the change in their resistances. Ordinary strain gages were bonded on the bottom surface of the specimen and ensured the induced tensile strains when the specimen was subjected to different four point bending loads. Figure 3.4 shows the ordinary strain gages used in this experiment, bonded to the bottom surface of the specimen.

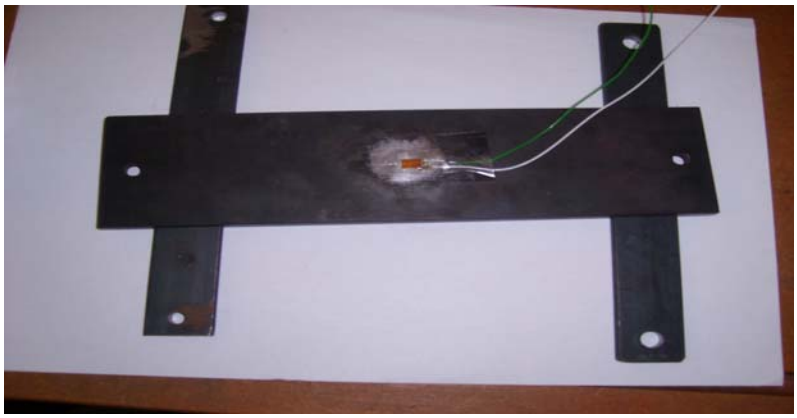

Figure 3.4. Bonded Strain Gauges for measuring tensile strains due to bending

3.4.4 Instrumentation

The Vishay Strain Indicators P 3500 and 3800 wide range models were used to record the strains. These strain indicators have a resolution of ± 2 μm/m. To account for temperature changes during the bending of the specimen, a three-wire temperature compensating circuit was used. The SB-10 Switch-and-Balance Unit was used to facilitate easy connection.

3.5 FOUR POINT BENDING TEST

The purpose of this test is to induce bending stresses on the specimen, where the top and the bottom surfaces experienced compression and tension respectively.

In this test, the simple bending theory assumptions were that the beam is perfectly homogeneous and isotropic, the material's elastic limit is nowhere exceeded and the Young's modulus for the material is the same in tension and in compression. The beam is simply supported on two roller supports and is considered to be in pure bending with constant bending moment in the section between the load application points hence the shear force is zero.

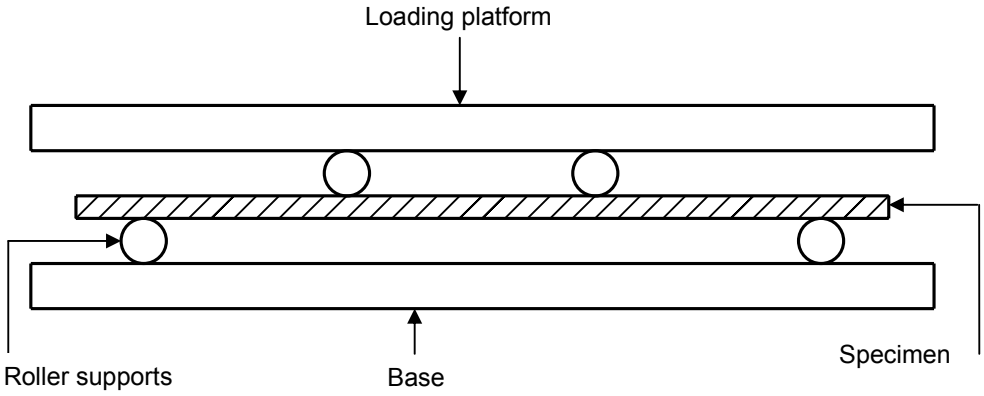

Figure 3.5. Beam loading set-up

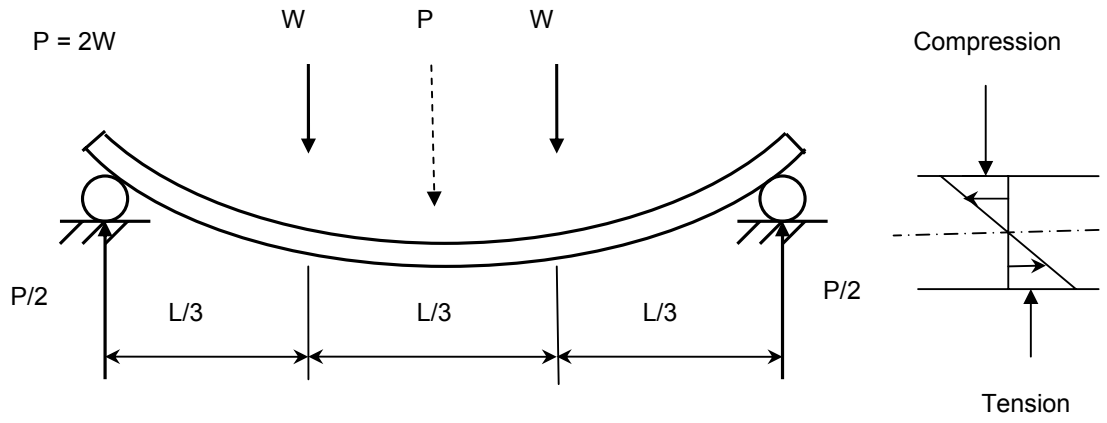

Figure 3.6. Specimen subjected to load

The strain gauges were bonded to the beam and connected to the 3800 wide range strain indicator by electrical cables. Before loading, the strain indicator was zeroed. The stresses from bending are computed from the following simple bending equation;

$$\frac{\sigma}{y} = \frac{M}{I} \tag{3.2}$$

Where I is the second moment of area given by;

$$I = \frac{bd^3}{12} \tag{3.3}$$

y is the distance to the uttermost fibres, i.e. d/2; σ and M are the bending stress and bending moment respectively.

$$\sigma = \frac{My}{I} = \frac{M\frac{d}{2}}{\frac{bd^3}{12}} = 6M/\left(b \times d^2\right) \tag{3.4}$$

Since the loading is symmetrical, the beam is sectioned in the middle as shown in the figure 3.7 below. Taking moments about the sectioned plane, a maximum bending moment is obtained as shown in equation 3.4.

$$M_{\max} = \frac{P}{2} \times \frac{L}{2} = \frac{PL}{4} \tag{3.5}$$

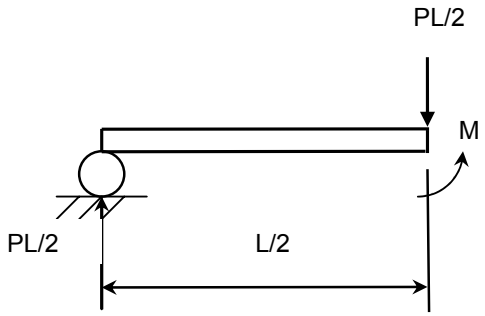

Figure 3.7. Beam sectioned in the middle with uniformly distributed load consideration

However, for thicker sections it is more suitable to treat the load as uniformly distributed. Thus the maximum bending moment, is given by:

$$M_{\max} = \frac{PL}{2}x - \frac{P}{2}x^2 = \frac{PL^2}{8} \quad \text{for x=L/2} \qquad (3.6)$$

Where P is the weight per metre.

3.6 DERIVATION OF THE APPLIED FORCE USING MACAULAY'S METHOD

In figure 3.8 below, the X-X is the cutting plane where the bending moment is determined at a distance x metres from the left hand end. Assuming P to be the applied concentrated load, the reaction A is therefore P/2. The Macaulay's bending moment equation is formulated as shown below.

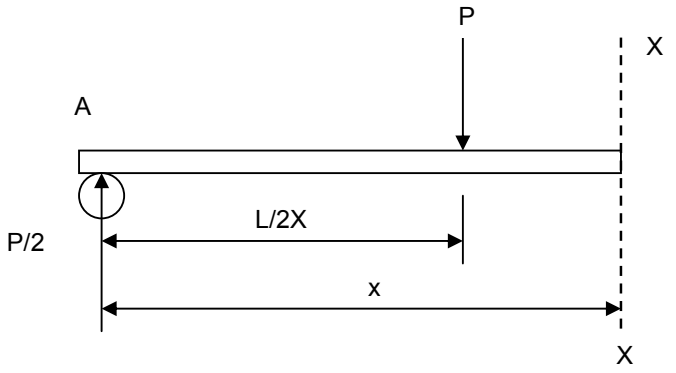

Figure 3.8. Free body diagram of beam

$$BM_{xx} = EI\frac{d^2y}{dx^2} = R_A[x] - P\left[x - \frac{L}{2}\right]$$ (bending moment equation)

$$EI\frac{dy}{dx} = \frac{R_A}{2}[x]^2 - \frac{P}{2}\left[x - \frac{L}{2}\right]^2 + A$$ (slope equation)

$$EIy = \frac{R_A}{6}[x]^3 - \frac{P}{6}\left[x - \frac{L}{2}\right]^3 + Ax + B$$ (deflection equation)

Applying boundary conditions:

When x = 0; y = 0 $\Rightarrow B = 0$

Also when x = L; y = 0

Substituting in the deflection equation yields;

$$0 = \frac{R_A}{6}[L]^3 - \frac{P}{6}\left[L - \frac{L}{2}\right]^3 + A[L] + 0$$

In terms of P, R_A and L, the constant A is found as follows:

$$A = \frac{PL^2}{48} - \frac{R_A L^2}{6}$$

Since R_A = P/2; the above equation can be reduced to:

$$A = -0.0625PL^2$$

For maximum deflection, x = L/2

$$y_{\max} = \frac{1}{EI}\left\{\left[\frac{PL^3}{96} - 0.03125PL^3\right]\right\} = \frac{-0.02083\dot{3}PL^3}{EI}$$ (3.7)

$$P = -\frac{EIy_{\max}}{0.02083\dot{3}L^3}$$ (3.8)

Where E is taken as 200 GPa and I = 4.55625 x 10^{-10} m^4 for the specimen geometry. The negative sign signifies a downward force. The derived formula, besides being used to determine the force applied to cause bending, can also be used to determine the deflection due to the applied force. The specimen must still remain in the elastic region after the application of the force and also ensuring that the problem will not in any way be treated as a large displacement problem requiring a non-linear solution in finite element analysis.

3.6.1 Procedure for conducting a Four Point Bending Test

The ordinary strain gauges are positioned in the middle of the work piece or specimen at the bottom whilst the rosette strain gauges are placed on the top also in the middle. The loading configuration induces compressive stresses on the top of the specimen and tensile stresses on the bottom. It can be noted that the drilling operation can exert a force which may cause further bending of the specimen. However, care was taken to ensure that the minimum force was exerted during drilling. The effect of the drilling force is shown by the change in the strain indicator reading. The drilling operation for residual stress measurement was facilitated by the RS-200 Milling Guide. Its description and how it was used to measure residual stresses follows.

3.7 DESCRIPTION OF THE RS-200 MILLING GUIDE

It is a precision fixture for accurate positioning and drilling of a hole through the centre of a special strain gage rosette. It is supported by three levelling screws with swivel mounting pads to facilitate attachment of uneven surfaces. The milling guide was aligned relative to the strain gage rosette using a special-purpose microscope into the guide's centering journal. This was achieved by adjusting the four X-Y screws, after which the journal was locked in position by the locking ring to restrict its movement after final adjustment. An illuminator which is attached to the base of the milling guide facilitated the optical alignment procedure. Figure 3.9 below shows the air turbine assembly mounted on the milling guide. High speed drilling was facilitated by filtered air that was supplied from the compressor via the pneumatic foot valve and tubing to the air turbine motor on which the end mill was mounted. The air supply was set at 276 kPa. The high pressure facilitates high speed drilling. Furthermore, the high speed drilling of about 300 000 – 450 000 revolutions per minute which minimises plastic deformation and heating.

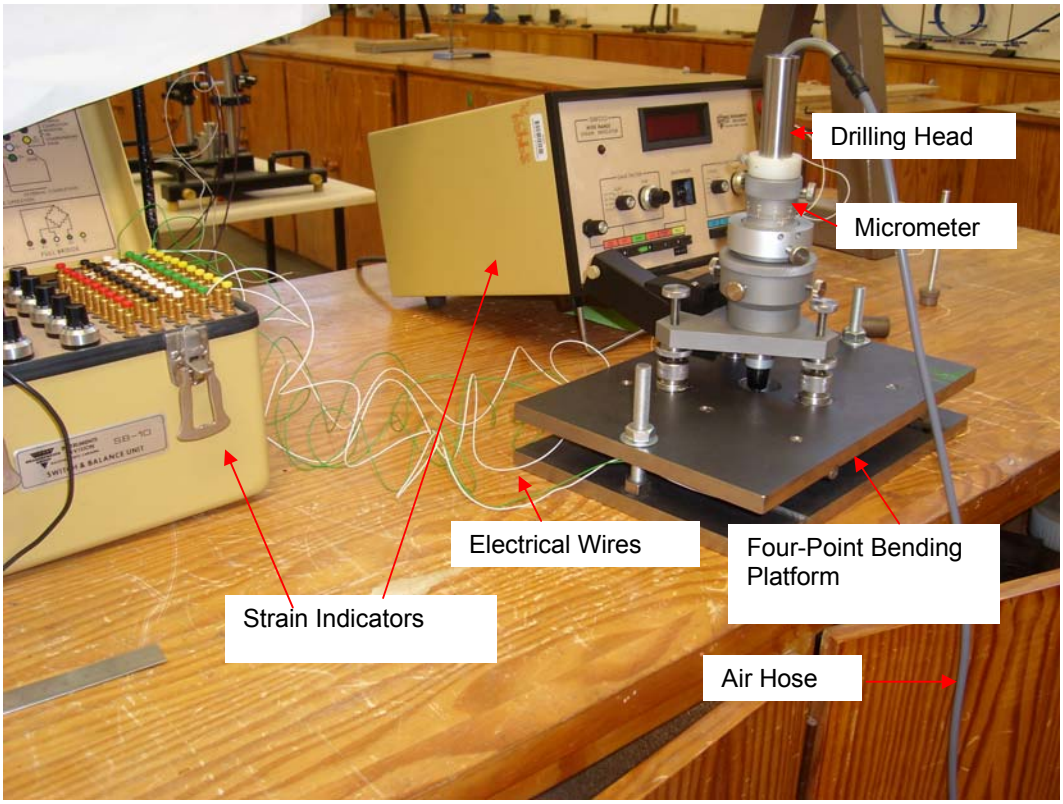

Figure 3.9. Hole-drilling equipment set-up using compressed air

3.7.1 Procedure for the Measurement of Residual Stress Using the RS-200 Milling Guide

1. A special three-element micro-measurements strain gauge rosette is bonded to the test part at points where residual stresses are to be determined.
2. Each rosette grid element is connected to a strain measuring instrument and “zero” readings are recorded.
3. The R-S 200 Milling Guide is positioned over the centre of the gauge and securely attached to the test part.
4. The R-S 200 is optically aligned so that its drilling axis is precisely positioned over the target at the centre of the strain gage rosette.
5. A hole is drilled through the centre of the rosette and into the test part.
6. Strain gage instrumentation is used to obtain strain readings.
7. Residual stresses are then computed, either manually or by using the Vishay Measurements Group’s RESTRESS software program. However in this work, the residual stresses were computed manually.

In cases where a larger diameter cutter is used and cannot be fitted into a turbine collet, the milling rod assembly together with the electric drill is used to introduce a hole on the specimen. The cutter selection used must correspond with the type of strain gauge rosette. The procedure of using the milling rod is mentioned below and figure 3.10 shows the set-up.

3.7.2 Procedure for Using the Milling Rod Assembly

1. Insert one end of double-ended milling cutter into the milling rod and lock it in place using a hexagonal wrench or Allen key.
2. The rod is gently rotated by hand until the end mill cuts through the protective coating and rosette backing and exposes the surface of the test part.
3. Slide the proper depth-setting gauge (1/16 in for 1/16-in diameter mill, and 1/8 in

   1/8-in diameter mill) between the stop collar of the boring rod and the locking rings of the triangular base. The micrometer depth-set is used for incremental drilling.

4. Zero the strain-measuring instrument of each grid rosette before milling.
5. Attach a variable-speed electric drill or manually operated hand drill to the universal joint at the top end of the boring rod. Moderate pressure is applied and the milling process slowly done until the stop collar on the milling rod reaches the end of travel.

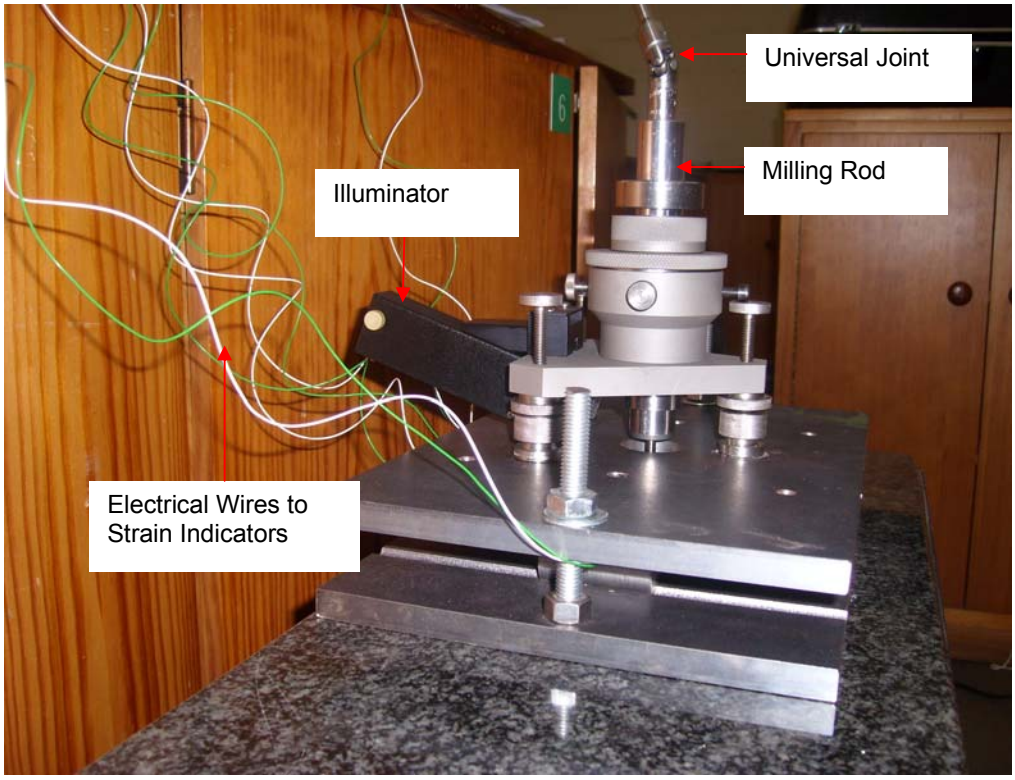

Figure 3.10. Hole-drilling equipment set-up using milling rod assembly and electric drill

The following sections present the results obtained from the experiments conducted. The results will be discussed and analysed.

3.8 PRESENTATION AND DISCUSSION OF RESULTS

The results obtained from the strain gages are recorded and presented in Appendix A. The procedure of computing the stresses from the strains is also outlined. The results are subsequently discussed in this section.

From the simple bending theory, the bending stress was calculated as:

$$\sigma_b = \frac{M_{\max} y}{I} \qquad (3.2)$$

The second moment of area, I, calculated from the section geometry was 4.55625 x 10^{-10} m^4 and y = half thickness = 0.00225 m;

The bending stress can also be given by: $\sigma_b = E\varepsilon$

The measured surface strain was 30 με and the Young's Modulus of Elasticity was 200 GPa.

From the two equations, a constant maximum bending moment can be obtained as follows:

Therefore, $M_{\max} = \frac{EI\varepsilon}{y} = \frac{200\times10^9 \times 4.55625\times10^{-10} \times 30^{-6}}{2.25\times10^{-3}} = 1.215Nm$

Since the bending moment is constant, the bending stresses at different depths can be found. In this case it was computed for the same depths as hole drilling for purposes of comparison.

When the clamping was done, the tensile strain increased to 80 με and went down to approximately 30 με upon settling. This translates into a surface stress of 6 MPa. The hole drilling technique was used to check if the same value of stress could be obtained. Five incremental drilling steps of 0.1 mm interval of a blind hole were made and the computed stresses were plotted on stress versus depth graph. Refer figure 3.11.

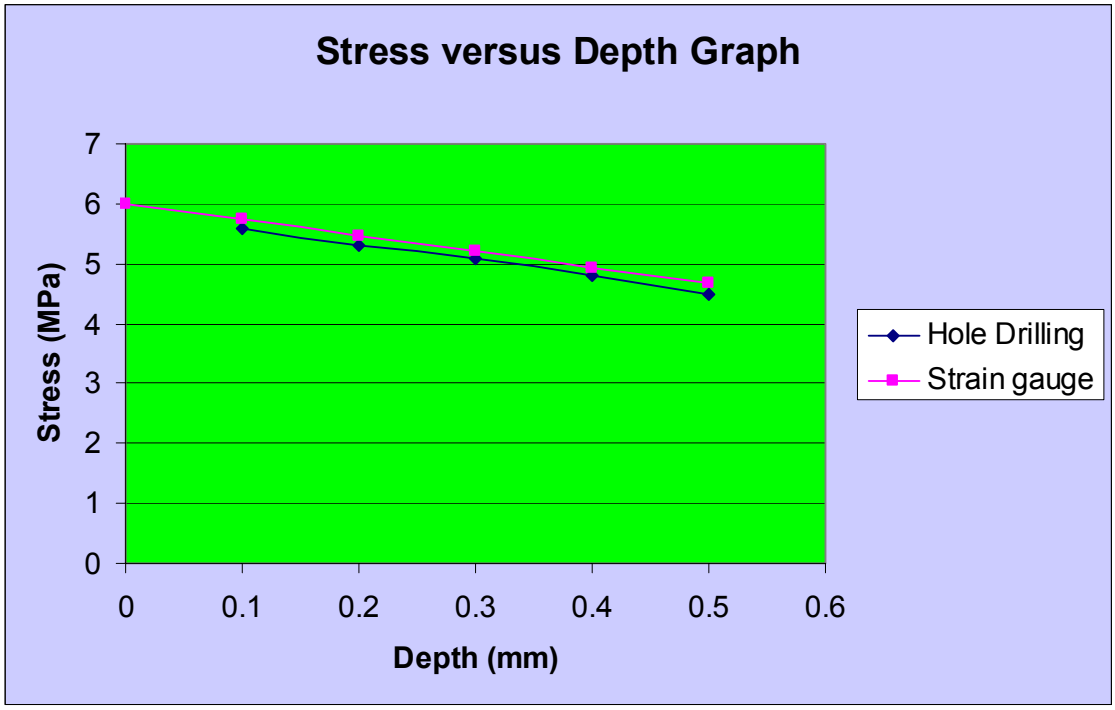

Figure 3.11. Graphical projection of surface stress by Uniform Stress Method

The strain gauge method recorded a maximum surface stress of 6 MPa. The subsurface values were obtained by assuming a linear distribution of stress, beginning with the value indicated by the strain gauge and approaching zero at the neutral axis. The hole drilling method recorded a stress value of 5.6 MPa at a depth of 0.1 mm. The drilling was done up to 0.5 mm and the data were plotted. The computed values of stress continued to decrease with depth as shown in figure 3.11. Since it is difficult to directly obtain the value of the surface stress, the best way was to plot a graph of stress versus depth and project it to get y-intercept. This y-intercept of 5.87 MPa represents the surface stress.

It is noted that the hole drilling method did not produce a perfect straight line because of the interpolated drilling coefficients used to compute the stress values. The strain gauge method produced a straight line because the obtained values of stress were based on a constant moment. A maximum force was obtained from this constant moment that was used in the FEA to show the magnitude and stress distribution on the specimen model.

3.9 VALIDATION OF RESULTS USING ANSYS

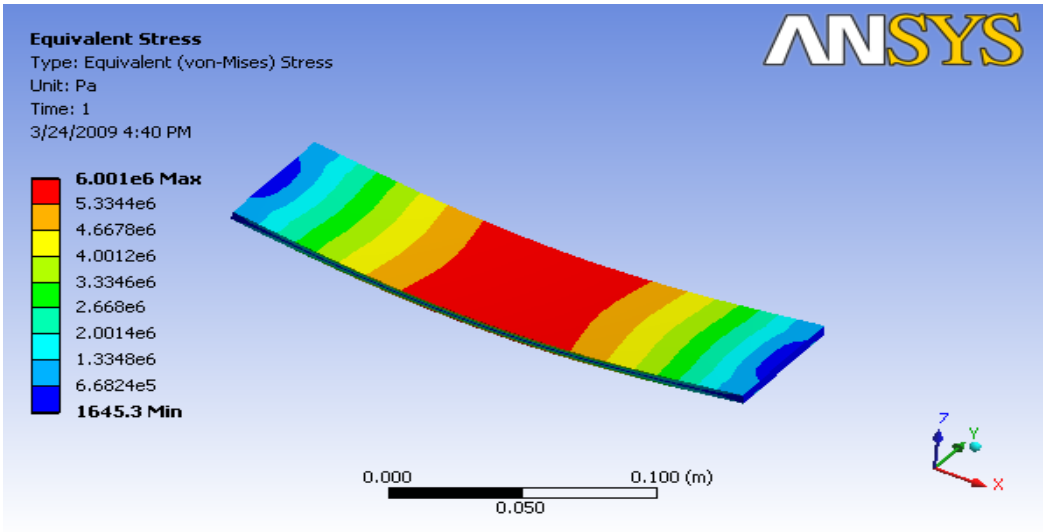

Figure 3.12. Stress distribution in the specimen

A simple static structural analysis was done in ANSYS to show the distribution of stresses in the specimen due to applied force. The results show that the maximum surface stress of 6 MPa was recorded at the centre of the specimen since the specimen was symmetrically loaded. The inputted boundary conditions, allowed the specimen to move in two directions at the supports while the other direction was fixed. The degrees of freedom of the specimen model took the Poisson's ratio effect into consideration.

3.10. CONCLUSION

The surface stress induced due to bending and determined using the strain gauge is in good agreement with the value of the surface stress extrapolated by the hole drilling method. A 2% difference is noted between the two values, i.e. 6 MPa versus 5.87 MPa respectively. Thus the experiment shows that the hole drilling method is an accurate method of determining stresses in materials.

CHAPTER FOUR

EXPERIMENTAL WORK

4.1 INTRODUCTION

This section deals with the experimental details of the three methods, namely, the Debro-30 Ultrasonic stress meter, the Hole Drilling method and Digital Shearography that were employed on the specimens to determine residual stresses. The manufacturing and treatment of the specimens, experimental procedure, methodology and discussion of results is covered.

4.2 MANUFACTURE OF THE SPECIMENS

The specimens made out of mild steel were machined to size on a milling machine. To ensure flatness and also to provide a clean surface for the Debro-30 probe head, the specimens were ground on the surface grinder. The final dimensions of the specimens were 250 mm long, 40 mm wide and 15.5 mm thick.

The material composition of the specimens is as shown in table 4.1. The percentage of carbon is higher than expected and this may be due to contamination of samples. More tests could not be carried out to verify this anomaly since the machine was out of order. The chemical composition was determined using the EDX facility of a Scanning Electron Microscopy, HITACHI X 650.

Table 4.1: Chemical composition of mild steel alloy.

Element	C	Si	P	S	Mn	Fe
Analysis (wt. %)	2.63	0.51	0.15	0.29	0.79	95.62

Machining processes induce residual stresses on the work piece. In order to relieve these stresses, the specimens were annealed. Annealing relieves internal stresses, refining the grain structure and cold working properties. The process is achieved by heating the specimen substantially for a while and allowing it to cool.

4.3 ANNEALING PROCEDURE

The procedure followed to fully stress relieve the specimens after they had been prepared, was heating and cooling at intervals of 100°C. The heating started at room temperature of 25°C to maximum temperature of 625°C while cooling was done from this maximum temperature to the room temperature. Table 4.2 below shows the recorded heating and cooling including holding times.

Table 4.2: Annealing heating and cooling cycles

Heating Cycle

Temperature (°C)	**Time**
25 – 125 (heating)	8 minutes
125 (holding time)	1 hour
125 – 225 (heating)	8 minutes
225 (holding time)	1 hour
225 – 325 (heating)	11 minutes
325 (holding time)	1 hour
325 – 425 (heating)	12 minutes
425 (holding time)	1 hour
425 – 525 (heating)	12 minutes
525 (holding time)	1 hour
525 – 625 (heating)	13 minutes
625 (holding time)	1 hour

Cooling Cycle

Temperature (°C)	**Time**
625 – 525 (cooling)	32 minutes
525 (holding time)	1 hour
525 – 425 (cooling)	52 minutes
425 (holding time)	1 hour
425 – 325 (cooling)	81 minutes
325 (holding time)	1 hour
325 – 225 (cooling)	124 minutes
225 (holding time)	1 hour
225 – 125 (cooling)	274 minutes
125 (holding time)	1 hour
125 – 50 (cooling)	420 minutes
Room temperature (cooling)	3 hours

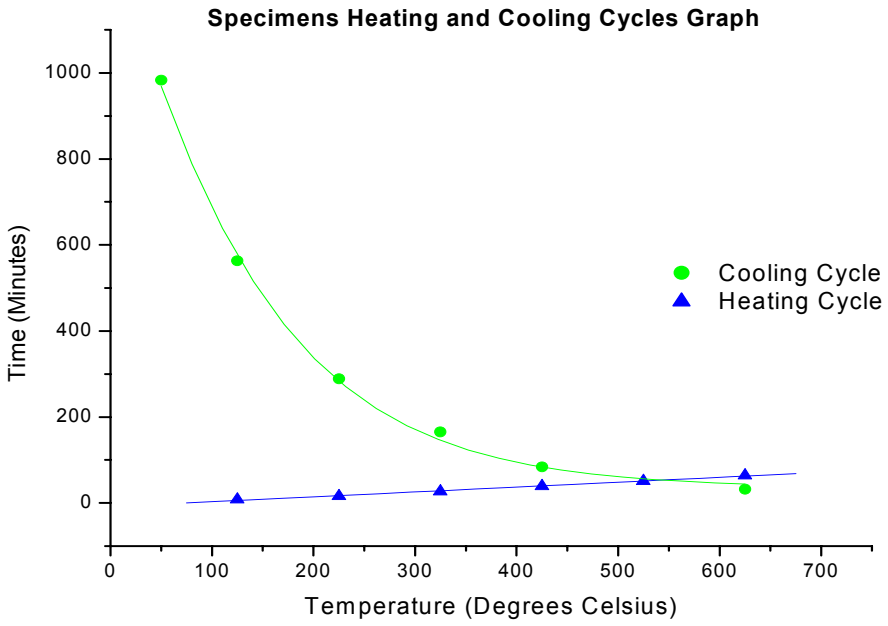

Figure 4.1. Combined Heating and Cooling Cycle Graphs at intervals of 100 °C

When the temperature was increased for intervals of 100 °C from 25 °C to 625 °C, the heating time in minutes increased from 8 to 13. The time increased more or less linearly with increase in temperature. The holding time at a maximum temperature for each interval was 1 hour (60 minutes).

Similarly, cooling was done from 625 °C to 50 °C and eventually to room temperature. The cooling graph is also shown in figure 5.1. The cooling cycle has a steeper gradient compared to the heating cycle. There was an increase in cooling times from 625 °C to 225°C and a much steeper gradient from this temperature to 50 °C when the furnace was switched off, down to room temperature. The annealing process generally produces a ferrite-pearlite microstructure.

4.4 INDUCING STRESSES ON THE SPECIMEN SURFACE BY SHOT PEENING

Emerging techniques such as laser shock peening and low plasticity burnishing are increasingly receiving attention to introduce beneficial compressive residual stresses on components. However, the most common technique known as shot peening was simulated to introduce stresses on stress free specimen surfaces. Shot peening involves impacting a surface with round metallic, glass or ceramic particles called shots with a force sufficient to create plastic deformation. The striking velocities can go up to 100 m/s (Schiffner & Droste gen. Helling, 1999). The phenomenon that can be best used to describe the development of

residual stress is; a Hertzian pressure that causes compressive residual stresses with a maximum near the surface and plastic stretching of the surface layers that leads to the residual stresses being recorded at the surface itself. Plastic deformation induces compressive residual stress layer on the surface of the specimen thereby changing some of its mechanical properties, that is, increased fatigue life, fracture strength and corrosion resistance. The transition between tensile and compression residual stress occurs at a certain distance beneath plate surface. The following equation agreed upon by many authors is used to calculate the plastic zone depth created by the impact of the shot (Barrios et al, 2005):

$$\frac{h_p}{R} = 3\left(\frac{2}{3}\right)^{1/4}\left(\frac{\rho V_0}{\bar{p}}\right)^{1/4} \qquad (4.1)$$

Where:

h_p = depth of plastic zone

R = radius of shot

ρ = material density of shot

V_0 = shot's initial velocity

$\bar{p}$ = average pressure

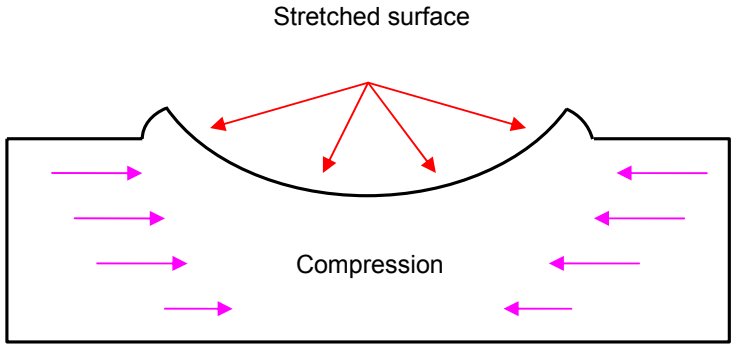

Figure 4.2. An illustration of the Shot Peening Process Phenomenon on a given metal surface

The stresses induced by shot peening are reasonably determined by the Almen strip (see description under 4.4.1). Debro-30 ultrasonic stress metering is done to determine and verify

the magnitude and distribution of the residual stresses in the specimens. Following are some of the parameters that influence the distribution of residual stresses on the surface of the specimen:

- Type of specimen material
- Specimen thickness
- Velocity of shots
- Radius of spheres/balls.

4.4.1 Classification of Almen strips

The stresses created by shot peening operation as mentioned above are measured by an Almen strip named after the inventor John Almen. The Almen strip made out of SAE 1070 spring steel is often used to specify measure and calibrate the peening impact energy. Requirements for tests and checks are specified in the SAE standards.

Almen strips are classified into 3 types (AMS standards):

“A” – predominantly used for shot peening with cast shot or cut wire shot. It is used for arc heights up to 0.61 mm.

“N” – are used usually for glass bead peen and ceramic bead peen. It is used for arc heights of less than 0.1 mm.

“C” – are used more rarely and are thicker than the other types. It is used for greater peening intensity of arc heights greater than 0.61 mm.

The standardized thin Almen plates are peened parallel to the real work-piece. The effect of the induced residual stresses on thin plates is bending them upwards. The resulting arc height is measured using an Almen gauge and the measurement denotes the Almen intensity. Thus the shot peening intensity is defined as the arc height of an Almen test strip at the saturation point. The mandatory standard for defining the saturation point is the arc height of an Almen test strip at the point at which this arc height increases by 10% after a two-fold increase in the shot peening time, measured by using an Almen gauge. Figure 5.3 below shows the general intensity curve for Almen strips.

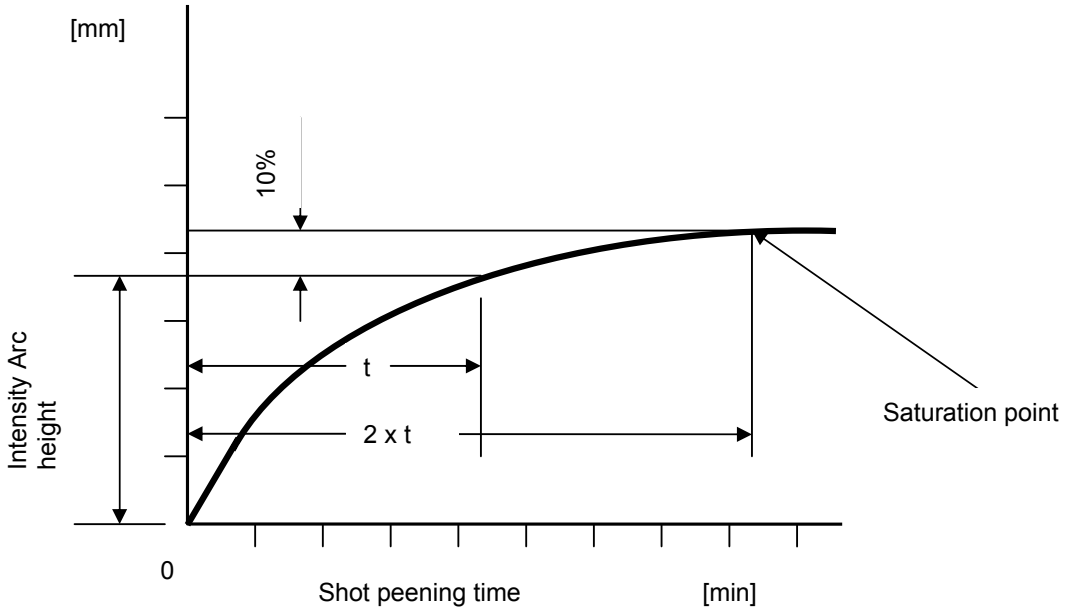

Figure 4.3. Shot Peening Intensity Curve

In order to set up a shot peening machine to the specified intensity, several shot peening intensity curves are initially recorded with different set ups. Five data points are recommended for these curves and the specified intensity at the saturation point is measured by the Almen gauge which eventually determines the correct machine set up.

The intensity of peening depends on such variables as shot velocity, angle of impingement and duration of peening.

It is important to note that there is no simple relationship between the Almen intensity and the residual stress distribution produced in the Almen strip. Arc height is a function of the induced total strain energy, or the area under the residual stress-depth distribution. The depth and magnitude of compression developed by the component being shot peened, generally having mechanical properties very different from the Almen strip, cannot be determined simply from the response of a steel Almen strip identically peened. Therefore, the only reliable method of controlling shot peening of a component is by measuring the subsurface residual stress distribution. Current researchers are using finite element methods to model and predict the residual stress distribution by shot peening. In this work, the “shot peened” specimens are measured for stresses using (a) the Debro-30 ultrasonic stress meter, (b) the hole drilling method and (c) Digital Shearography.

Facts about Shot Peening

- Stress increases almost linearly with low coverage but reaches a maximum at about 80% coverage. At 100% coverage the induced compressive surface residual stress is about 20% lower than at the maximum.
- A uniform state of stress is usually achieved at a particular number of shots.
- The increase of velocity improves the residual stress distribution up to a particular point.
- The peening intensity is directly proportional to the portion of the total energy of the shot stream transferred to the component. The energy is governed by the velocity and weight of the shot pellets and also by the angle of impingement.
- The maximum compressive residual stress produced in the surface layer is typically near the yield strength of the material.
- Shot-peening can cause an almost equal-biaxial compressive residual stress, with a high gradient distribution in the depth (Min et al, 2006).

4.5 MATERIAL AND EQUIPMENT

4.5.1 Debro-30 Ultrasonic stress meter

The instrument was developed by the Polish Academy of Sciences for the purpose of measuring thermal stresses in railway lines and stress increments in steel objects subjected to unidirectional stress state. It uses piezoelectric transducer techniques to measure stresses. The use of piezoelectric transducers necessitates the use of a couplant with suitable acoustic transmission properties. The Debro-30 unit includes a cathode ray oscilloscope as well as interchangeable probe heads that may be used for different applications. The primary probe head, 6L 150, which was used in this work measures stress changes in the test-piece for a stress direction that is parallel to the longitudinal wave propagation direction. The probe head consists of a six (6) transducers that emit and receives subsurface longitudinal waves. The arrangement of the transducers minimises the influence of surface roughness of the object under test on measurement results. The functions of the Ultrasonic stress meter can be summarised as:

- Receiving the ultrasonic pulse from the probe
- Processing and storing data
- Displaying the results on the screen

The difference between the measured times is interpreted as the travel time of the ultrasonic waves along the distance between the receiving transducers. Thus the reference time of

flight for longitudinal waves generated by the transmitters respectively is given by: $T_1 = t_{1-3} - t_{1-2}$; where the t_{1-3} and t_{1-2} are measured times from transducer to receivers 1 and 2 respectively. The reference time of flight will be used to compute the material's acousto-elastic constant.

Ultrasonic wave velocity is influenced by temperature. Any slight increase in temperature significantly causes stress changes; hence temperature corrections must be done in ultrasonic stress measurement. A temperature sensor on the probe head monitors the temperature of the specimen which is automatically taken into account when calculating the stress value.

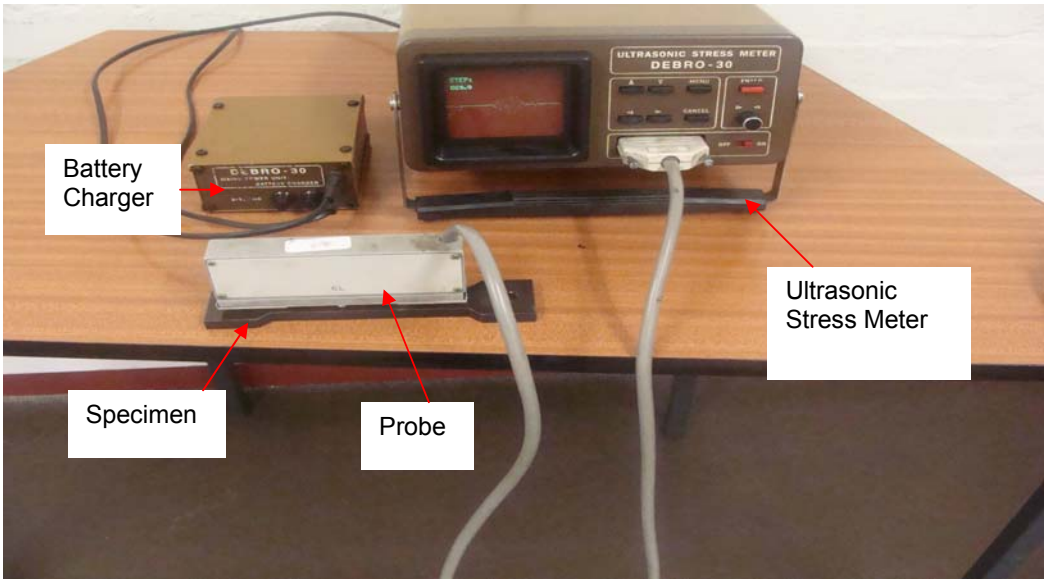

Figure 4.4. Ultrasonic Stress Meter – Debro-30 and Accessories

In order to evaluate and adjust the precision and accuracy of measurement equipment, a calibration procedure was performed as outlined below.

4.5.2 Calibration Procedure

1. Calibrate the Debro-30 residual stress measuring device using stress free specimens (calibration samples) similar to the one to be tested. The probe head, 6L150 which does the measurement is connected to the Debro-30 ultrasonic stress meter by an electric cable. Calibration enables the stress readings to be corrected for variations in material characteristics.
2. Record the time of flight at least thrice to get the average, referred to as the reference time which is then stored in the memory of the device.

3. Apply different tensile loads to the stress free specimen and record corresponding times of flight for the stressed material. The loads that should be applied must create stresses that are below the yield stress of the material in order to obey Hooke's law.
4. Determine the acousto-elastic constant from the recorded times of flight and store it in the stress measuring device. The calculation of the acousto-elastic constants is done using the following equation:

$$\beta_L = \left(\frac{T_L{}^{\sigma_0} - T_L{}^{\sigma_k}}{T_L{}^{\sigma_k} \times \sigma_k} \right) \tag{4.2}$$

Where:

$T_L{}^{\sigma_0}$ - Time of flight of longitudinal wave for zero (0) stress.

$T_L^{\sigma_k}$ - Time of flight of longitudinal wave for stress equal to σ_k

σ_k - Applied stress

β_L - Acousto-elastic constant for a particular material using a particular probe head.

The acousto-elastic constants or coefficients vary for different materials and also with crystallographic orientation. Hence the reference times of flight and the calculated acousto-elastic constants are stored in the Ultrasonic stress meter (Debro-30) before the commencement of the measuring cycle.

The equation for calculating stress change ($\Delta\sigma$) from the travel-times (Δt) is given by Bray & Bray (2007) as:

$$\Delta\sigma = \frac{E(t - t_0)}{\beta t_0} = \frac{E\Delta t}{\beta t_0} \tag{4.3}$$

Where - E – Young's Modulus

t_0 – Travel-time in stress free conditions

The measured travel-time change (Δt) indicates the stress change since the other variables remain constant throughout the measuring cycle.

4.5.3 Measuring Procedure

The specimen to be tested was smeared with oil which was used as a coupling medium. The coupling medium promotes transfer of sound waves into the test specimen by displacing air from the test surface and allowing high frequency sound waves generated from the transmitter of the probe head to be introduced into the test piece with negligible attenuation. The travel time from the transmitter to the receivers is a function of the stress in the test piece. In the initial stages of measurement, the ultrasonic pulse of the longitudinal wave detected by the first receiver is displayed on the oscilloscope. The V-shape marker must cancel out the first maximum amplitude by positioning the arms of the marker on the same level as the amplitude. By pressing the “ENTER” button thrice after this exercise, the results are instantaneously displayed on the screen of the Debro-30 signifying the end of the measuring cycle. The data can either be printed from the data acquisition equipment with the help of RS 232 cable or can be transmitted to the computer equipped with a serial interface RS 232 using PCDEBRO program.

The calibration process began by first measuring the reference times of flight for a zero or non stressed specimen. The mean value of reference times of flight was stored in the Debro-30 before subjecting the same specimen to uniaxial tensile stress. The specimen used for the calibration of the Debro-30 was assumed isotropic and homogenous.

NB. All dimensions are in mm.

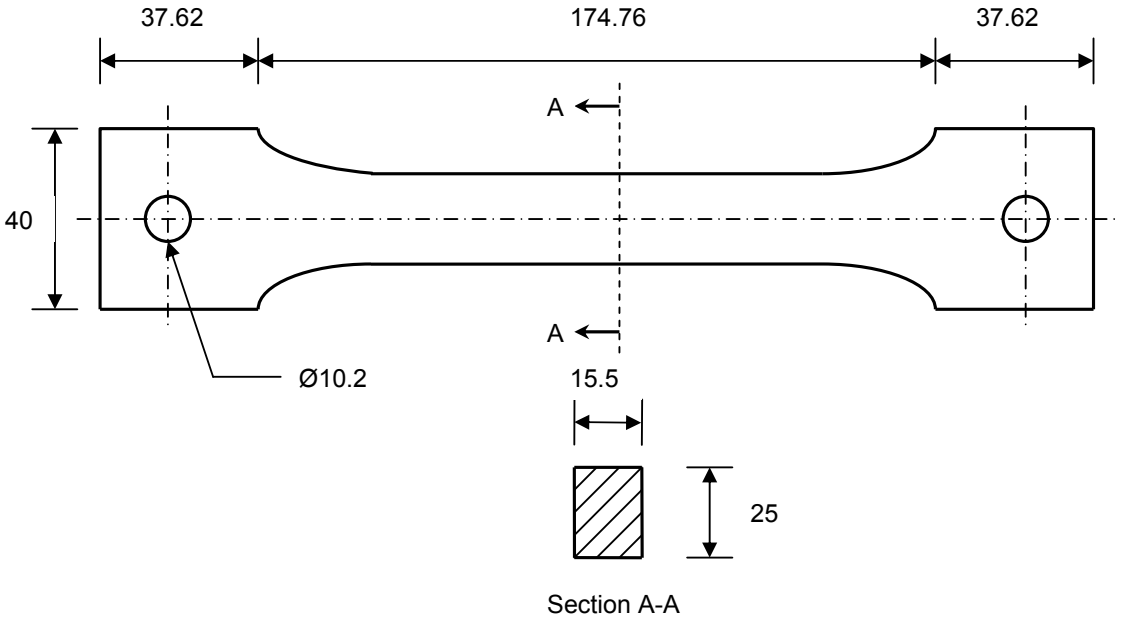

Figure 4.5. Schematic of the Specimen used for the calibration in uniaxial loading

The specimen was gradually loaded and times of flight were recorded at respective loads. This was facilitated by a magnetic 6L150 probe head that was attached to the specimen and connected to the Debro-30 device. The choice for the probe head was influenced by comments from acousto-elastic studies done by many researchers which showed that the bulk longitudinal wave propagating parallel to the applied force exhibited the greatest acousto-elastic effect.

The temperature of the specimen at the time of measurements was noted since the probe head is equipped with a temperature monitoring sensor. The Debro-30 device can properly operate with the probe heads when the temperature of the sample ranges from -5 to +40 °C.

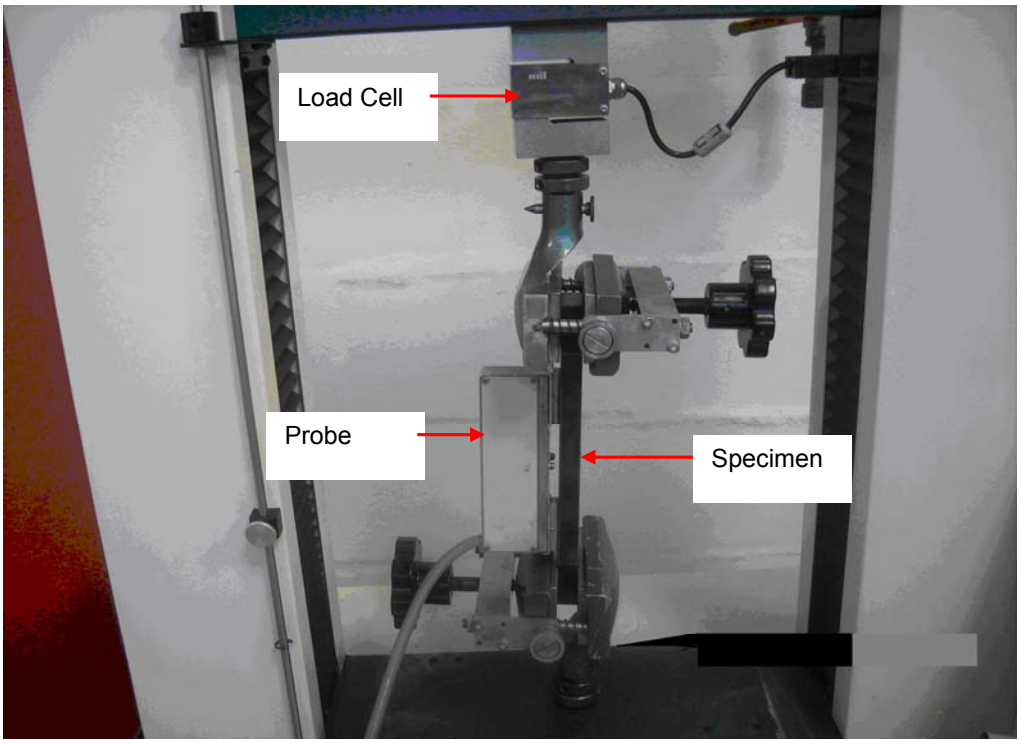

Figure 4.6. Tensile Test set-up for calibrating the Debro-30 Ultrasonic system

Calibration Results

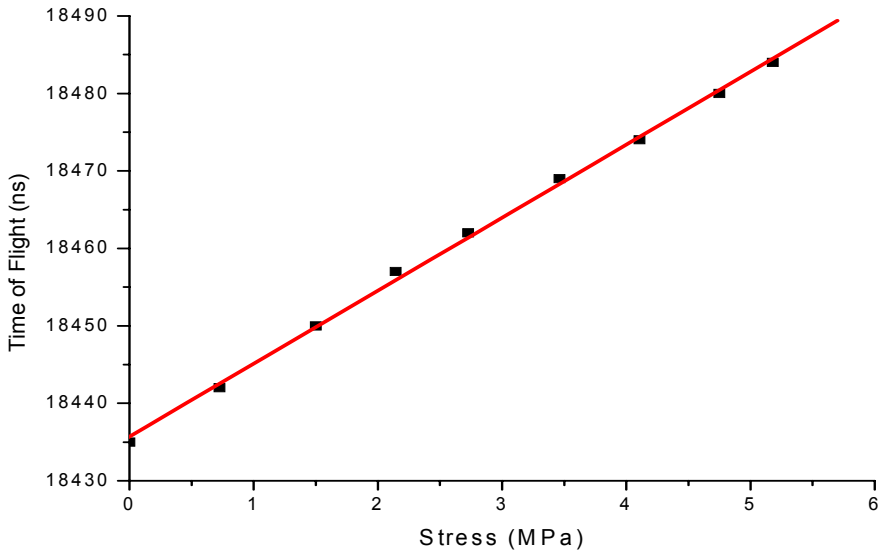

Figure 4.7. Determination of Acousto-elastic constant of specimen using the Debro-30 6L Probehead

The determination of the acousto-elastic constant was done using equation 4.2. From the graph, the time of flight is increasing with increase in stress. The best linear fit was drawn through the data points since the acousto-elastic constant for a given material is constant. The value of acousto-elastic constant obtained for this test could not be relied upon because of improper grips; suspected of inducing a little bending on the specimen and also allowing slippage. For this reason, it was decided that the compression test could yield better results for the acousto-elastic constant determination.

4.5.4 Compression Test

Due to the improper clamping system for the tensile test, the best option available was to do a compression test and compare the results. The compression test produced better results than the tensile test; therefore the reference time of flight and the acousto-elastic constant obtained from a compression test were stored into the Debro-30 to be used for the stress measurement of the shot peened specimens.

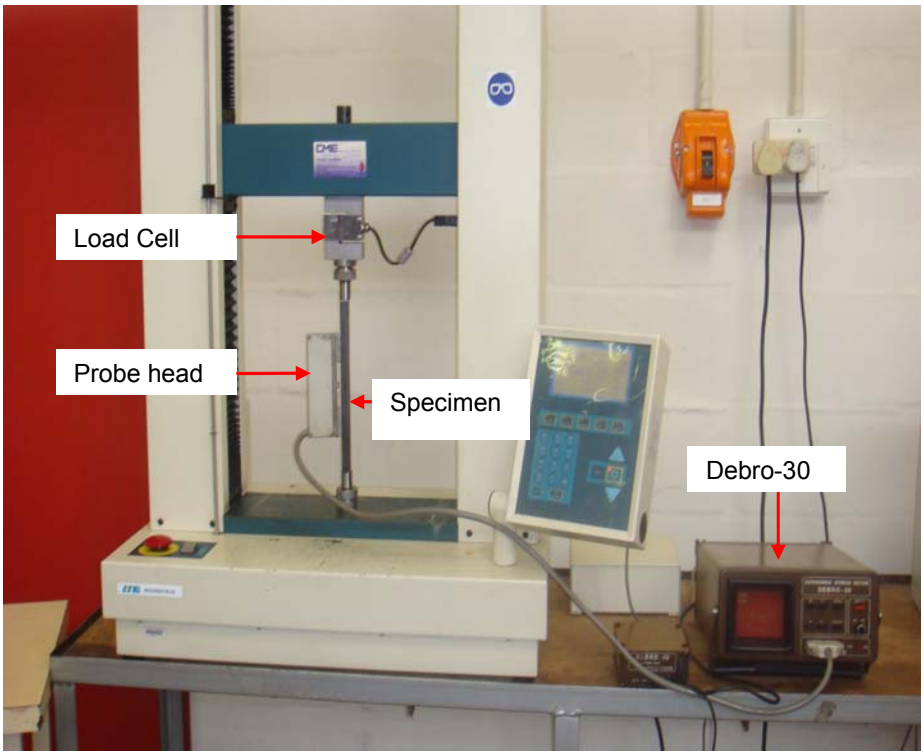

Figure 4.8. Compression Test set-up for calibrating the Debro-30 system

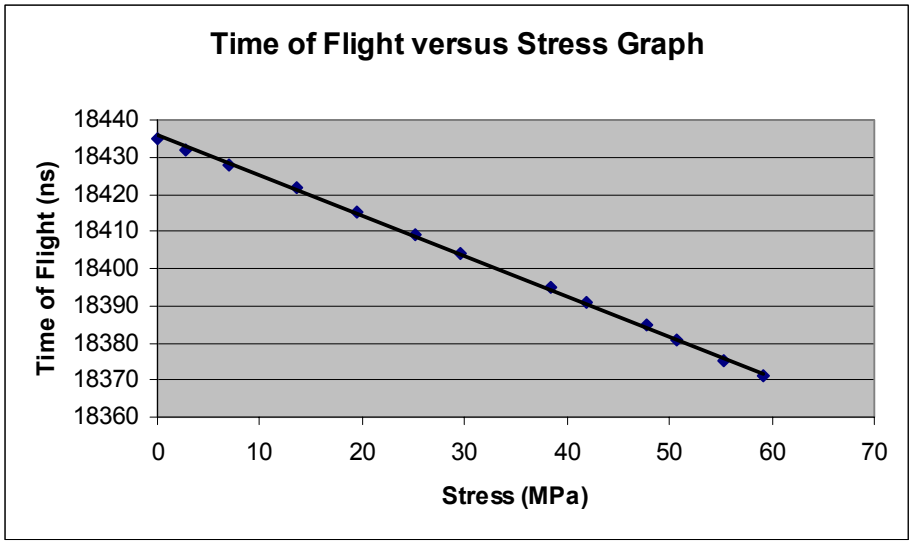

Figure 4.9. Determination of Acousto-elastic constant of specimen using the 6L Probehead in a compressive test

4.6 DISCUSSION OF CALIBRATION RESULTS

The graph shown in figure 4.9 indicates that the time of flight is decreasing with increase in stress. Thus the speed of wave propagation is faster in a material stressed under compression than tension. The graph facilitates in the determination of the acousto-elastic constant as follows; for example the equation of a straight line drawn from this graph is given as:

$y = -1.0802x + 18436$; thus the stress value and a corresponding time of flight are obtained from this equation. At a stress value of say, 25 MPa the corresponding time of flight is obtained as follows.

At x = 25

$$y = -1.0802(25) + 18436 = 18409$$

Using equation 4.2, the acousto-elastic constant, β is obtained as below.

$$\beta = \frac{(18436 - 18409)}{18409 \times 25} = +5.8678 \times 10^{-5}\, MPa^{-1}$$

The acousto-elastic constant is positive since the time of flight decreases with increase in stress. However since the sign of the acousto-elastic constant is a fixed negative on the Debro -30, the value was inputted as a negative. Furthermore the value of the constant must be a three digit number raised to 10^{-7}, hence the inputted valued is $587 \times 10^{-7}\, MPa^{-1}$

Studies done by Hu et al (2009) on the influence of surface roughness on the determination of acousto-elastic constant showed that for a surface roughness of Ra0.8 μm, a coupling error of 5 nanoseconds yielded a stress determination error of 58 MPa. They recommended a surface roughness not greater than Ra0.8 μm. In this work the surface roughness was not measured but assumed sufficiently smooth since it was ground on a surface grinder to a smooth finish.

4.7 STRESS MEASUREMENTS ON SPECIMENS

Three specimens were subjected to different ways of inducing stresses on one surface. For specimen one, the stresses were induced by impacting the surface with the tips of the bristles of a wire brush while specimen two was “shot peened” by covering the surface with 1.5 mm diameter steel “bearing” balls and impacting them with a hammer. This form of cold

working of the two specimens' surfaces was used as it proved impossible to procure a shot peening facility.

Figure 4.10. Specimen surface impacted with the tips of bristles of a wire brush

The photos for specimens two and three clearly indicate a small blind hole of 1.5 mm that was introduced at the centre of the specimens when performing a hole drilling process to measure the residual stress from the relieved strain (See figures 4.11 and 4.12).

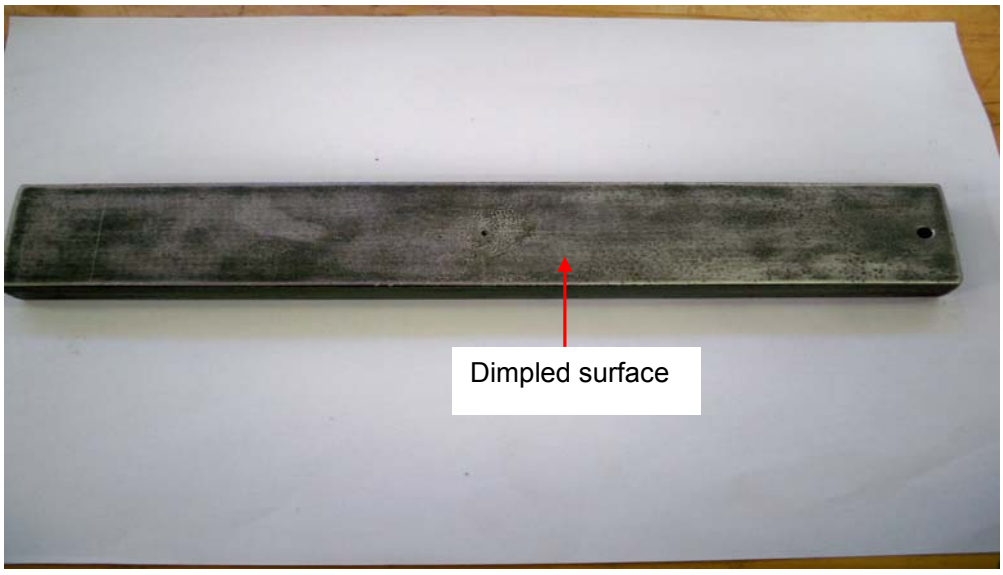

Figure 4.11. Specimen surface subjected to hammering the 1.5 mm steel bearing balls that covered the surface

For the third specimen, compressive stress was introduced on one of its surfaces by heating it to a dull orange colour and suddenly exposing one surface to cooling water; that is, quenching it.

Figure 4.12. Specimen surface heated to dull orange colour with oxy-acetylene flame and quenched in water

The results of stress level introduced on the specimens by the random methods employed are as shown in table 4.3.

Table 4.3: Ultrasonic stress measurement results for the three mild steel specimens.

Specimen Identity	**Stress (MPa)**
Specimen 1 (surface impacted with the tips of bristles of a wire brush)	3
Specimen 2 (hammering the 1.5 mm steel bearing balls in contact with the surface)	5
Specimen 3 (surface heated with oxy-acetylene flame and quenched in water)	6

4.7.1 Discussion of Ultrasonic Stress Measurement Results

The stress values as measured with the Debro-30 ultrasonic stress meter show that “shot peening” by heating and quenching induced the greatest stress. The dimpled surface as a result of hammering the 1.5 mm steel bearing balls in contact with the surface had more stress compared to the one where the wire brush was used because of the level of surface indentation observed. There was no way of predicting in comparison the level of stress induced by quenching the third specimen.

4.8 THE HOLE DRILLING METHOD

The CEA-06-062UM-120 rosette and a 1.5 mm cutter diameter were used for all the drilling operations of the specimens. Before the commencement of each drilling operation, the grid resistances of the strain gauges were checked by a multi-meter and in all cases recorded a resistance of 120 ± 0.4% Ω. The nominal gage factor of 2.08 ± 1% was set on the strain indicator.

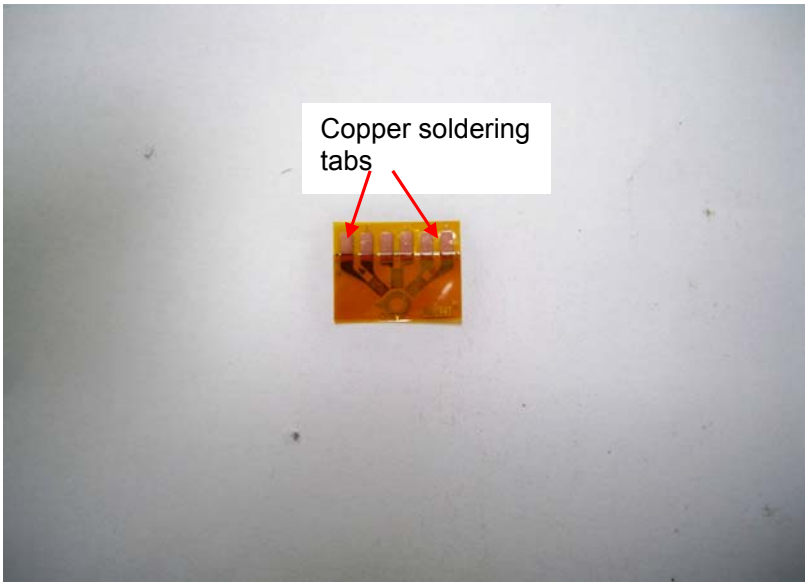

Figure 4.13. CEA-06-062UM-120 rosette

The specimens were glued on the surface of a flat plate, one at a time for stress measurement. The strain gauge was cemented on the surface of the specimen. The wires were carefully soldered on the tabs of the strain gauges and then connected to the P-3500 strain indicator and the SB-10 Switch-and-Balance Unit. The connections were done according to the gauge numbering on the strain gauge. In all cases for consistency, gauge 1 was oriented along the axis of the specimen. The milling guide base assembly was positioned on the flat plate by gluing its three pads to the plate and ensuring that the centre of the journal hole and the gauge circle diameter of the strain gauge were more or less in alignment. During setting, a small spirit level was used to ensure that the entire assembly was level by adjusting the levelling screws of the miller. The final adjustment of the journal hole to the gauge circle diameter was facilitated by four adjusting screws and a microscope assembly. The complete microscope is moved up or down until the centre of the rosette is clear and in focus. A locking ring was then fastened to restrict any further movement when

the final adjustment was done. The three gauge readings were zeroed before the high speed drilling commenced.

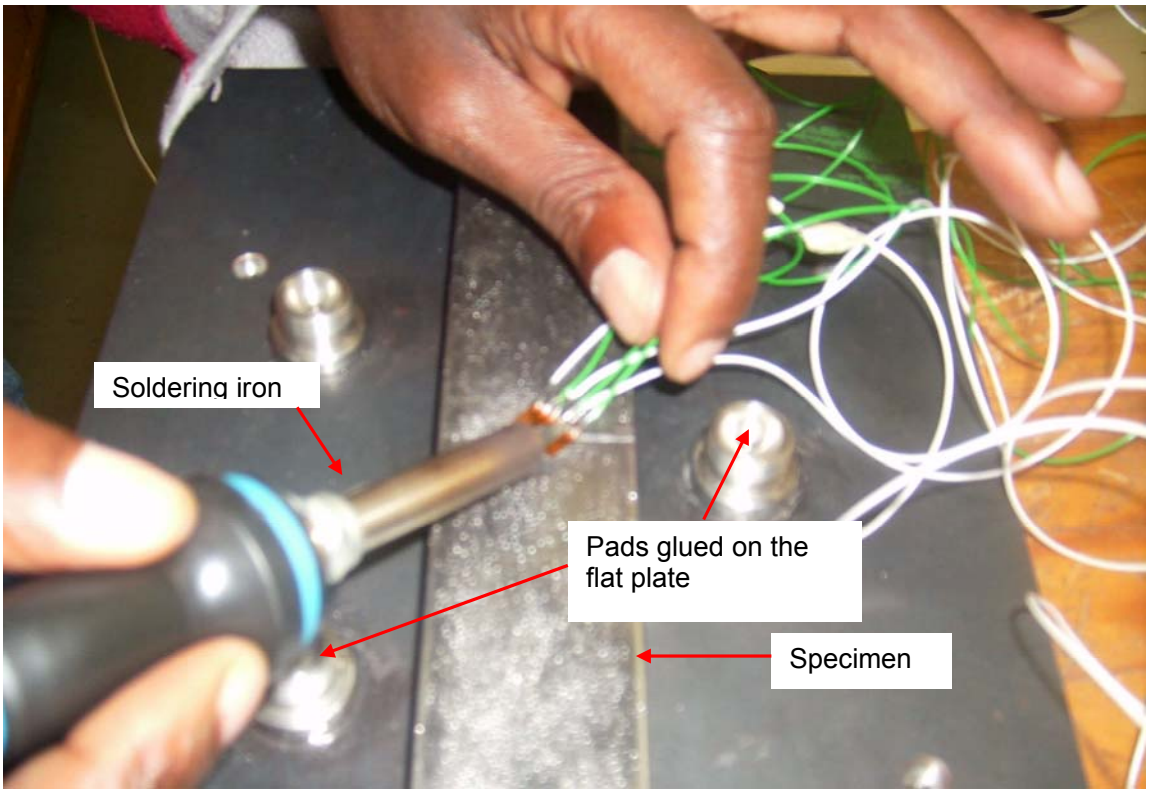

Figure 4.14. Soldering of electrical wires on the tabs of the CEA-06-062UM-120 rosette

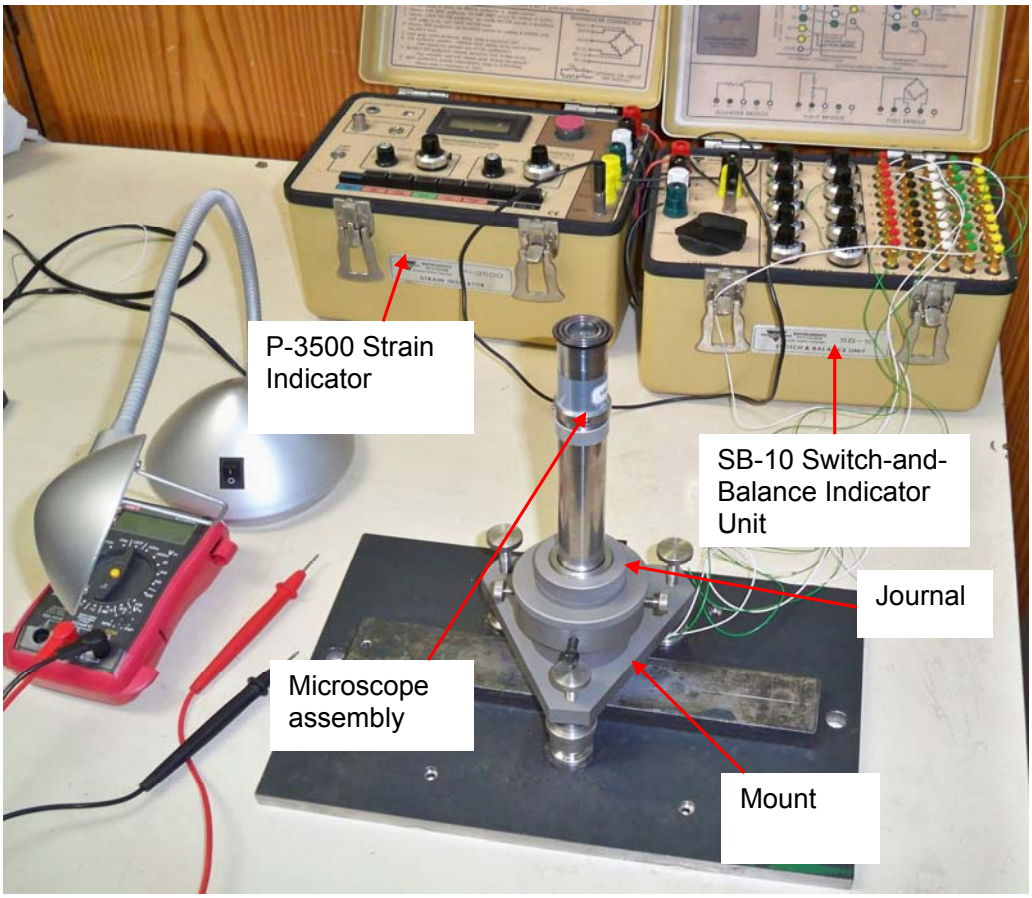

Figure 4.15. Milling Guide Base Assembly with a microscope assembly

Table 4.4 below shows the computed near surface stresses as a result of drilling for the three specimens. The recorded strain readings and computation of stresses was done in Appendix A.

Table 4.4: Hole Drilling stress measurement results.

Specimen Identity	**Stress (MPa)**
Specimen 1 (surface impacted with the tips of bristles of a wire brush)	3.2
Specimen 2 (hammering the 1.5 mm steel bearing balls in contact with the surface)	4.76
Specimen 3 (surface heated with oxy-acetylene flame and quenched in water)	5.84

4.8.1 Discussion of the Hole Drilling Method Stress Measurement Results

For the three specimens investigated, the surface residual compressive stresses were measured as average stress at the depth of the drilled hole. According to Bahadur et al (2007) and Rajendran et al (2008), mechanical relaxation is really complete when the depth of the hole approaches 1.2 times the diameter. The ASTM E837 -01 reports that within the close vicinity of the hole, the relief is nearly complete when the depth of the drilled hole approaches 0.4 of the mean diameter of the strain gauge circle, that is, Z/D = 0.4.

Furthermore, the discussion of stress distribution is in the context of uniform equivalent principal stress. This stress is uniformly distributed and would produce the same total relieved strain at any depth of the hole. In order to qualitatively understand the variation of stress with depth, it is important to obtain the uniform equivalent stress.

The heated and quenched specimen had the greatest stress of 5.84 MPa and the least of 3.2 MPa was obtained for the wire brush impacted specimen. The dimpled surface that was produced by steel bearing balls had a stress value of 4.76 MPa.

The hole drilling experimental errors due to the plasticity were eliminated since the equivalent stress values obtained were far less than the yield strength of the specimens. Nobre et at (2006) mention that the plasticity effect induced by stress concentration factor around the hole produces high residual stresses that lead to local plastic deformation if the equivalent stress reaches the material's yield stress.

A quick comparison of stress values for both the Ultrasonic method and the Hole drilling method are in good agreement. The largest percentage error is 7%.

The Shearography technique which is discussed as follows produced qualitative results. The equivalent quantitative results obtained by analytical means are presented in Chapter 5.

4.9 DIGITAL SHEAROGRAPHY

4.9.1 Introduction

This section deals with the feasibility of using the shearographic technique to detect and possibly quantify residual stresses in materials. A Shearographic Unit developed by the Non Destructive Testing Laboratory of the University of Cape Town, Mechanical Engineering Department was used for the purpose. The treatment of specimens, experimental procedures, methodology and discussion of results are presented.

4.10 Surface Preparation of Specimens

The specimens employed for the Ultrasonic (Debro-30) and Hole drilling stress measurements were also used for the shearographic technique, the aim being a direct comparison of the residual stress values for the three methods.

The specimens were firstly de-greased using M5 solvent. Strain gauges were cemented on the surfaces of the specimens at the position where the specimens would be clamped as cantilever beams. The purpose of cementing the strain gauges on the surface of the specimens was to measure the strain at the “roof” of the cantilever that would result from the loading of the cantilever. Grey primer was sprayed on the surfaces of specimens to facilitate the capture of good contrast images by the digital camera on the shearographic system.

Figure 4.16. Strain Gauge cemented on specimens

4.11 Material and Equipment

Digital Shearographic Unit

The shearographic unit consists of a shearographic head that is mounted on a tripod and an industrial personal computer that is used to acquire and process data. The shearographic head has various components that include the focus and aperture that control the digital camera lens, pan and tilt that control the direction and magnitude of shearing, and the tilt and pan that controls the positioning of the laser. Figure 5.2 shows the shearographic unit. A full description of the shearographic technique was presented under literature review on Shearography, pages 22 to 28.

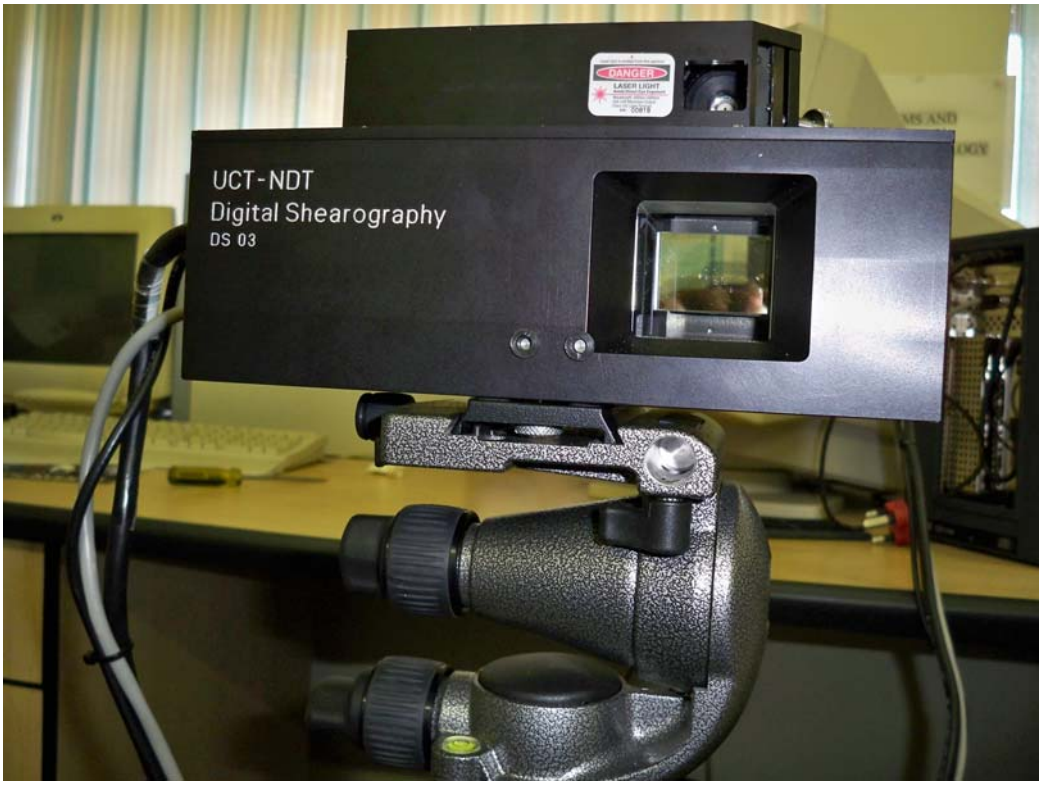

Figure 4.17. Digital Shearographic Unit System

4.12 Experimental Procedure

This section describes the attempt made to measure the stresses that were present in the specimens and previously measured by the Ultrasonic and Hole Drilling methods. The stress free specimen would act as reference.

Each of the specimens was clamped as a cantilever in a precision vice. The free end was subjected to a pulling force induced by the rope running over the pulley with weights on a hanger suspended on its end. CEA-06-125UN-120 strain gauges were cemented on the surface of each specimen and connected to the strain indicator to measure the maximum surface strain that is expected at the “built-in” end, as shown in figure 4.18 below.

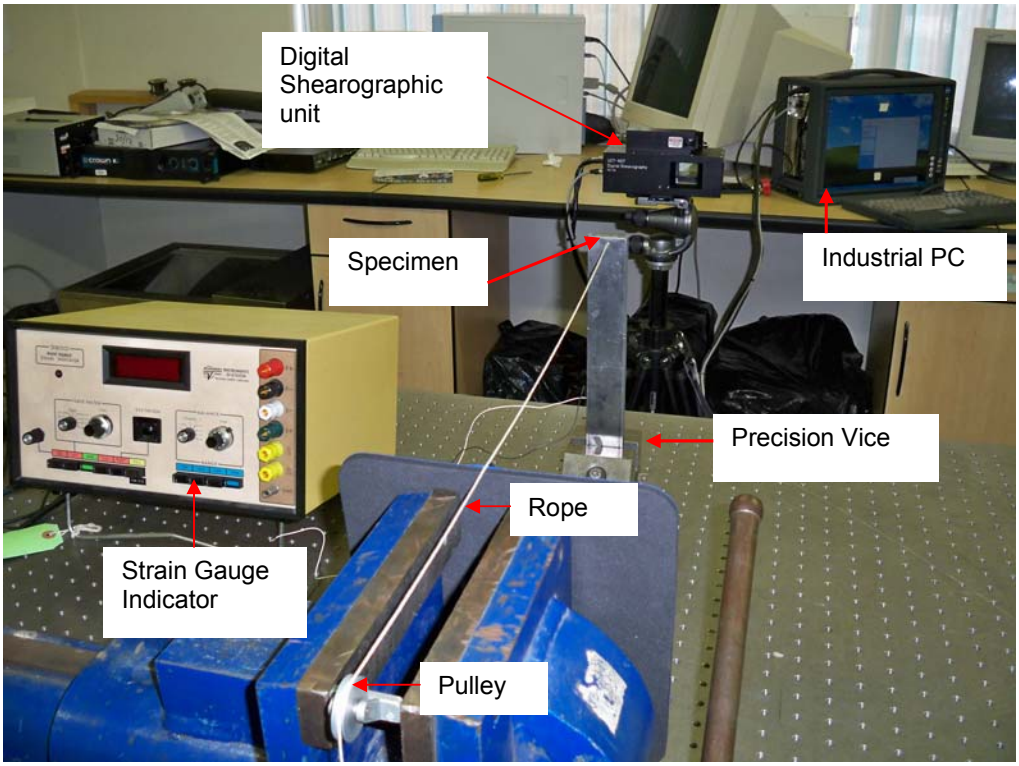

Figure 4.18. Shearography Experimental set-up

In the “cantilever beam” set-up in figure 4.18, the force exerted at the free end induces a maximum bending moment at the built-in end on the specimen. The maximum beam deflection of course occurs at the free end. The beam deflection under the action of the force, within the elastic limit of the test material, is proportional to the applied force and in turn the stress level in it. Since the geometry of the beam section is known, i.e. rectangular section, its moment of inertia can easily be calculated. In order to compute the maximum bending stress that is induced on the surface of the specimen, the maximum value of bending moment is used. The maximum bending stress is compared to the one obtained from a strain reading on strain indicator and computed to stress. According to Gryzagoridis et al (2004), residual stresses may inhibit or aid surface displacement with respect to externally applied loads depending on their nature i.e. compressive or tensile stresses. In this work, the surfaces of the specimens which were under compressive stress were subjected to tensile

stress by the mass attached to the rope. The compressive residual stress would have to be "neutralised" by the load before any displacement of the cantilever took place.

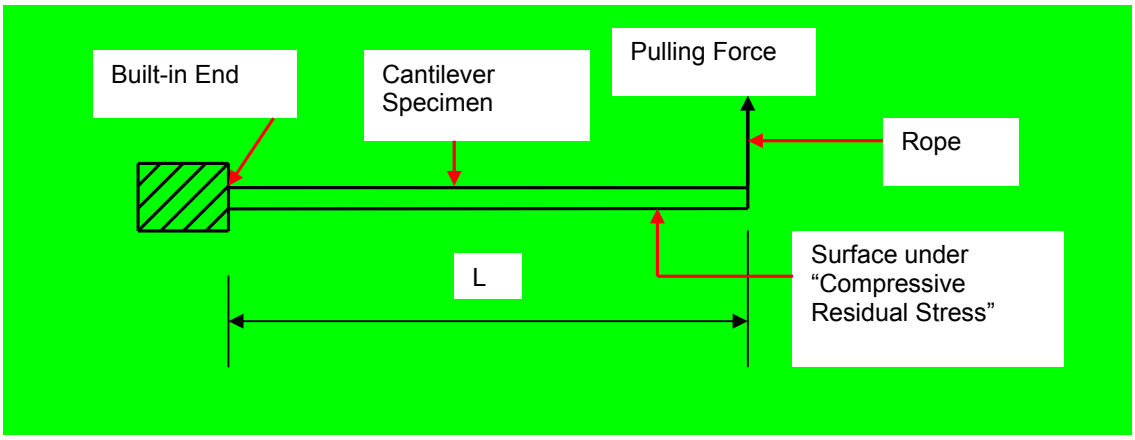

Figure 4.19. Schematic of the Mechanical Loading of the Cantilever

The digital shearographic measuring procedure is outlined below.

4.13 Shearography Measurement Procedures

The shearography head was positioned on the tripod by sliding the saddle located on the underside of the shearography head onto the tripod head and securing it with the locking screw. The unit was placed approximately one metre away from the test specimen which was mounted on a cantilever. After all the power supply connections and adjustments were done, the diode laser was turned on to illuminate the test specimen and its image was viewed and captured using the Digital Camera by the PC's frame grabber. The shearing device produces two identical images separated by a small distance known as the shearing distance. The sheared image of the unloaded specimen is stored in the PC and acts as the reference "strain" level of the object. This image will be compared with the "loaded" image of the specimen and the result displayed on the system's monitor as a shearogram.

The specimen was loaded by placing weights on the hanger. The total mass including the mass of the hanger was 1.2 kg. In this experiment, the choice of this mass was done by loading the specimen and observing the quality and number of the fringes produced. The density of the fringes on the specimen is an indication of the amount of strain as a result of the application of the load.

The measuring steps are summarised below:

(a) Open the Digital Shearography Control Screen by clicking the icon marked "Inspector".
(b) Initiate a live video image on the PC screen by clicking on the "Video" button in the floating toolbar and click the green arrow on the top toolbar. This process sends a typical image of the specimen to the Image Digitiser and displaying it on the screen.
(c) Adjust the Shearography Head via the tripod controls so that the area under inspection is central in the displayed image.
(d) Adjust (if necessary) the laser illumination via the laser tilt control, central to the desired test area.
(e) Focus the video image on the computer monitor by rotating the focus control located at the rear face of the Shearography Head.
(f) Adjust (if necessary) the camera iris such that the image viewed on the computer is not excessively bright.
(g) Set the Shearography Head shearing mirrors to get the required amount of shear. This is achieved by turning the pan and tilting control knobs on the back face of the Shearography Head.
(h) Commence the inspection routine by selecting the desired option i.e. by clicking on "Shear" for intensity based shearography or "Phase" for phase stepping shearography followed by the green arrow on the top of the floating toolbar creating a new blank video document. In this work, the phase stepping shearography was done. Video feed control enables the desired colour quality by adjusting the brightness, darkness and contrast sliders. The computer program then takes a sample of video feed and stores the digitised image as a master image ready to compare the live video feed with the stored master image.
(i) Load the specimen as desired. This produces the interference patterns called fringes on the test object in response to the applied load, depicting displacement gradient.
(j) Filter the image to remove random speckle noise by clicking the "Filter" button and adjusting the filtering slider to the desired level.
(k) Unwrap the phases by clicking the "Unwrap" button on the floating toolbar to display different images. The unwrapping of the phases is facilitated by phase unwrapper software.
(l) Save the desired images by clicking the "Save As" option from the pull-down file menu.

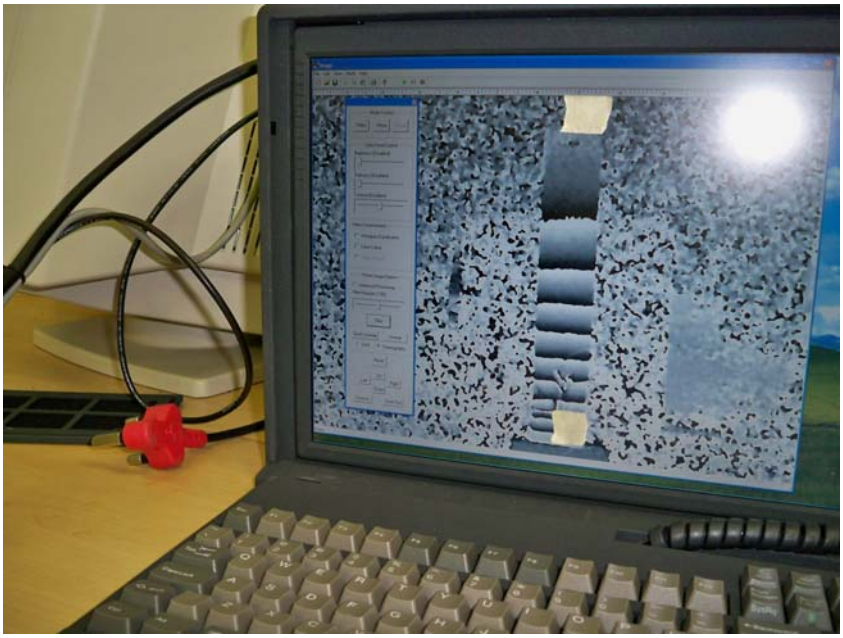

Figure 4.20. Captured filtered phase image during measurement

In this experiment, the strain readings were simultaneously recorded while the specimen was under load.

4.14 Discussion of Shearography Results

The results are a full-field displacement gradient of the specimens as a result of the applied load. A comparison of the specimens in figure 4.21, (a) the stress free and (b) the one with residual stress induced by impacting the surface with tips of bristles of a wire brush, shows that the stress free exhibits more fringes. This obviously indicates that the one with residual stresses offered more resistance to the load than the stress free one. The other specimens exhibited the same pattern by their phase images. See Appendix D, where also detailed digital shearography results on gradient and displacement of all the four specimens are shown.

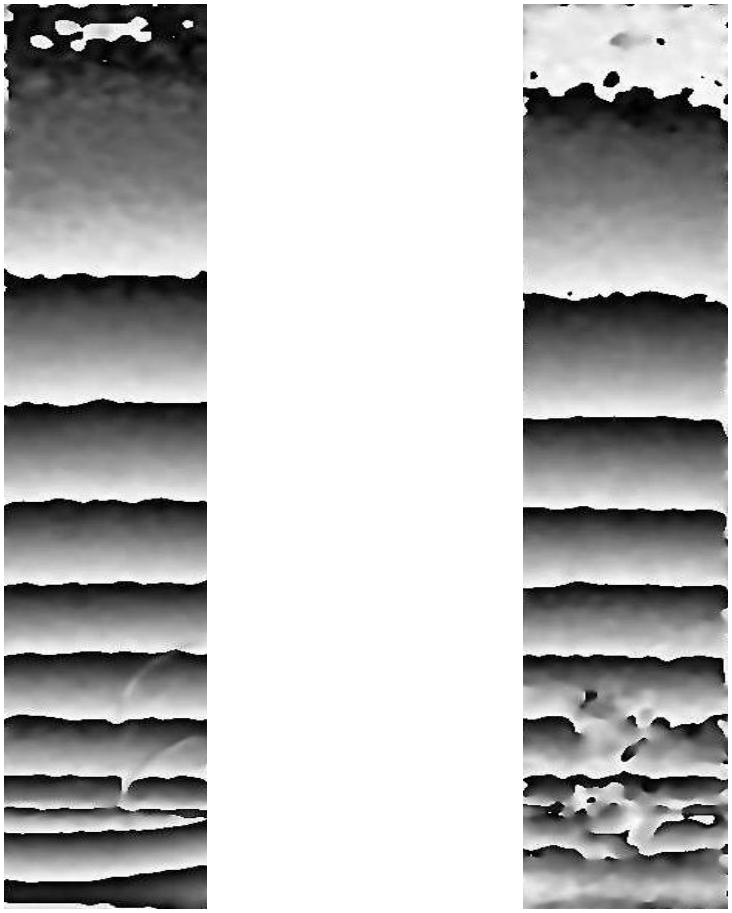

(a) (b)

Figure 4.21. (a) Phase Image for stress free surface; (b) Phase Image for a surface impacted with tips of bristles of a wire brush.

4.15 Conclusion

The experimental procedures and results for the three stress measurement techniques namely; Ultrasonic (Debro-30), Hole Drilling and Digital Shearography were discussed. Predicted results from theory are compared to digital experimental results in the next chapter.

CHAPTER FIVE

ANALYTICAL RESULTS

5.1 INTRODUCTION

This Chapter deals with the predicted results from theory compared to digital shearography experimental results. Both experimental and analytical results are graphically represented. The results are discussed.

5.2 ANALYTICAL RESULTS

Calculation by Direct Integration Method

Assumptions

- The beam is initially straight and unstressed.
- The weight of the beam is negligible.
- The beam is isotropic and homogenous.
- The limit of proportionality is not exceeded.

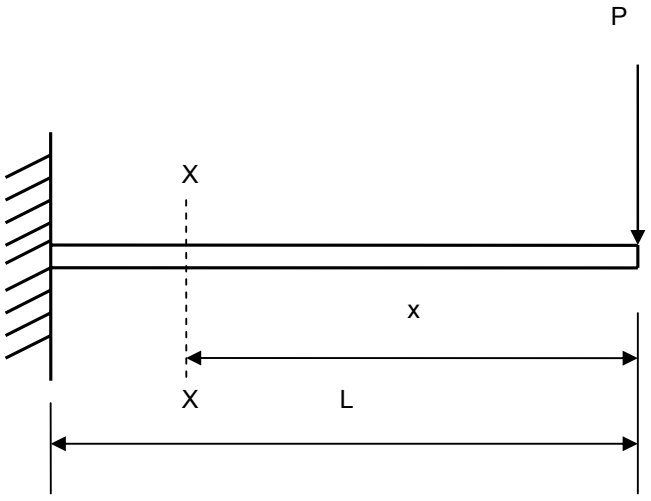

Figure 5.1. Cantilever Beam loading set-up

Young's Modulus of the beam is assumed initially to be 200 GPa

The beam inertia is calculated from; $I = \frac{bd^3}{12}$ (3.3)

$BM_{xx} = EI\frac{d^2y}{dx^2} = -Px$ (The negative sign means the beam is hogging).

$EI\frac{dy}{dx} = -\frac{Px^2}{2} + A$ A is the constant of integration

$EIy = -\frac{Px^3}{6} + Ax + B$ B is another constant of integration.

Assuming that the stiffness of the beam, EI is constant and applying the boundary conditions;

When $x = L$, $\frac{dy}{dx} = 0$ $\therefore A = \frac{PL^2}{2}$

When $x = L$, $y = 0$ $\therefore B = \frac{PL^3}{6} - \frac{PL^2}{2}L = -\frac{PL^3}{3}$

$\therefore y = \frac{1}{EI}\left[-\frac{Px^3}{6} + \frac{PL^2x}{2} - \frac{PL^3}{3}\right]$. This equation is simplified to:

$$\therefore y = \frac{P}{6EI}\left[-x^3 + 3L^2x - 2L^3\right] \quad (5.1)$$

This equation gives the value of deflection at any point on the beam. The maximum deflection however occurs at the tip of the beam i.e. when $x = 0,$

Therefore the **maximum deflection**, $y_{\max} = \frac{1}{EI}\left[-\frac{PL^3}{3}\right] = -\frac{PL^3}{3EI}$ (5.2)

The slope is found in the same way as deflection by substituting all the values in the slope equation, giving the value of slope at any point on the beam;

$\frac{dy}{dx} = \frac{1}{EI}\left[-\frac{Px^2}{2} + \frac{PL^2}{2}\right]$ .This equation is simplified to:

$$\frac{dy}{dx} = \frac{P}{2EI}\left[L^2 - x^2\right] \quad (5.3)$$

The **maximum slope** occurs when $x = 0,$

$$\therefore \left(\frac{dy}{dx}\right)_{\max} = \frac{1}{EI}\left[\frac{PL^2}{2}\right] = \frac{PL^2}{2EI} \qquad (5.4)$$

Bending Theory

$$\frac{\sigma}{y} = \frac{M}{I} \Rightarrow \sigma_b = \frac{My}{I} \qquad (3.2)$$

$$Moment \quad , M = P \times \chi = 1.2\,kg * 9.81 = 11.77\ N$$

$$I = \frac{bd^3}{12} = \frac{0.04 \times 0.0155^3}{12} = 1.241292 \times 10^{-8}\ m^4$$

$$Length \quad / \ Span \quad = \quad 225 \quad mm$$

$$\sigma = \frac{My}{I} = \frac{M\frac{d}{2}}{\frac{bd^3}{12}} = 6M/\left(b \times d^2\right)$$

Since the bending moment at any given point on the beam is known, then also the bending stress at that particular point can be found. In addition, the deflection and slope at any given point on the beam is found from equations 5.1 and 5.3 respectively.

Assuming a constant load of 1.2 kg to be applied at the free end on a stress free specimen, graphs of variation of bending stress, deflection and slope with distance from the built-in end; are plotted in figures 5.2, 5.3 and 5.4 respectively. These graphs are compared later with stressed specimens to determine the effect of residual stresses in those specimens. In practical applications, this information could be of importance to engineers who could incorporate the effect of residual stresses in the design of components.

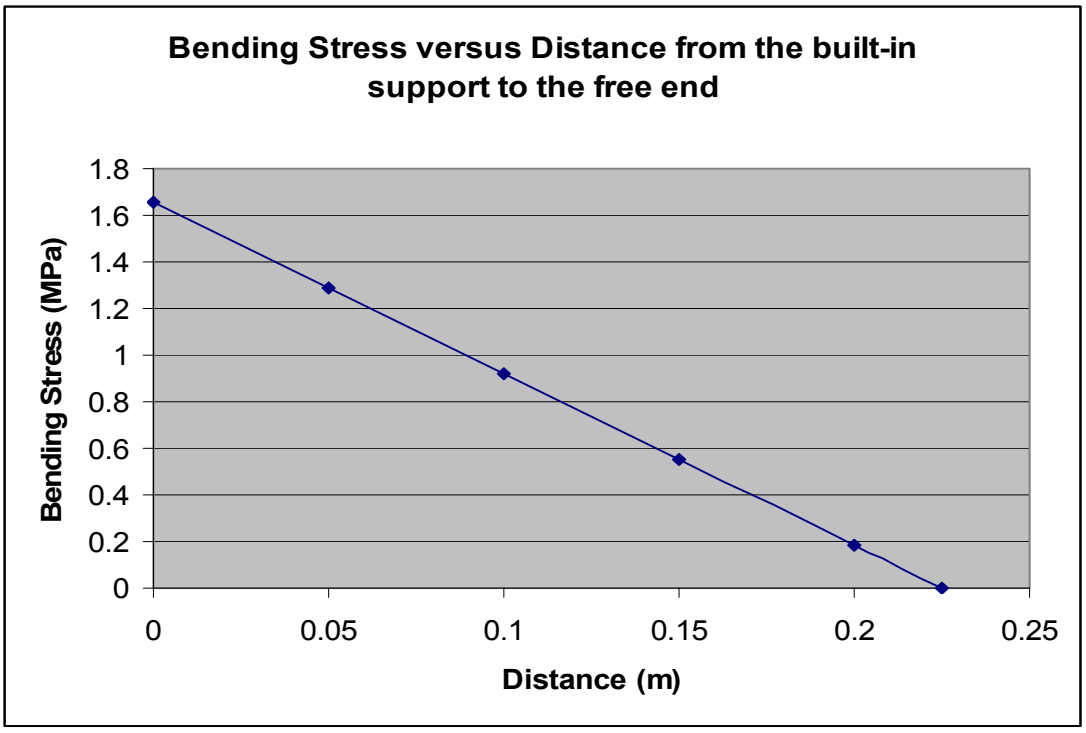

Figure 5.2. Variation of bending stress with distance from the built-in support

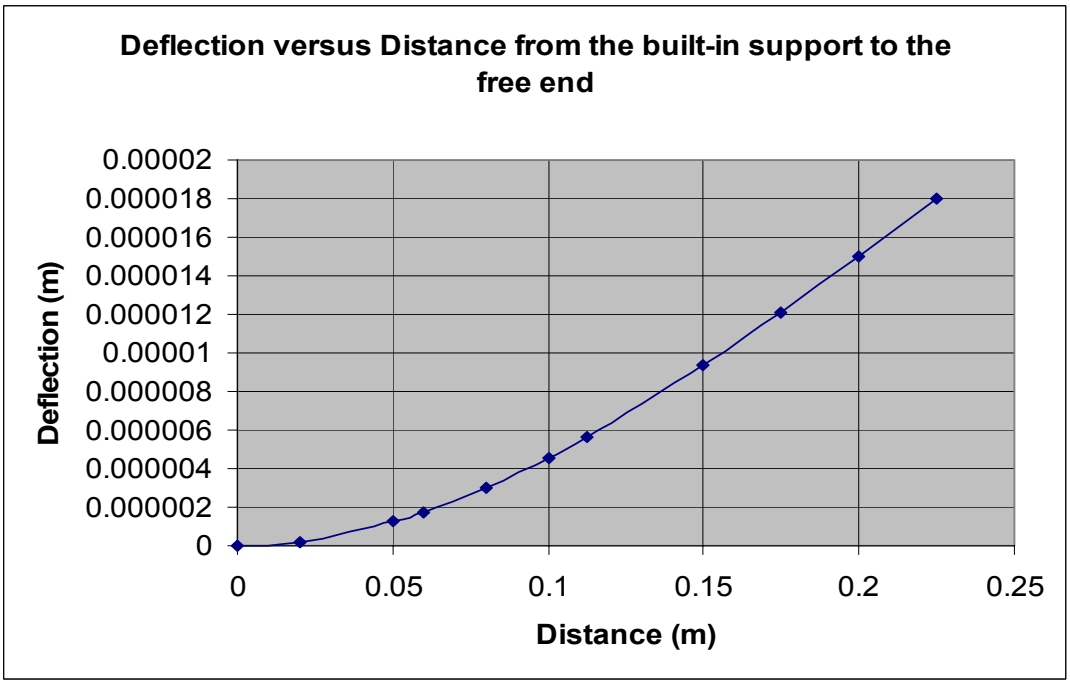

Figure 5.3. Variation of deflection with distance from the built-in support to the free end

The maximum deflection is recorded at the free end and zero at the built in support.

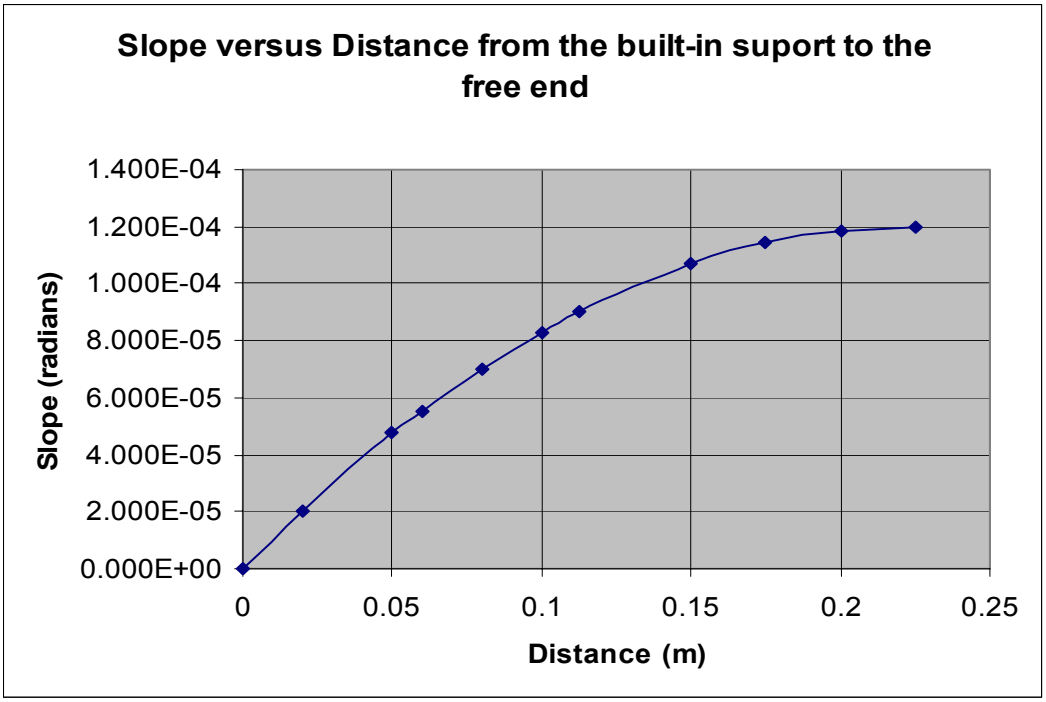

Figure 5.4. Variation of slope with distance from the built-in support to the free end

The slope is zero radians at the built-in support and maximum 1.2 x 10^{-4} radians at free end.

Derivation of equations required to compute strain and stress of the beam

The key formula used here to study the behaviour of the beam section as a result of the load system is given as:

$$\frac{\sigma}{y} = \frac{M}{I} = \frac{E}{R} \qquad \text{(Theory of Bending)} \quad (3.2)$$

Where

- σ is the bending stress
- E is the Young's Modulus
- M is the bending moment
- I is the second moment of area
- R is the radius of curvature
- y is the distance from the neutral axis to the uttermost fibres of the beam section

Assumptions

1. The above relation assumes that the stress is proportional to strain
2. Valid for small deflections and rotations
3. The pure bending case is considered and deflections caused by shear force are not accounted for.

$$\sigma_b = \frac{My}{I} = \frac{Ey}{R} \quad \text{also} \quad \sigma_b = E\varepsilon$$

From Euler-Bernoulli Theory of Bending:

$$R = \frac{EI}{M} \tag{5.5}$$

This equation relates the radius of curvature to the bending moment, M and the stiffness of the material, EI.

Mathematically, the curvature equation is given by:

$$\frac{1}{R} = \frac{d^2y/dx^2}{\left[1+(dy/dx)^2\right]^{3/2}} \tag{5.6}$$

The above can be simplified for actual beams because the slope dy/dx is small and its square is even smaller and can be neglected as a higher order term. Hence equation 5.6 can be simplified as;

$$\frac{1}{R} = \frac{d^2y}{dx^2} = y'' \tag{5.7}$$

By substituting equation 5.7 into equation 5.5 gives the bending moment at any point along the beam as;

$$EI\frac{d^2y}{dx^2} = M_x = EIy'' \tag{5.8}$$

It can also be shown from bending theory formula that the radius of curvature is related to strain.

$$\varepsilon = \frac{y}{R} \qquad (5.9)$$

Where y is the distance from the neutral axis, which in this case is taken as half of thickness, t/2

Now relating the radius of curvature to the second derivative of the deflection equation (equation 5.1) gives:

$$\frac{1}{R} = \frac{d^2y}{dx^2} = \frac{P}{2EI}\left[-2x\right] = \frac{Px}{EI}$$ (Working the free end to the built-in support)

Or $\frac{1}{R} = \frac{d^2y}{dx^2} = \frac{P}{6EI}\left[6L - 6x\right] = \frac{P}{EI}\left[L - x\right]$ (Working the built-in support to the free end)

These equations are the same as equation 5.5 for a constant bending moment.

Therefore $\varepsilon_x = \frac{Pxy}{EI} = \frac{t}{2} \cdot \frac{Px}{EI}$ (Longitudinal strain at any point along the beam)

$$\varepsilon_{\max} = \frac{t}{2} \cdot \frac{PL}{EI} \qquad (5.10)$$

The strain is proportional to stress hence the maximum stress is given by:

$$\sigma_{\max} = \frac{3Ety_{\max}}{2l^2} \qquad (5.11)$$

Where

- E is the Young's Modulus
- t is the thickness of the beam
- l is the length of the beam
- $y_{\max}$ is the maximum deflection which occurs at the point of load application

Alternatively, the maximum stress can be obtained by multiplying the maximum strain by the Young's Modulus from the relationship; $\sigma_b = E\varepsilon$

Thus $$\sigma_{\max} = \frac{PLt}{2I} \qquad (5.12)$$

Where

- P is the load
- t is the thickness of the beam
- L is the length of the beam
- I is the second moment of area of the beam

Figure 5.5 shows the variation of strain with distance along the beam.

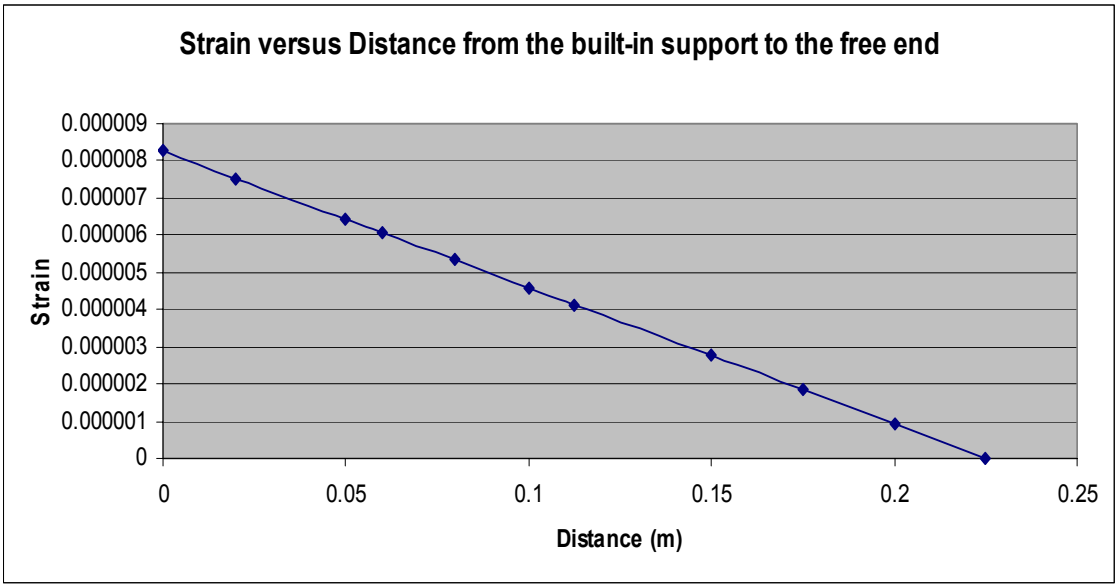

Figure 5.5. Variation of strain with distance

5.3 Shearography Measurements

Each of the specimens used in the shearography experiment was measured for displacement and gradient under the load of 1.2 kg applied to the free end. Strain gauges were also cemented on the surface of each specimen at the built-in end, to measure the amount of stress when the load was applied.

The surface displacement of each specimen was computed from equation 2.21 in chapter 2, repeated here, simply by counting the number of fringes as they appeared on the surface of the beam.

$$\frac{\partial \delta p}{\partial x} = \frac{N\lambda}{2S} \qquad (2.21)$$

The width of the measured image was 30 mm and the shearing distance was 20 mm. The original width of the specimen was 40 mm. Thus the scaling factor of 0.75 was applicable to all the measurements on the images. Figure 5.6 depicts the experimental and analytical results for a stress free specimen.

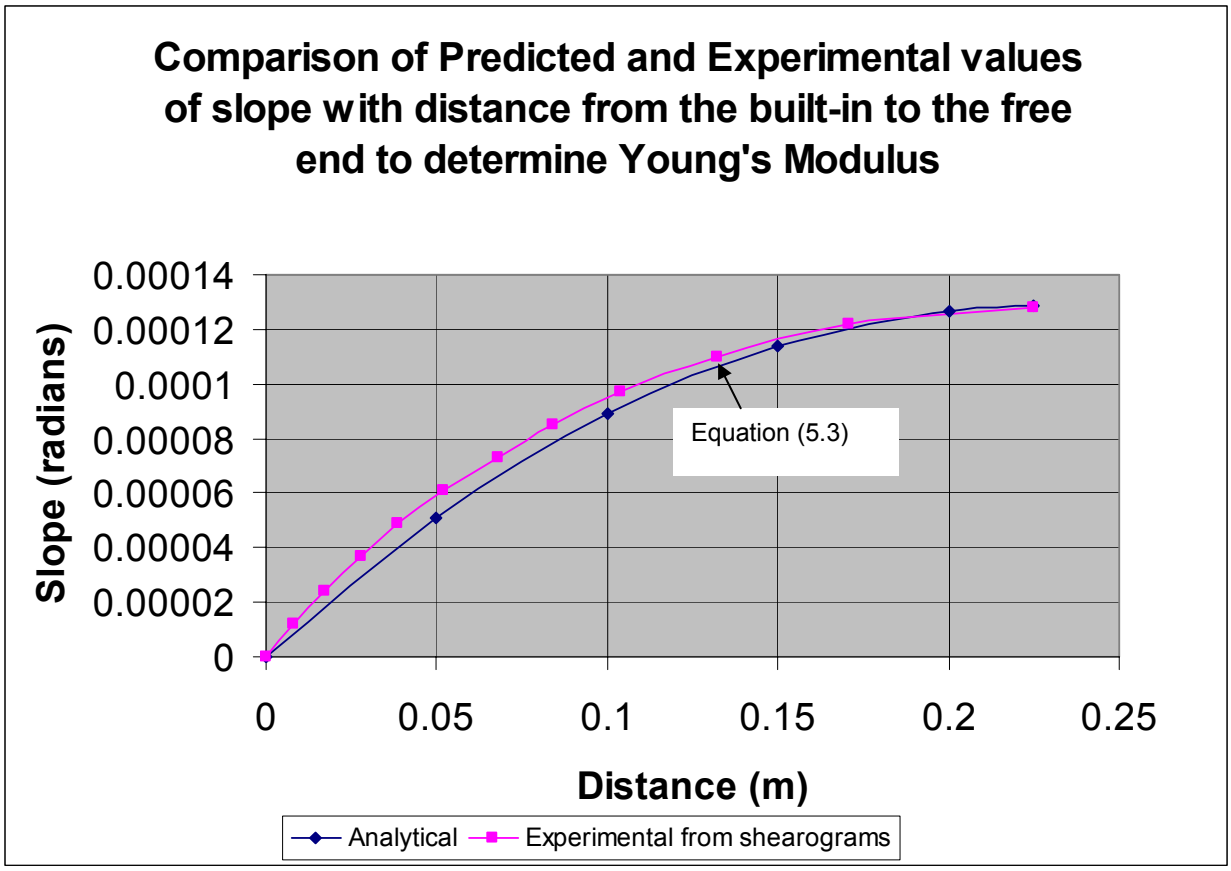

Figure 5.6. Variation of slope with distance from the built-in support to the free end

There is a good correlation between the two results for the stress free specimen. However a change in the Young's Modulus value in the analytical solution initially assumed as 200 GPa brings the predicted values closer to the experimentally obtained values. A better match of the curves is obtained with a Young's Modulus of 187 GPa. Note that this approach holds promise of determining experimentally the value of Young's Modulus of materials.

From the slope equation for shearograms,

$$\frac{dy}{dx} = \frac{\lambda N}{2S} \qquad (2.21)$$

The deflection of each specimen can be obtained by integrating equation 2.21.

$$y = \frac{\lambda N}{2S} x + C \qquad (5.13)$$

The constant of integration C is obtained by applying boundary conditions;

When $x = L$; $y = 0$ at the built-in support

$$C = -\frac{\lambda N}{2S} L$$

Equation 5.13 can be rewritten as:

$$y = \frac{\lambda N}{2S} x - \frac{\lambda N}{2S} L = \frac{\lambda N}{2S} (x - L) \qquad (5.14)$$

The maximum deflection occurs when $x = 0$

$$y_{\max} = \frac{\lambda N}{2S} L \qquad (5.15)$$

From equation 5.11 the maximum stress is given as:

$$\sigma_{\max} = \frac{3Et\lambda N}{4SL} = \frac{0.75Et\lambda N}{SL} \qquad (5.16)$$

Equation 5.16 shows that the stress can be computed for different positions on the beam where the fringes are situated.

Stress measurements for all four specimens obtained by the shearographic technique are shown in figure 5.7 below.

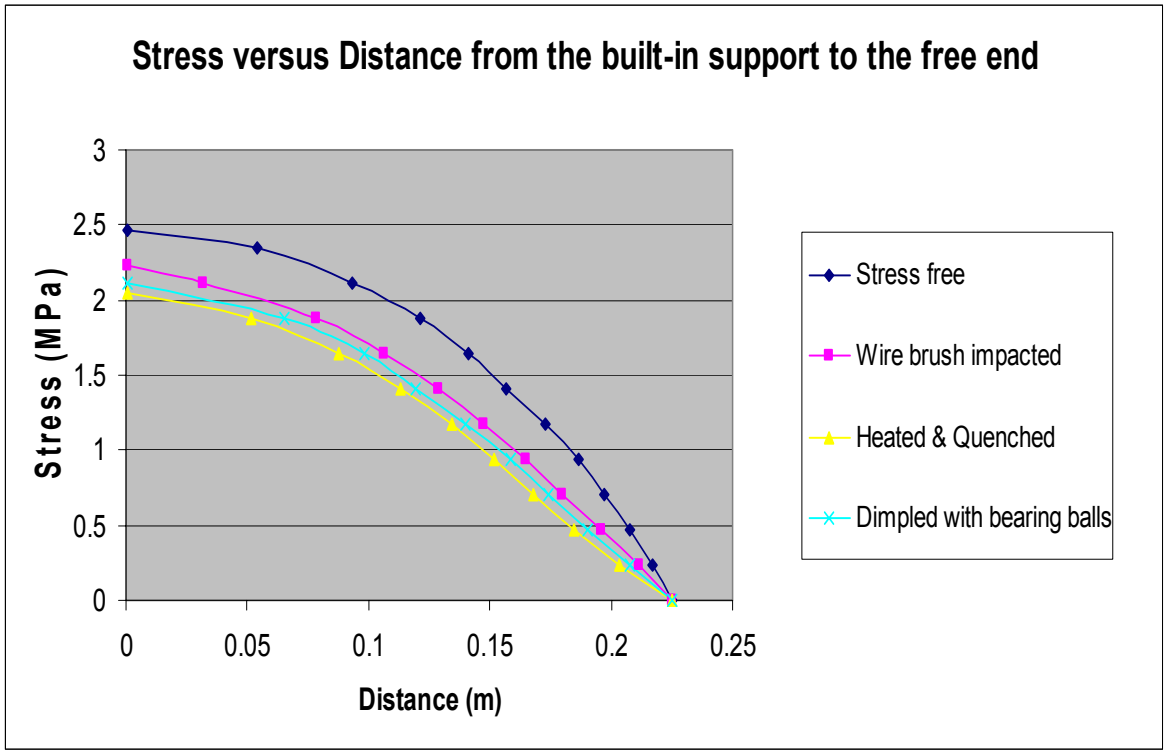

Figure 5.7. Variation of stress with distance from the built-in support to the free end for all specimens

As expected the residual stress laden specimens offered resistance to bending and hence exhibited lesser stress compared to the “stress free” specimen

Figure 5.7 has been composed from equation 5.16 by determining the stress at positions where the fringes are located.

With the inclusion of the stress free curve quantification of the existing residual stress is possible. In other words the difference of the values between the stress free specimen and say the heated and quenched specimen is 0.42 MPa reveals the value of residual stress in that specimen.

5.4 Strain Gauge Measurements

The strain for each specimen at the built-in support was recorded for different masses and the results were plotted as depicted in figure 5.8.

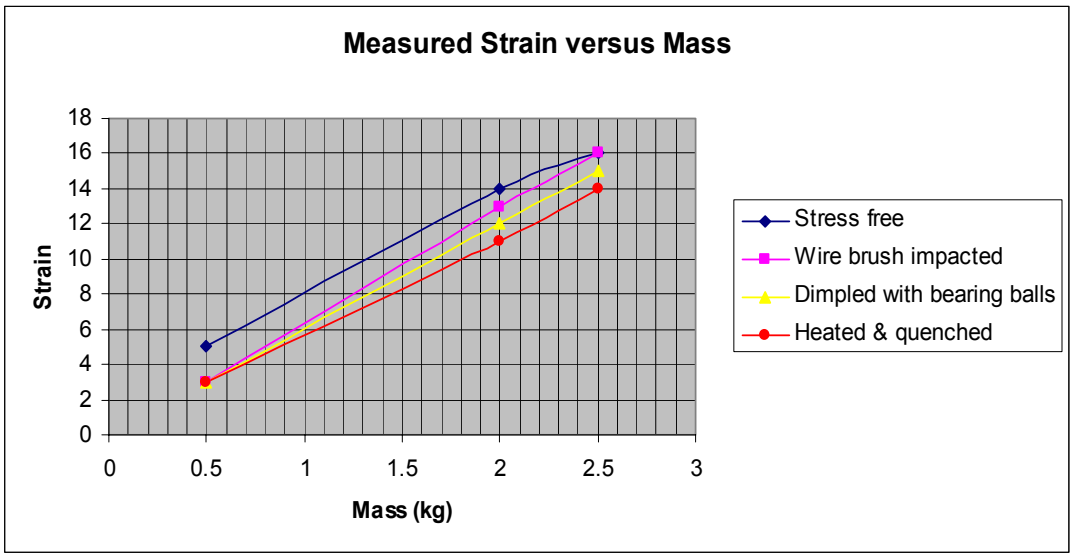

Figure 5.8. Variation of measured surface strain with mass at the built-in support for the four specimens

The value of mass used for the experiment was 1.2 kg and the respective strain for each specimen can be interpolated from figure 5.8. The recorded strain for each specimen was compared to the analytical solution that used the determined Young's Modulus of Elasticity. Refer figure 5.9.

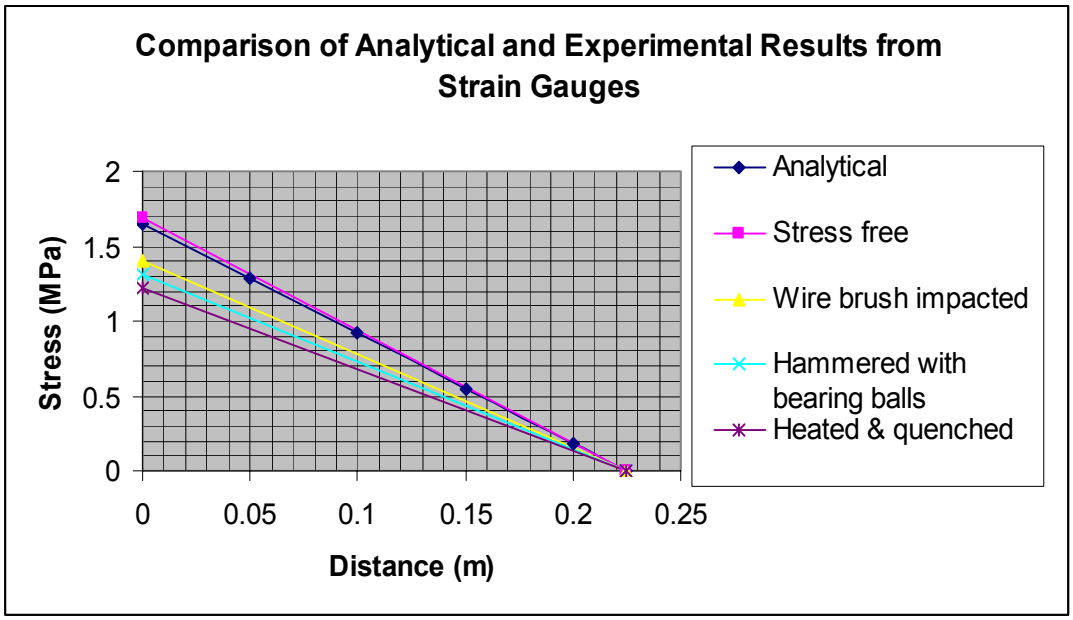

Figure 5.9. Variation of measured surface strain with distance from the built-in support to the free end for all the specimens

The maximum stress for each specimen was computed from a relationship;

$$\sigma_b = E\varepsilon$$

Where E, Young's Modulus was experimentally determined as 187 GPa from shearography.

5.5 Comparison of Strain Gauge and Shearography Results

Table 5.1: Computed stress values for all the specimens

Specimen Identity	**Stress Measurement Method**	
	(MPa) Strain Gauge	(MPa) Shearography
Stress Free	1.68	2.5
Wire Brush Impacted	0.28	0.24
Dimpled with bearing balls	0.37	0.35
Heated and Quenched	0.47	0.42

The standard deviation is within 4% for all the specimens showing a good correlation except for the stress free specimen that recorded a much higher value. It is assumed that the strain gauge for the stress free specimen was not completely picking up the strain due to improper bonding.

Cold working and heat treatment processes on surfaces of components induce different levels of stresses and may cause changes in the elastic properties. The next section on Finite Element Analysis attempts to investigate the effects of these elastic constants on stress and displacement.

5.6 Finite Element Analysis on "Stress Free" Specimen

A simple structural analysis was performed on a specimen model to investigate the effects of elastic constants on the displacement and stress. The analysis was done in ANSYS Workbench. It was found out that the stress remains constant over a wide range of Young's Modulus of Elasticity i.e. from 180 to 240 GPa. However, displacement decreases with increases in Young's Modulus for various Poisson's ratio values. Refer figure 5.9 below.

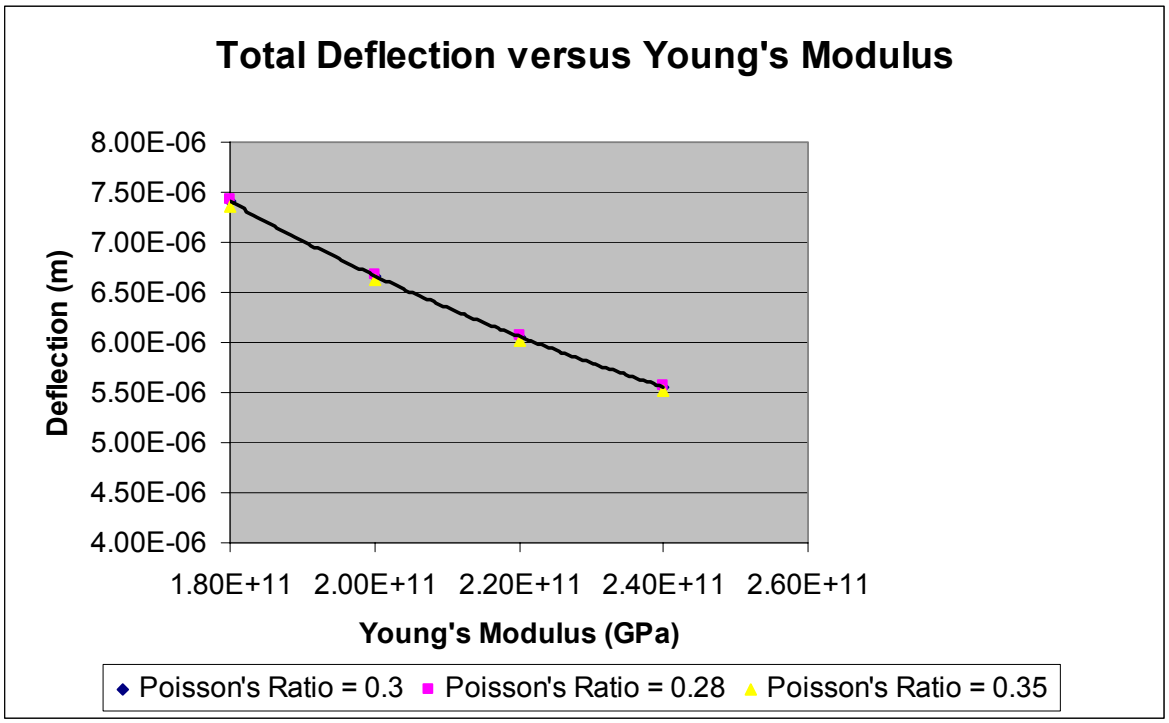

Figure 5.10. Effect of elastic constants on displacement

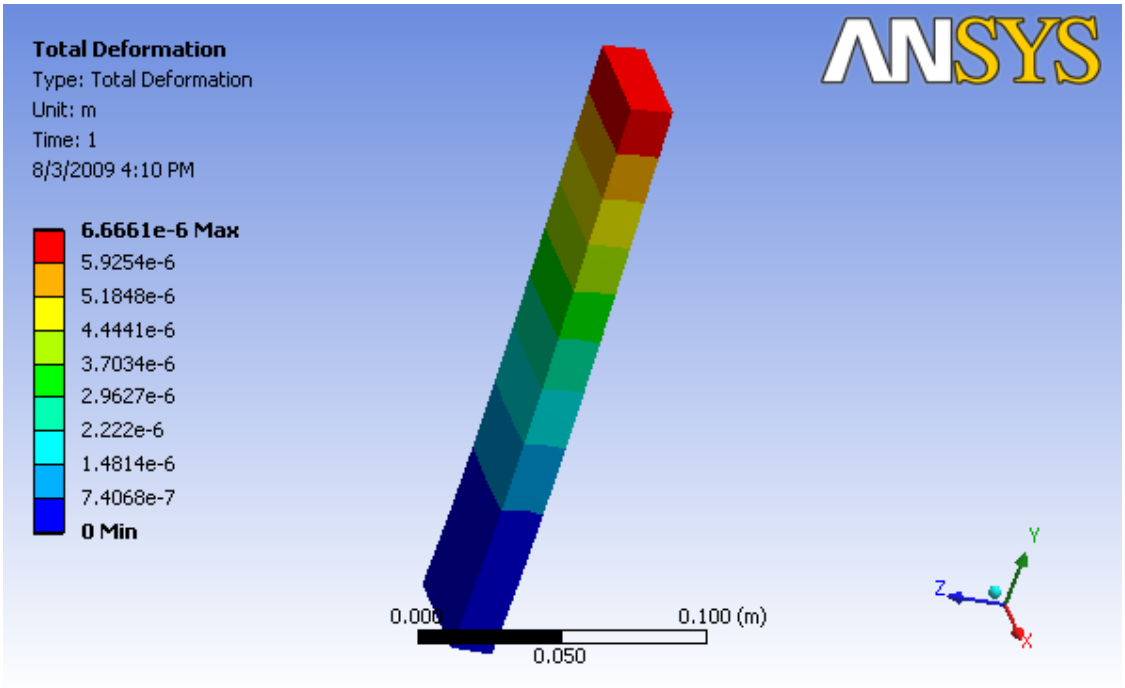

Figure 5.11. Variation of displacement from the built-in support to the free end

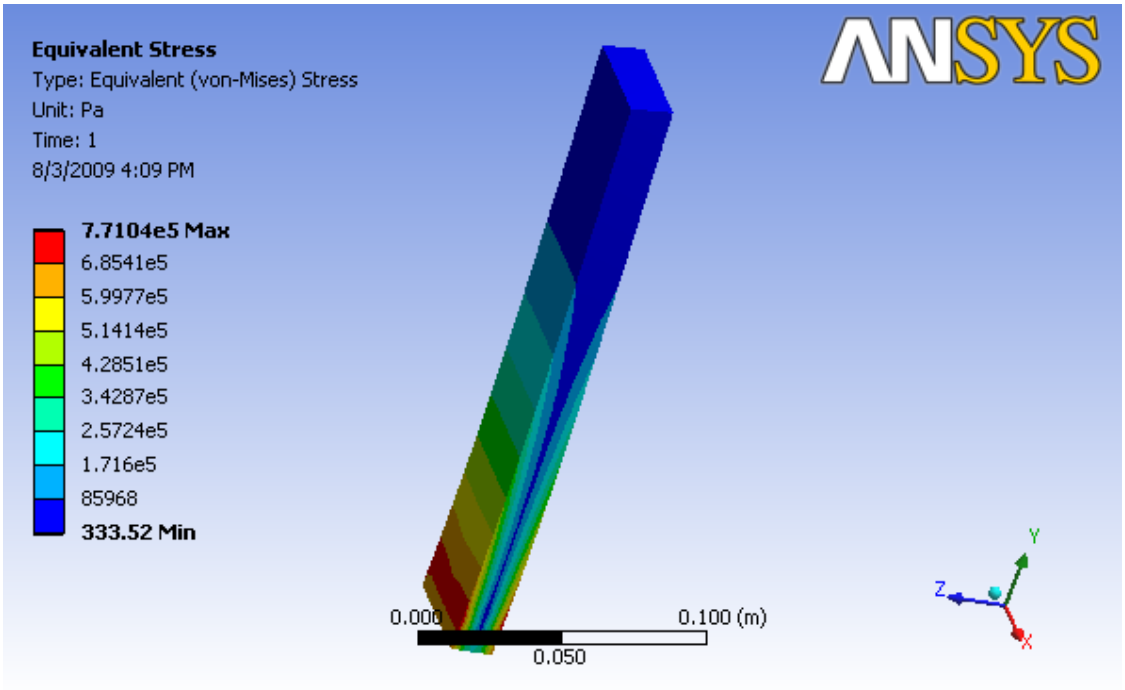

Figure 5.12. Variation of stress from the built-in support to the free end

The maximum value of stress is recorded at the built-in support as expected although this value is lower than both the theoretical and experimental.

5.7 Conclusion

Analytical and FEA were performed to validate the experimental results.

CHAPTER SIX

CONCLUSIONS AND RECOMMENDATIONS

6.1 CONCLUSIONS

This work is aimed at determining residual stresses in steel bars for the purpose of comparing three different residual stress measurement techniques. The residual stresses were induced by methods similar to the "shot peening" method namely; impacting the surface with the tips of the bristles of a wire brush, hammering tiny steel bearing balls that covered the surface of the bar and by heating one of the specimens (using oxy-acetylene flame) and quenching its surface in water. These methods of stress inducing were devised because the procurement of a shot peening facility was not possible. Three methods were used to measure the residual stresses, that is, the Hole drilling, the Debro-30 Ultrasonic system and Digital Shearography. Four test specimens were used to conduct the experiments for the purposes of comparison of results between the techniques, three that had residual stresses induced and an additional as a reference specimen assumed to be free of residual stresses having been annealed. The Hole drilling method was also performed on a specimen subjected to four point bending as described in Chapter 3. All the specimens used were initially annealed in an oven to relieve stresses induced during the machining operations such as milling and grinding.

Ultrasonic measurements were done by first determining the acousto-elastic constant of the test specimens by conducting a compression test on the annealed specimen obviously made of the same material. The acousto-elastic constant and recorded reference time were inputted into the Debro-30 Ultrasonic system before actual stress measurements on test specimens were conducted. The result from each specimen was recorded.

The hole drilling method was facilitated by the use the equipment comprising the RS 200 Milling Guide, strain indicator and the SB-10 Switch-and-Balance Unit. The relieved strains from the drilling process were recorded and manually computed to stresses. It was found that residual stresses varied with depth.

An attempt has been made to quantify residual stresses using digital shearography, a technique originally proposed for strain measurements and lately used in detecting flaws or defects in materials. In this work, quantification of residual stresses was facilitated by using a reference or "residual stress free" specimen. For all shearography experiments, the cantilever beam set-up was used to support the load that was applied at the free end of the specimen. The strain field along the length of the cantilever was obtained and from this

record the stresses were computed. The bending stresses in the “shot peened” specimens were compared to the reference specimen or “residual stress free” specimen values under the same load. The “residual stress free” specimen had the greatest bending stress value at the built-in edge as expected. The difference between “residual stress free” value and the bending stress value for each specimen at the built-in end gives an indication of the amount of existing residual stress in that particular specimen. However that is not conclusive because a cantilever beam set-up is expected to give lower stress values due to the nature of load application i.e. the load cannot be physically applied at the tip of the specimen, but most importantly the modelling of the built-in end. Furthermore, the assumption that the distribution of stresses in the “shot peened” specimens is uniform may not be the case. Nevertheless one would nearly predict the amount of residual stresses based on the stress profiles depicted in figure 5.6 in Chapter 5. It has been shown that shearography can be used to measure residual stresses in components or materials. It was also found that Young’s Modulus can possibly be determined using the shearographic technique by matching the analytical-graphical solution to the experimental graph of a given reference specimen.

Direct comparison of the three methods reveals some similarities and differences. The Debro-30 Ultrasonic system is fairly quick to quantitatively determine residual stresses when compared to the Hole Drilling method. Shearography on the other hand provides a quicker way to qualitatively analyse residual stresses. According to Honner et al (2004) shearography can be used in place of the hole drilling method through the use of a micro-indenter to relieve stresses instead of drilling a hole; however they admit that quantification of the stresses relieved by indentation is a difficult task due to the complexity of the mechanics of plastic indentation. Of the three methods, the hole drilling technique is the most time consuming because of the need to critically align the strain gauge circle diameter to coincide with the journal hole of the milling guide, not to mention the time required to prepare the specimen and of course the processing of the drilling results.

The major aim of the research was to determine the accuracy of the above mentioned methods in measuring residual stresses and it has been shown that the ultrasonic and the hole drilling method lie within 7% of each other. However, the accuracy of methods depends among other things on an in-depth understanding of the underlying principles of each method and the expertise required in using the respective measuring apparatus.

The novel contribution to the existing body of knowledge is the attempt here to quantify residual stresses using digital shearography, which at best can be termed as a feasibility study. In this regard shearographic non-destructive testing is not limited to defect or flaw detection but can also be used to determine stress levels of manufactured materials and

components, before commissioning. It is a fact that the formation of residual stresses in manufacturing processes is inevitable and therefore cannot be ignored. Although residual stress measurement methods discussed in this study have been in existence for some time, the reliability factor still requires attention because of the complexity involved with each technique; hence the call for ongoing research on these methods and others in measuring residual stresses.

6.2 RECOMMENDATIONS

- Tedious and laborious manual computation of measured strains into stresses using the hole drilling technique could have been eased by the use of relevant software.
- Future work should include further investigation into the quantification of residual stresses by digital shearography.

REFERENCES

Aerospace Material Specification, AMS-S-13165 (1997), "Shot Peening of Metal Parts", SAE International.

Andhee A, Gryzagoridis J, Findeis D. 2005. Comparison of Normal and Phase Stepping Shearographic NDE. NDT laboratory, Department of Mechanical Engineering, University of Cape Town.

Bahadur A, Mitra A, Ravi Kumar B, Palit Sagar S. 2007. Evaluation and Correlation of Residual Stress Measurement in Steel. Journal for Nondestructive Evaluation 26:47-55.

Balalov V.V, Pisarev V.S, Moshensky V.G. 2007. Combined implementing the hole-drilling method and reflection hologram interferometry for residual stresses determination in cylindrical shells and tubes. Optics and Lasers in Engineering 45: 661 – 676.

Baldev Raj, V. Rajendran, P. Palanichamy 2004. Science and Technology of Ultrasonics, Alpha Science International Ltd., Pangbourne.

Barrios D.B, Angelo E, Goncalves E, "Finite Element Simulation of Shot Peening Simulation for Residual Stresses. Analysis and Comparison with Experimental Results". MECOM 2005- VIII Congreso Agentino de Mecánica Computational.

Bray D, Bray D. E (2007). Ultrasonic Stress Measurement L_{CR} Wave. http://www.rssummit.org/rrobin/UT_overview.pdf

Bray D. E Tang W. Subsurface stress evaluation in steel plates and bars using the L_{CR} ultrasonic wave. Nuclear Engineering and Design 207 (2001) 231-40.

Bray D.E. "Current Directions of Ultrasonic Stress Measurement Techniques", 15th World Conference on Non-destructive Testing, Roma (Italy) 15 – 21 October 2000.

Dobmann G, Meyendorf N, Schneider E, "Non-destructive characterisation of materials A growing demand for describing damage and service-life-relevant aging processes in plant components". Nuclear Engineering and Design 171 (1997) 95 – 112.

Duggan T.V, Byrne J (1979). Fatigue As A Design Criterion, The Macmillan Press Ltd. London.

Duquennoy M, Ouaftouh M, Qian M.L, Jenot, F, Ourak M, "Ultrasonic characterization of residual stresses in steel rods using a laser line source and piezoelectric transducers": NDT & E International 34 (2001) 355-362.

Findeis D, Gryzagorids J. A, Matlali M. (2005). Phase Stepping Shearography and Electronic Speckle Pattern Interferometry. NDT laboratory, Department of Mechanical Engineering, University of Cape Town.

Findeis D, Gryzagorids J. A. (2004). Comparison of the Capabilities of Portable Shearography and Portable Electronic Speckle Pattern Interferometry. NDT laboratory, Department of Mechanical Engineering, University of Cape Town.

Groves R.M, James S.W, Tatam R.P. Shape and Slope Measurement by Source Displacement in Shearography. Optics and Lasers in Engineering 41 (2004) 621 – 634.

Gryzagorids J, Findeis D. (2005). Simultaneous Shearographic and Thermographic NDT of the Aerospace materials. NDT laboratory, Department of Mechanical Engineering, University of Cape Town.

Hathaway R.B, Hovanesian J.D, Hung Y.Y. Residual Stress Evaluation using Shearography with Large-shear Displacements. Optics and Lasers in Engineering 27 (1997) 43 – 60.

Hearn E.J. 1985. Mechanics of Materials, 2nd Edition, Volume 2. Oxford, 790-803.

Honner M, Litoš P, Švantner M, Thermography analyses of the hole-drilling stress measuring technique: Infrared Physics & Technology 45 (2004) 131-142.

Hosford W.F, 2005. Mechanical Behavior of Materials. Cambridge University Press, New York.

Hu, E. He, Y, Chen Y. Experimental study on the surface stress measurement with Rayleigh detection technique. Applied Acoustics, Volume 70, Issue 2, (2009) 356-360.

Hung Y.Y, Luo W.D, Lin L, Shang H.M. Evaluating the soundness of bonding using shearography. Composite Structures 50 (2000) 353-362.

Hung Y.Y. Applications of Digital Shearography for testing of Composite Structures. Composites: Part B 30 (1999) 765 – 773.

James M.N, Hughes D.J, Chen Z, Lombard H, Hattingh D.G, Asquith D, Yates J.R, Webster P.J, Residual stresses and fatigue performance: Engineering Failure Analysis, Volume 14, Issue 2, March 2007, pages 384-395.

Kudryavtsev Y, Kleiman J, Gushcha O, Smilenko V, Brodovy, V, "Ultrasonic Technique and Device for Residual Stress Measurement". Integrity Testing Laboratory Inc. & Paton Welding Institute.

"Measurement of Residual Stresses by the Hole-Drilling Strain Gage Method", Tech Note TN – 503-6, Vishay Micro-Measurements.

Min Y, Hong M, Xi Z, Jian L. Determination of residual stress by use of phase shifting moiré interferometry and hole-drilling. Optics and Lasers in Engineering 44 (2006) 68-79.

Mordfin L, "Mechanical relaxation of residual stresses", American Society for Testing and Materials 1988.

Nobre J.P, Loureiro A, A Batista A.C, Dias A.M. Evaluation of Welding Stress Using Incremental Hole-Drilling Technique. Materials Science Forum Vols. 514 – 516 (2006) pp 768-733.

Rajendran R, Baksi P, Bhattacharya S, Basu S. Evaluation of Nonuniform Residual Stress using Blind-Hole Drilling Technique. Experimental Techniques May/June 2008.

Schiffner K, Droste gen. Helling C, "Simulation of residual stresses by shot peening". Computers and Structures 72 (1999) 329 – 340.

Smith D.J, Farrahi G.H, Zhu W.X, McMahon C.A, Experimental measurement and finite element simulation of the interaction between residual stresses and mechanical loading: International Journal of Fatigue, Volume 23, Issue 4, April 2001, pages 293-302.

"Standard Test Method for Determining Residual Stresses by the Hole Drilling Strain Gage Method", E 837 – 01.

"Strain Gages and Instruments", Tech Note TN – 515, Vishay Micro-Measurements.

Totten G, Howes M, Inoue T (2002). Handbook of Residual Stress and Deformation of Steel, ASM International, USA.

Weng C.C, Lo S.C. "Measurement of residual stresses in welded steel joints using hole drilling method" Materials Science and Technology, March 1992, Volume 8, pages 213-218.

Withers P.J, Bhadeshia H.K.D.H, Residual Stress; Part 1 – Measurement Techniques: Material Science and Technology, Volume 17, April 2001.

Wyatt J.E, Berry J.T, A new technique for the determination of superficial residual stresses associated with machining and other manufacturing processes: Journal of Materials Processing Technology 171 (2006) 132 -140.

Ya M, Marquette P, Belahcene F, Lu J, "Residual stresses in laser welded aluminium plate by use of ultrasonic and optical methods". Materials Science and Engineering A 382 (2004) 257 – 264.

APPENDICES

APPENDIX A: STRAIN RESULTS AND COMPUTATION OF STRESSES

PROCEDURE FOR COMPUTATION OF STRESSES

Designation and specification of the Rosettes used:

EA-06-062RE-120 for high speed drilling using small drill bits ranging from 1.5 – 2 .3 mm.

EA-06-125RE-120 used in conjunction with an electric hand drill using drill bits ranging from 3 – 4.1 mm.

CEA-06-062UM and CEA-06-125UN -120

Cutter diameter, D_o = 2.3 mm; Gauge circle diameter, D = 5.13 mm $\Rightarrow$ D_o/D = 2.3/5.13 = **0.45**

The drilling coefficients, $\bar{a}$ and $\bar{b}$ will be evaluated at this ratio, as functions of non-dimensional hole depth and diameter, (Z/D).

These coefficients are interpolated from the figure 12 below derived from finite-element studies done by Schajer for uniform stress with depth and from E 837 -01 for out of range values. An example of the computation of equivalent uniform stresses at a depth of 0.1 mm for Type A rosette is done below.

E = 200 GPa and v = 0.3; $\bar{a} = 0.063$ $\bar{A} = -\frac{1+\nu}{2E} \times \bar{a} = -2.048 \times 10^{-13} (Nm)^{-2}$ $\bar{b} = 0.113$ $\bar{B} = -\frac{1}{2E} \times \bar{b} = -2.825 \times 10^{-13} (Nm)^{-2}$

The minimum and maximum stresses are 3.2 MPa and 5.65 MPa respectively. The orientation of the principal stresses follow the rules outlined below (Measurement Group Tech Note TN-503-4):

$\varepsilon_3 > \varepsilon_1 : \alpha$ refers to σ_{max}

$\varepsilon_3 < \varepsilon_1 : \alpha$ refers to σ_{min}

$\varepsilon_3 = \varepsilon_1 : \alpha = \pm 45^\circ$ refers to σ_{max}

$\varepsilon_2 < \varepsilon_1 : \sigma_{max} at + 45^\circ$

$\varepsilon_2 > \varepsilon_1 : \sigma_{max} at - 45^\circ$

Where $\tan 2\alpha = \frac{\varepsilon_1 - 2\varepsilon_2 + \varepsilon_3}{\varepsilon_3 - \varepsilon_1}$

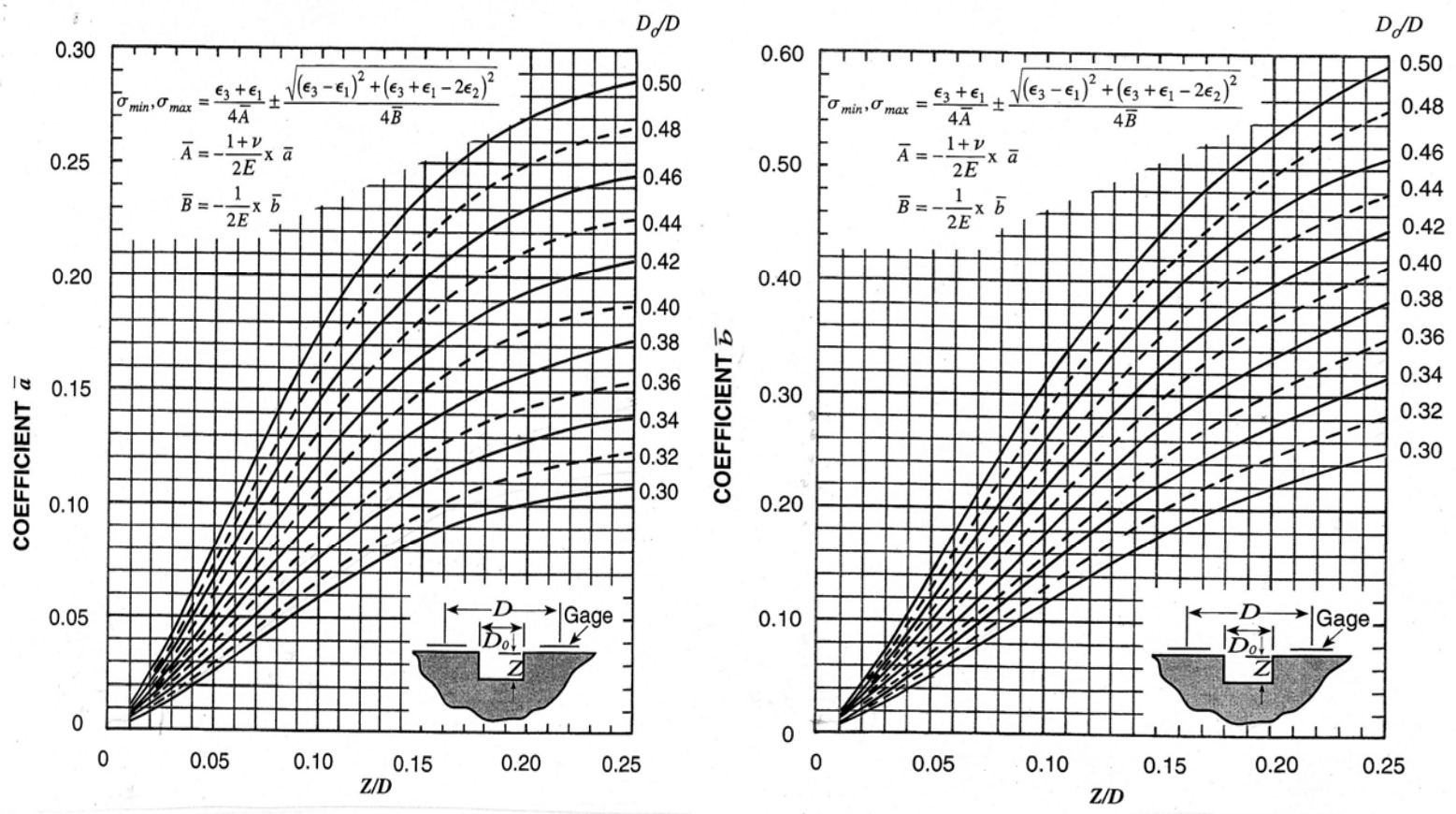

Figure A1. Data reduction coefficients $\bar{a}$ and $\bar{b}$ for RE and RK rosettes, as functions of nondimensional hole depth and diameter [Measurement Group Tech Note TN-503-4]

PRESENTATION OF RESULTS

Table A1 : RESULTS AND COMPUTATION OF STRESSES FOR EA-XX-125RE-120 ROSETTE

DEPTH		MEASURED STRAINS με		RELIEVED STRAINS			COEFFICIENTS Multiplier of (10^{-13}) for $\overline{A}$ and $\overline{B}$				α	Equiv. Uniform Stress (MPa)	
Z (mm)	Z/D			$\varepsilon_3 + \varepsilon_1$	$\varepsilon_3 - \varepsilon_1$	$\varepsilon_3 + \varepsilon_1 - 2\,\varepsilon_2$						σ_{min}	σ_{max}
0.1	0.019	ε_1	-2	1E-6	5E-6	1E-12	$\overline{a}$	0.063	$\overline{b}$	0.113	6°	3.2	-5.65
		ε_2	0				$\overline{A}$	-2.048	$\overline{B}$	-2.825			
		ε_3	3				$4\overline{A}$	-8.192	$4\overline{B}$	-11.3			
0.2	0.039	ε_1	-1	1E-6	3E-6	-4E-6	$\overline{a}$	0.063	$\overline{b}$	0.113	-27°	3.2	-5.65
		ε_2	2				$\overline{A}$	-2.048	$\overline{B}$	-2.825			
		ε_3	2				$4\overline{A}$	-8.192	$4\overline{B}$	-11.3			
0.3	0.058	ε_1	-3	1E-6	7E-6	-6E-6	$\overline{a}$	0.115	$\overline{b}$	0.21	-20°	3.7	-5.06
		ε_2	3				$\overline{A}$	-3.738	$\overline{B}$	-5.25			
		ε_3	4				$4\overline{A}$	-14.95	$4\overline{B}$	-21			
		ε_1	-4										

0.4	0.078			1E-6	9E-6	-6E-6	$\overline{a}$	0.136	$\overline{b}$	0.25	-17°	3.6	-4.89
		ε_2	3				$\overline{A}$	-4.42	$\overline{B}$	-6.25			
		ε_3	5				$4\overline{A}$	-17.68	$4\overline{B}$	-25			
0.5	0.097	ε_1	-5	1E-6	1.1E-5	-4E-6	$\overline{a}$	0.138	$\overline{b}$	0.255	-10°	4.03	-5.15
		ε_2	2				$\overline{A}$	-4.485	$\overline{B}$	-6.375			
		ε_3	6				$4\overline{A}$	-17.94	$4\overline{B}$	-25.5			
1	0.05	ε_1	-	-	-	-	$\overline{a}$	-	$\overline{b}$	-	-	-	-
		ε_2	-				$\overline{A}$	-	$\overline{B}$	-			
		ε_3	-				$4\overline{A}$	-	$4\overline{B}$	-			
2	0.39	ε_1	-11	2E-6	2.4E-5	1.8E-5	$\overline{a}$	0.239	$\overline{b}$	0.576	-18°	4.56	-5.85
		ε_2	9				$\overline{A}$	-7.768	$\overline{B}$	14.4			
		ε_3	13				$4\overline{A}$	-31.07	$4\overline{B}$	-57.6			

Rosette Design: CEA-06-062UM

HEATED AND QUENCHED SPECIMEN

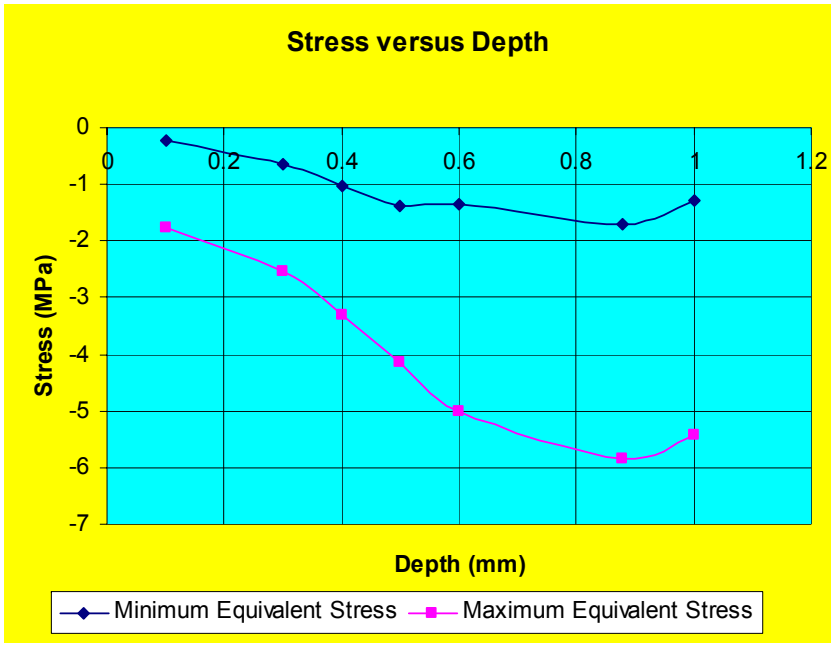

Figure A2: Stress versus depth for a heated and quenched specimen

SPECIMEN DIMPLED WITH STEEL BEARING BALLS

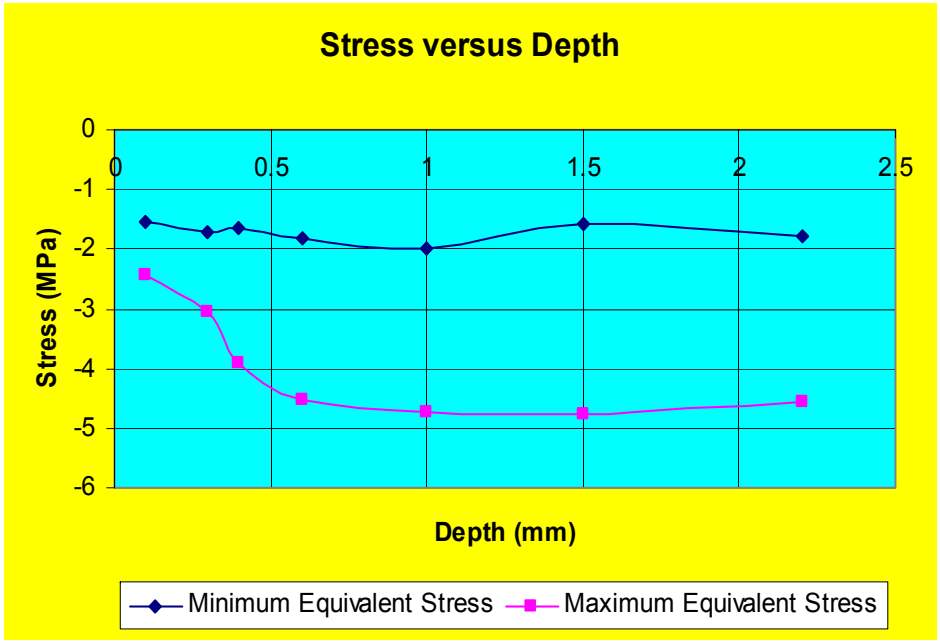

Figure A3: Stress versus depth for a dimpled surface specimen

WIRE BRUSH IMPACTED SPECIMEN

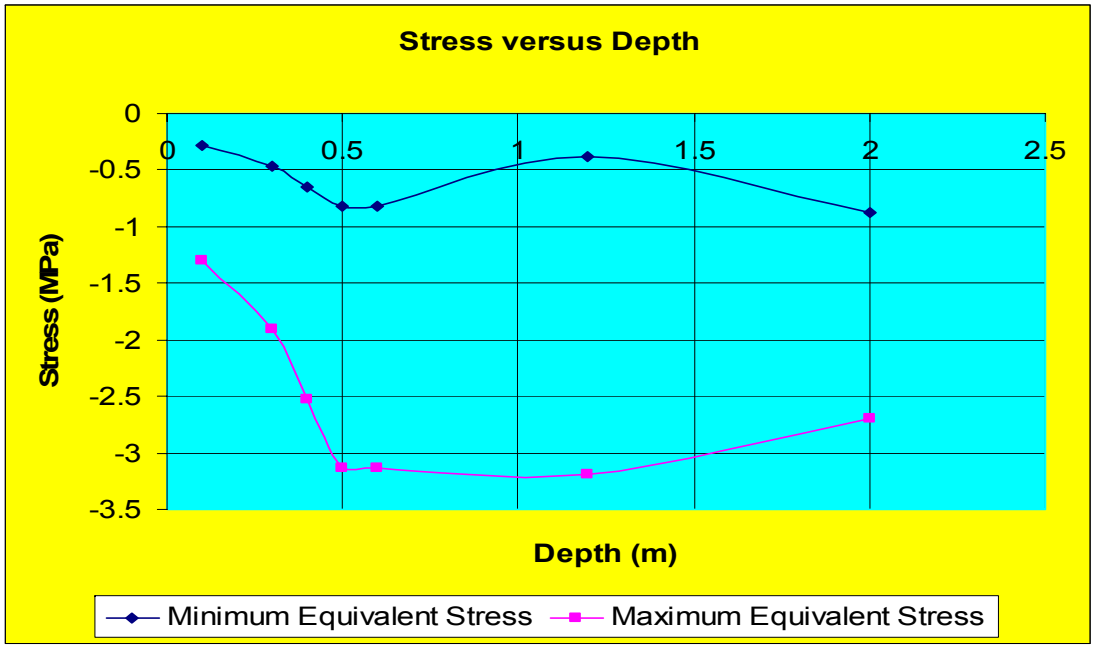

Figure A4: Stress versus depth for a specimen impacted with tips of bristles of a wire brush

APPENDIX B: Fundamental Properties of Ultrasonic Waves in some solid media

Table B1: *Fundamental Properties of Ultrasonic Waves in some solid media*

Constants of some solid media at a temperature 20 °C

medium	density $.10^3$ [$kg.m^{-3}$]	Poisson's number μ	propagation velocity c [$m.s^{-1}$]		wave resistance $Z_e = \rho.C_L.10^6$ [$Pa.s.m^{-1}$]
			longitudinal	transverse	
metals					
tin	7.30	0.33	3320	1670	24.2
aluminium	2.70	0.34	6320	3080	17.0
magnesium	1.73	0.30	5780	3050	10.0
cast iron	7.20	-	3500 – 5600	2200 – 3200	25 – 40
brass	8.10	0.35	3830	2123	31.0
nickel	8.80	0.31	3830	2960	49.5
steel	7.80	0.28	5900 – 6000	3200	46.3
non-metals					
ice	1	0.33	3980	1990	3.98
organic glass	1.18	0.35	2670	1121	3.2
polystyrene	1.06	0.32	2350	1120	2.40
porcelain	2.40	-	5300 – 5500	-	13
quartz glass	2.60	0.17	5570	3515	14.5
teflon	2.2	-	1350	-	3
rocks					
basalt	2.72	0.3	5930	3140	16.2
slate	2.74	0.27	6300	3610	17.8
marble	2.66	0.30	6150	3260	16.4
granite	2.62	0.18	4450	2780	11.6

APPENDIX C: Debro-30 Measurement Results

Calibration Specimen: Determination of Ref. Time

Step 1	Step 2	Step 3	Step 4	T_L^0	T_L^σ	Force (N)	Temp.(°C)	Stress (MPa)	β (MPa^{-1})
24.3	7.4	24.3	7.4	18437			24		
24.3	7.4	24.3	7.4	18438			24		
24.3	7.4	24.3	7.4	18433			24		
24.3	7.4	24.3	7.4	18435			24		
24.3	7.4	24.3	7.4	18434			24		
24.3	7.4	24.3	7.4	18433			24		
24.3	7.4	24.3	7.4	18435			24		
			Mean	**18435**					

Specimen One: Determination of Reference Time

Step 1	Step 2	Step 3	Step 4	T_L^0	T_L^σ	Force (N)	Temp.(°C)	Stress (MPa)	β (MPa^{-1})
24.3	7.4	24.3	7.5	18437			24		
24.3	7.4	24.3	7.5	18434			24		
24.3	7.4	24.3	7.5	18435			24		
24.3	7.4	24.3	7.5	18436			24		
24.3	7.4	24.3	7.5	18433			24		
24.3	7.4	24.3	7.4	18435			24		
24.3	7.4	24.3	7.4	18434			24		
			Mean	**18435**					

Specimen Two: Determination of Reference Time

Step 1	Step 2	Step 3	Step 4	T_L^0	T_L^σ	Force (N)	Temp.(°C)	Stress (MPa)	β (MPa^{-1})
24.3	7.4	24.6	7.4	18436			24		
24.3	7.4	24.6	7.4	18435			24		
24.3	7.4	24.6	7.4	18433			24		
24.3	7.4	24.6	7.4	18438			24		
24.3	7.4	24.6	7.4	18432			24		
24.3	7.4	24.6	7.4	18436			24		
24.3	7.4	24.6	7.4	18434			24		
			Mean	**18435**					

Specimen Three: Determination of Reference Time									
Step 1	**Step 2**	**Step 3**	**Step 4**	**T_L^0**	**T_L^σ**	**Force (N)**	**Temp.(°C)**	**Stress (MPa)**	**β (MPa^{-1})**
24.3	7.4	24.3	7.4	18433			24		
24.3	7.4	24.3	7.4	18432			24		
24.3	7.4	24.3	7.4	18436			24		
24.3	7.4	24.3	7.4	18434			24		
24.3	7.4	24.3	7.4	18432			24		
24.3	7.4	24.3	7.4	18433			24		
24.3	7.4	24.3	7.4	18439			24		
			Mean	**18434**					

Specimen Four: Determination of Reference Time									
Step 1	**Step 2**	**Step 3**	**Step 4**	**T_L^0**	**T_L^σ**	**Force (N)**	**Temp.(°C)**	**Stress (MPa)**	**β (MPa^{-1})**
24.3	7.4	24.3	7.4	18438			24		
24.3	7.4	24.3	7.4	18437			24		
24.3	7.4	24.3	7.4	18434			24		
24.3	7.4	24.3	7.4	18432			24		
24.3	7.4	24.3	7.4	18435			24		
24.3	7.4	24.3	7.4	18433			24		
24.3	7.4	24.3	7.4	18432			24		
			Mean	**18434**					

Table C1: Calibration Results for Acoustoelastic Constant Determination by Compression Test

T_L^0 (ns)	**T_L^σ** (ns)	**Area** (m^2)	**Force** (N)	**Stress** (N/m^2)	**σ** (MPa)	**β** (MPa^{-1})
18435	18432	6.20E-04	1750	2822581	2.822581	5.76637E-05
	18428		4380	7064516	7.064516	5.37697E-05
	18422		8442	13616129	13.61613	5.18266E-05
	18415		12062	19454839	19.45484	5.58252E-05
	18409		15565	25104839	25.10484	5.62582E-05
	18404		18335	29572581	29.57258	5.69587E-05
	18395		23758	38319355	38.31935	5.67469E-05
	18391		25950	41854839	41.85484	5.71612E-05
	18385		29635	47798387	47.79839	5.68975E-05
	18381		31400	50645161	50.64516	5.80078E-05
	18375		34285	55298387	55.29839	5.90488E-05
	18371		36700	59193548	59.19355	5.88536E-05
					Mean	**5.65848E-05**

APPENDIX D: Shearography Results for all the Four Specimens

Stress Free Specimen

Figure D1. Phase Image

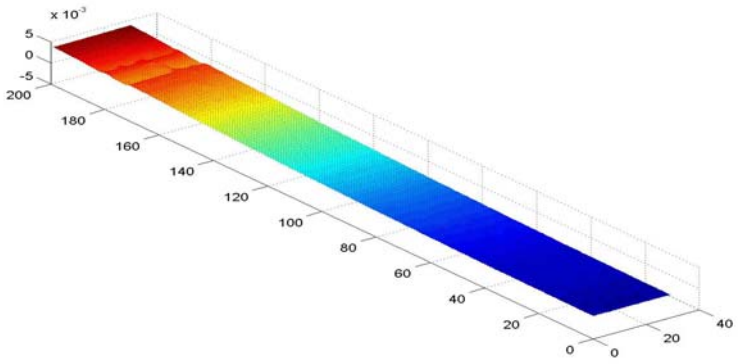

Figure D2. Gradient Image

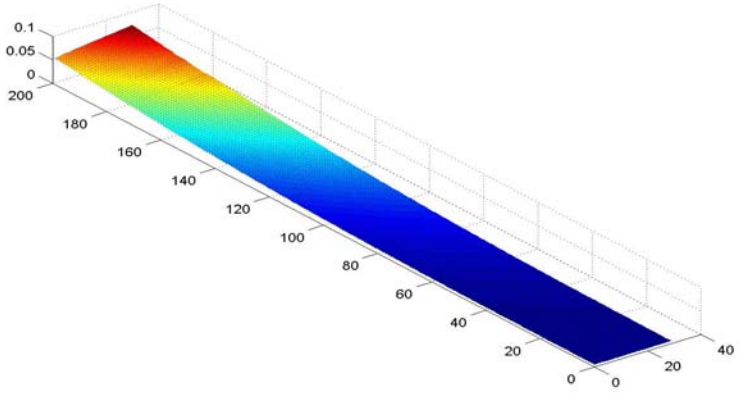

Figure D3. Displacement Image

Surface impacted with the tips of bristles of a wire brush

Figure D4. Phase Image

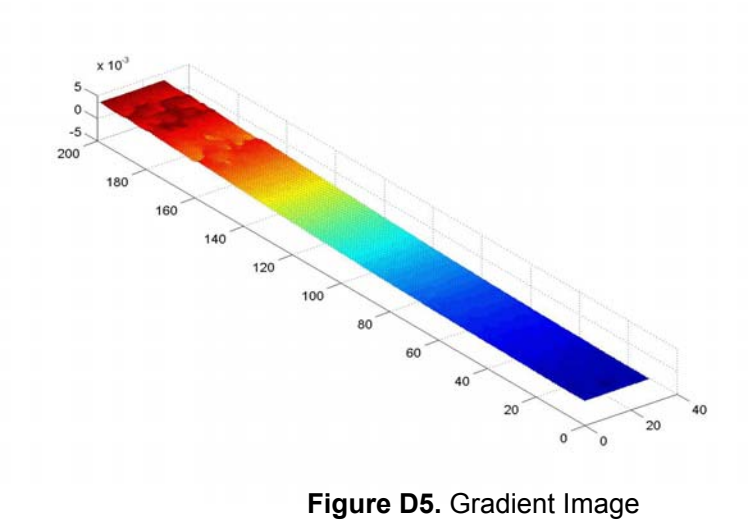

Figure D5. Gradient Image

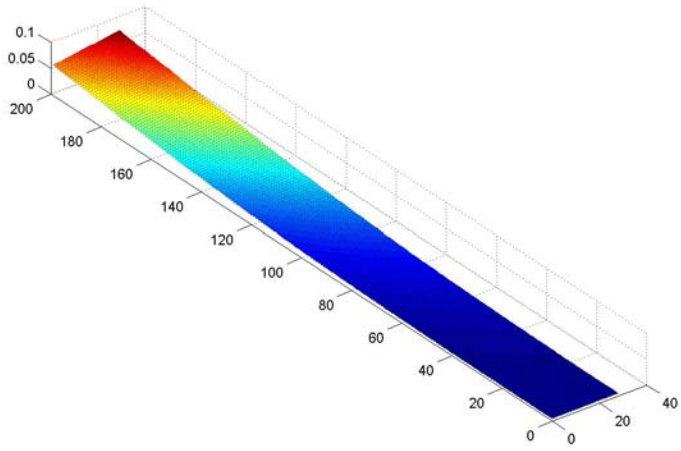

Figure D6. Displacement Image

Surface produced by hammering 1.5 mm steel bearing balls in contact with the surface

Figure D7. Phase Image

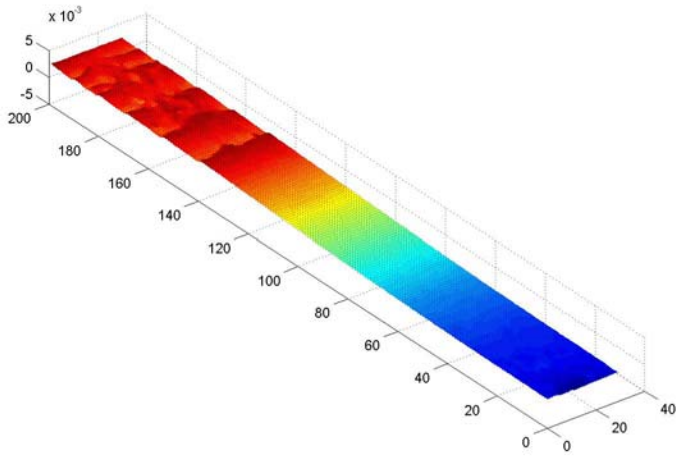

Figure D8. Gradient Image

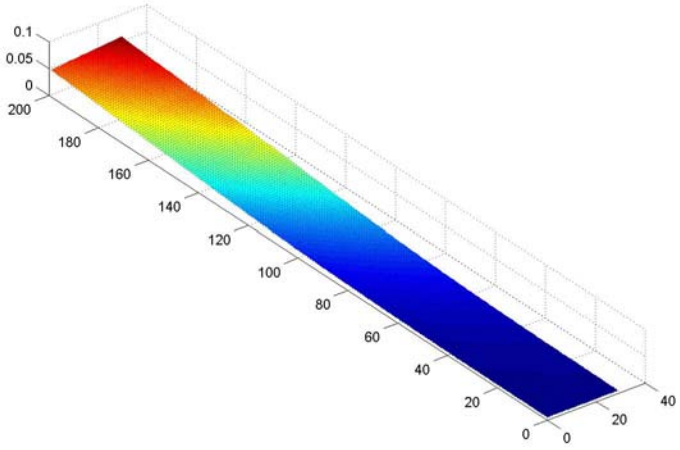

Figure D9. Displacement Image

Surface heated with oxy-acetylene flame and quenched in water

Figure D10. Phase Image

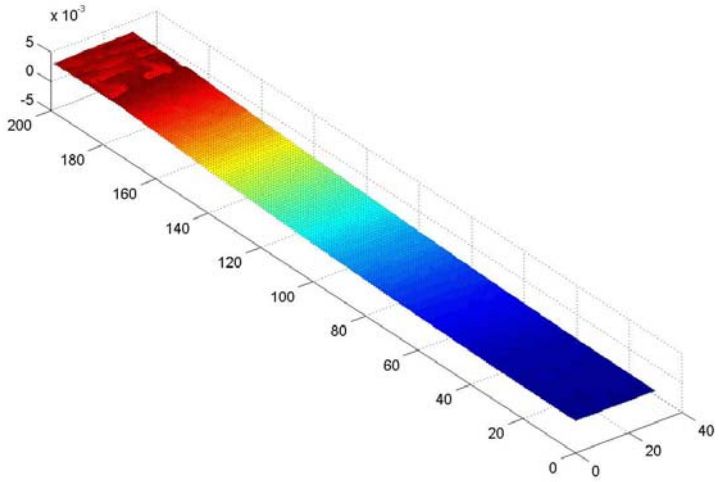

Figure D11. Gradient Image

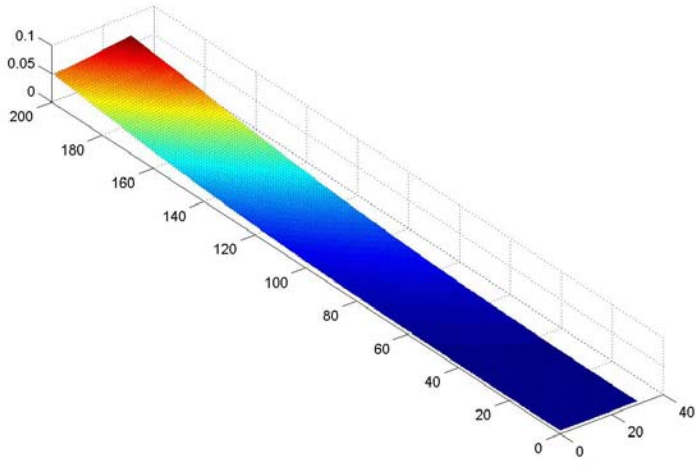

Figure D12. Displacement Image